UNIVERSITÄT
LEIPZIG

Fakultät für Physik und Geowissenschaften
Fortgeschrittenen-Praktikum
Advanced Physics Lab

X-ray diffraction (XRD)

Analysis of structure of powder samples and epitaxial thin films

Experiment in Advanced Physics Lab

tasks and preparation

English

version of 28.04.2023

Supervisor:
Prof. Dr. Michael Lorenz

Tasks for preparation:

Summarize in writing the basics of the experiment and include it as introductory part in your protocol:

- Generation of X-rays, Bremsstrahlung and characteristic spectrum (see Appendix Cullity et al., p. 1-19)
- Nomenclature of designation of characteristic X-ray lines (p. 1-19)
- Absorption and filtering of X-rays (p. 1-19)
- Derivation of Bragg-equation (Cullity p. 167-168, Kittel chapter 2)
- Crystal systems, derivation of Miller's indices (Kittel chapter 1, Cullity p. 44-52)
- Relation of lattice spacing d and lattice constants for the 7 crystal systems (p. 44-45 and 619-621)
- Penetration depth of X-rays
- Errors in goniometer measurement and methods for elimination of errors (p. 363-369)
- Structure of polycrystalline samples and heteroepitaxial thin films (p. 174-177, 399-402, …)

Experimental tasks:

Important note: Before you start to operate the X-ray diffractometer, wait for the instructions of the supervisor including the special safety instructions for X-rays.

1. Analysis of two polycrystalline bulk samples (selected from silicon Si, aluminum Al, copper Cu, and zinc oxide ZnO)

1. Measure with the Philips X'Pert diffractometer in Bragg-Brentano geometry the X-ray diffraction patterns (2θ-ω scan) of two selected polycrystalline bulk samples with the following 2θ range:

- Si: **$20° \leq 2\theta \leq 140°$**
- Al: **$30° \leq 2\theta \leq 120°$**
- Cu: **$40° \leq 2\theta \leq 140°$**
- ZnO: **$30° \leq 2\theta \leq 130°$**

For all samples the step size is 0.02°, and the measuring time 0.5 sec. per step. Using the X'Pert High Score software, a list of all peaks can be generated without and with deconvolution of the $K\alpha_1/K\alpha_2$ peaks.

- Derive the Miller's indizes (hkl) by comparison with suitable patterns from the PC-PDF data base. Optionally you may try to derive the hkl for the cubic materials Si / Al by combining the formulae for the lattice parameter with the Bragg equation, without any data base, see the literature.

- Show and discuss by means of a scheme in the protocol the unit cells of Si / Al and ZnO including the c and a lattice parameters, see Cullity p. 51-52.
- Calculate from the lattice spacing d of all peaks the lattice constants a (Si, Al) or a and c (ZnO). Note that for h, k = 0 or l = 0 you can determine either a or c, respectively. Check the consistency of a and c for all reflections of the same material.
- Perform the error correction of the a- and c-lattice parameters of the single peaks by extrapolating these lattice parameters to $\theta = 90°$ using three different functions: $\cos^2\theta$; $\cot\theta$; and the Nelson-Riley-function $1/2\,[(\cos^2\theta)/\theta + (\cos^2\theta)/(\sin\theta)]$.
- Check and discuss the agreement of experimental lattice constants (single values and extrapolated values from the three different extrapolation functions) in comparison to the PC-PDF data base values.

2. Epitaxial ZnO thin films grown on a-plane and r-plane oriented single-crystalline sapphire substrates

2.1. Measure the XRD patterns (2θ-ω scans, 0.02°, 0.5 sec.) of two different ZnO thin films (about 1 µm thick) on single-crystalline sapphire substrates with different crystalline orientation of the substrate surface.

Sapphire is chemically Al_2O_3 with rhombohedral structure. Consider the given ω-offset values to take into account the miscuts of the sapphire substrates. Note the sample orientation in the diffractometer ("vorn" = this side should show to you).

- ZnO thin film on a-plane sapphire (11-20): **$30° \leq 2\theta \leq 130°$**
- ZnO thin film on r-plane sapphire (01-12): **$20° \leq 2\theta \leq 130°$**

Note: The Millers-Bravais (hkil)-notation with four indices corresponds to the usual (hkl)-notation of the Miller's indices as follows: i = - (h + k) (see Cullity S. 51-52).

- Assign the peaks of ZnO and sapphire using the PC-PDF data base. Use the tool "Spectral lines" in Data Viewer software to identify the weak Cu Kβ and W Lα peaks.
- Compare the appearance of ZnO Kα-peaks with that of the polycrystalline ZnO sample of task 1. Discuss the structure (orientation, epitaxy) of the ZnO thin films in dependence of the substrate orientation and give the crystallographic growth direction of the two ZnO films.

Note: After peak assignment you have to measure the ω-scans according to task 2.2., as shown below. Do not remove the sample from the sample stage of the goniometer.

2.2. Measure for each of the two thin film samples the ZnO and sapphire peaks with the highest 2θ-value (*note: the peak selection can be confirmed by the supervisor*) the ω-scans (scan range 5°, step 0.01°, 0.5 sec.) with the detector position fixed at the 2θ position of the selected peak maxima from task No. 2.1.

- Determine by using the Data Viewer software the $K\alpha_1$ peak positions and the full width of half maximum (FWHM) values of the in total four selected 2θ-ω peaks (two ZnO and two for sapphire) and the four ω-peaks and compare all FWHM values in a table.
- From the $K\alpha_1$ peak positions, calculate the out-of-plane lattice constants c or a of the ZnO thin films perpendicular to the film surface (i.e. out-of-plane) and compare them with that of task 1 and with the PC-PDF values of ZnO.
- The measurements in task 2.2. are the so called ω-scans. They are called in case of use of a high-resolution goniometer "rocking curve". The FWHM of the rocking curves is an important and widely used structural quality criterion of textured and epitaxial thin films and single crystals. Discuss the FWHMs of the 2θ-ω peaks (keywords: deviations of lattice plane distance d and coherence length) and ω-scan peaks (keyword: tilt mosaizity) in dependence on the substrate orientation and concerning their relevance for the crystalline sample structure.

3. Phase analysis of an unknown oxide powder

Prepare and measure a powder sample of an unknown oxide (mention number of the powder bottle) as 2θ–ω-scan in the range from **10° to 90°** in 2θ with step size of 0.02°, and time of 0.5 sec per step.

- Perform a phase analysis using the software X'Pert High Score with implemented PC-PDF data base using an automatic best fit of measured and data base diffraction patterns. You get a table of phase proposals with decreasing score value. Contact the supervisor. Proof the result of the software-based search for different search algorithms related to the different input restrictions (for example without/with consideration of peak intensities).
- Compare and discuss the three best-fit (highest score) search results concerning agreement of peak positions. Discuss crystalline structure and lattice constants of the identified oxide material.

Note: Include all measured XRD patterns with assignment of all peaks in the protocol.

References:

[1] B. D. Cullity, S. R. Stock, Elements of X-ray diffraction third edition, Prentice Hall, Upper Saddle River, p. 1-19; 44-45; 51-52; 167-171; 174-177; 295-302; 363-369; 399-402; 619-621; 632-633

[2] Charles Kittel, Introduction to Solid State Physics, 7th edition, J. Wiley, New York, p. 1-37

[3] L. Spieß, R. Schwarzer, H. Behnken, G. Teichert, Moderne Röntgenbeugung, Teubner, Wiesbaden 1st edition 2005 or 2nd edition 2009, see German XRD description, or our University Library in Liebigstraße.

Operation X-Ray Diffraction Instrument Philips X'Pert

1. open both cooling water valves and switch on the water cooler,
2. goniometer electronics and the PC should be always on, if not ask experienced person.
3. if not already started: start *X'Pert Data Collector* software**,** User: **User-1**, PW: **galaxy,** wait
   Instrument, connect: **Configuration 1, diffracted beam path 1,** wait,
   Message X-ray tube: quit OK.
4. X-Ray generator: press "Power on", press "HT on" and wait as long as the two green LEDs are on, increase slowly high voltage (first) and then current (for voltage wait around 10 sec per step), close doors (doors open lamp should be off),
   open corresponding Shutter,
   Parameters of X-Ray tube*:* polycrystalline samples: **40 kV, 30 mA;**
   Single crystals, epitaxial films: **30 kV, 25 mA** (≤ 1 Mio. cps in peak maximum)
5. To measure a scan: *Measure*, *manual scan, select scan axis*: $2\theta-\omega$ oder ω-scan.
   The scan range has to be controlled by the ***Position*** (center position of scan in the Configuration-1 window) and ***Range*** (Scan range symmetricaly around the center),
   For example for $20° \le 2\theta \le 120°$: fix Position 70° and give Range 100°.
   Continuous scan mode, *Step size* 0.05° bis 0.01°, *Time per step* 0.5 sec. Check total scan time, press Start.
   Note: manual scans are not saved automatically, has to be done immediately after manual scan is finished
6. Software *X'Pert Data Viewer*:
   - Show and *compare* diffraction patterns
   - Get Peak parameters (position, intensity FWHM)
   - Show spectral lines of X-Ray tube such as copper Kβ, tungsten Lα)
   - *Convert into* ASCII (csv- and xy-) format
   - Save current screen as emf graphics file
7. Software *X'Pert High Score*
   - Treatments: *Behandeln, Kα2 eliminieren*
   - Peak search: *Behandeln, Reflexe suchen, akzeptieren* (Reflexliste)
   - Print results: *Berichte* (Reports as MS word file ….)
   - Phase analysis of polycrystalline samples: *Analyse, Suchen und vergleichen* (search-match, looks for agreement with reference cards of JCPDS data base)
   - Screenshot of score list: press "Druck", insert into "Paint", save image file.

Leipzig, 28 April 2023 Prof. Dr. Michael Lorenz

CHARLES KITTEL

Introduction to Solid State Physics

SEVENTH EDITION

John Wiley & Sons, Inc., New York, Chichester,
Brisbane, Toronto, Singapore

1

Crystal Structure

UNITS: 1 Å = 1 angstrom = 10^{-8} cm = 0.1 nm = 10^{-10} m.

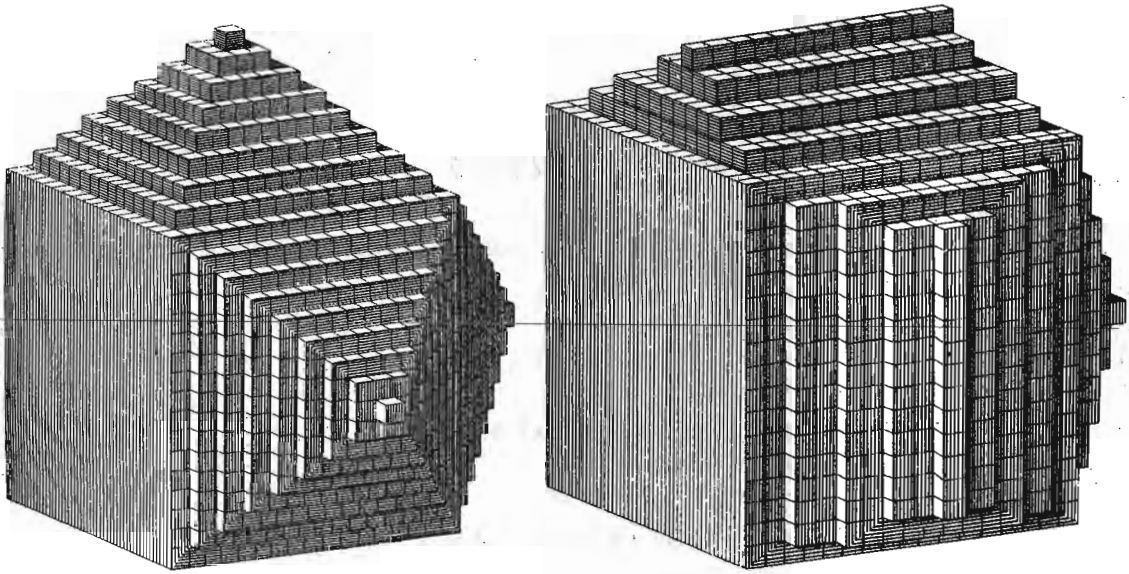

(a) (b)

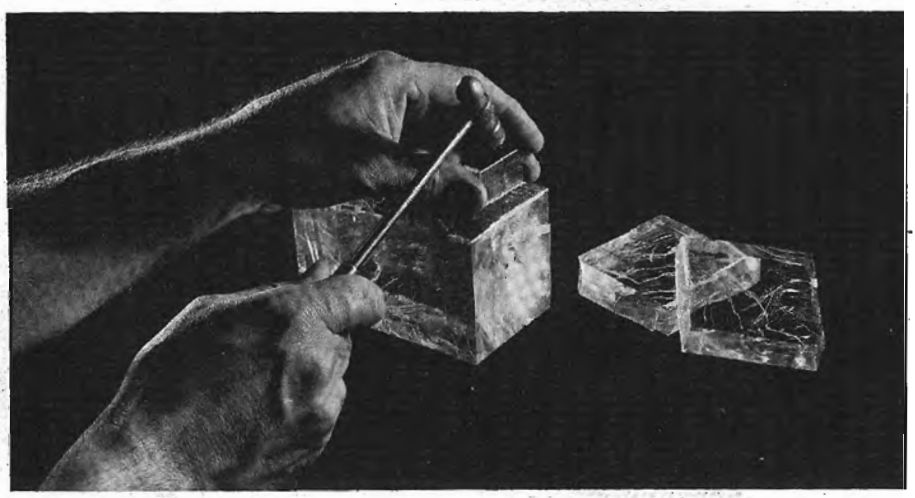

(c)

Figure 1 Relation of the external form of crystals to the form of the elementary building blocks. The building blocks are identical in (a) and (b), but different crystal faces are developed. (c) Cleaving a crystal of rocksalt.

Solid state physics is largely concerned with crystals and electrons in crystals. The study of solid state physics began in the early years of this century following the discovery of x-ray diffraction by crystals and the publication of a series of simple calculations and successful predictions of the properties of crystals.

When a crystal grows in a constant environment, the form develops as if identical building blocks were added continuously (Fig. 1). The building blocks are atoms or groups of atoms, so that a crystal is a three-dimensional periodic array of atoms.

This was known in the 18th century when mineralogists discovered that the index numbers of the directions of all faces of a crystal are exact integers. Only the arrangement of identical particles in a periodic array can account for the law of integral indices,[1] as discussed below.

In 1912 a paper entitled "Interference effects with Röntgen rays" was presented to the Bavarian Academy of Sciences in Munich. In the first part of the paper, Laue developed an elementary theory of the diffraction of x-rays by a periodic array. In the second part, Friedrich and Knipping reported the first experimental observations of x-ray diffraction by crystals.[2]

The work proved decisively that crystals are composed of a periodic array of atoms. With an established atomic model of a crystal, physicists now could think much further. The studies have been extended to include amorphous or noncrystalline solids, glasses, and liquids. The wider field is known as condensed matter physics, and it is now the largest and probably the most vigorous area of physics.

PERIODIC ARRAYS OF ATOMS

An ideal crystal is constructed by the infinite repetition of identical structural units in space. In the simplest crystals the structural unit is a single atom, as in copper, silver, gold, iron, aluminum, and the alkali metals. But the smallest structural unit may comprise many atoms or molecules.

The structure of all crystals can be described in terms of a lattice, with a group of atoms attached to every lattice point. The group of atoms is called the basis; when repeated in space it forms the crystal structure.

[1]R. J. Haüy, *Essai d'une théorie sur la structure des cristaux*, Paris, 1784; *Traité de cristallographie*, Paris, 1801.

[2]For personal accounts of the early years of x-ray diffraction studies of crystals, see P. P. Ewald, ed., *Fifty years of x-ray diffraction*, A. Oosthoek's Uitgeversmij., Utrecht, 1962.

Lattice Translation Vectors

The lattice is defined by three fundamental translation vectors $\mathbf{a}_1$, $\mathbf{a}_2$, $\mathbf{a}_3$ such that the atomic arrangement looks the same in every respect when viewed from the point $\mathbf{r}$ as when viewed from the point

$$\mathbf{r}' = \mathbf{r} + u_1\mathbf{a}_1 + u_2\mathbf{a}_2 + u_3\mathbf{a}_3 , \tag{1}$$

where u_1, u_2, u_3 are arbitrary integers. The set of points $\mathbf{r}'$ defined by (1) for all u_1, u_2, u_3 defines a **lattice**.

A lattice is a regular periodic array of points in space. (The analog in two dimensions is called a net, as in Chapter 18.) A lattice is a mathematical abstraction; the crystal structure is formed when a basis of atoms is attached identically to every lattice point. The logical relation is

$$\textbf{lattice} + \textbf{basis} = \textbf{crystal structure} . \tag{2}$$

The lattice and the translation vectors $\mathbf{a}_1$, $\mathbf{a}_2$, $\mathbf{a}_3$ are said to be primitive if any two points $\mathbf{r}$, $\mathbf{r}'$ from which the atomic arrangement looks the same always satisfy (1) with a suitable choice of the integers u_1, u_2, u_3. With this definition of the **primitive translation vectors**, there is no cell of smaller volume that can serve as a building block for the crystal structure.

We often use primitive translation vectors to define the crystal axes. However, nonprimitive crystal axes are often used when they have a simpler relation to the symmetry of the structure. The crystal axes $\mathbf{a}_1$, $\mathbf{a}_2$, $\mathbf{a}_3$ form three adjacent edges of a parallelepiped. If there are lattice points only at the corners, then it is a primitive parallelepiped.

A lattice translation operation is defined as the displacement of a crystal by a crystal translation vector

$$\mathbf{T} = u_1\mathbf{a}_1 + u_2\mathbf{a}_2 + u_3\mathbf{a}_3 . \tag{3}$$

Any two lattice points are connected by a vector of this form.

To describe a crystal structure, there are three important questions to answer: What is the lattice? What choice of $\mathbf{a}_1$, $\mathbf{a}_2$, $\mathbf{a}_3$ do we wish to make? What is the basis?

More than one lattice is always possible for a given structure, and more than one set of axes is always possible for a given lattice. The basis is identified once these choices have been made. Everything (including the x-ray diffraction pattern) works out correctly in the end provided that (3) has been satisfied.

The symmetry operations of a crystal carry the crystal structure into itself. These include the lattice translation operations. Further, there are rotation and reflection operations, called **point operations**. About lattice points or certain special points within an elementary parallelpiped it may be possible to apply rotations and reflections that carry the crystal into itself.

Finally, there may exist compound operations made up of combined translation and point operations. Textbooks on crystallography are largely devoted to

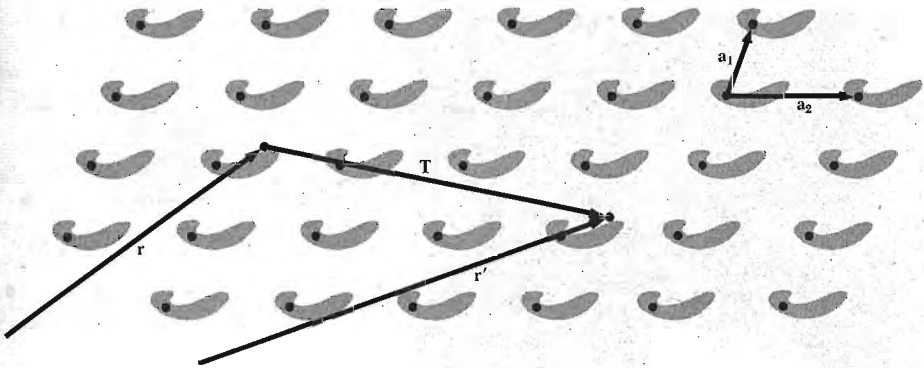

Figure 2 Portion of a crystal of an imaginary protein molecule, in a two-dimensional world. (We picked a protein molecule because it is not likely to have a special symmetry of its own.) The atomic arrangement in the crystal looks exactly the same to an observer at $\mathbf{r}'$ as to an observer at $\mathbf{r}$, provided that the vector $\mathbf{T}$ which connects $\mathbf{r}'$ and $\mathbf{r}$ may be expressed as an integral multiple of the vectors $\mathbf{a}_1$ and $\mathbf{a}_2$. In this illustration, $\mathbf{T} = -\mathbf{a}_1 + 3\mathbf{a}_2$. The vectors $\mathbf{a}_1$ and $\mathbf{a}_2$ are primitive translation vectors of the two-dimensional lattice.

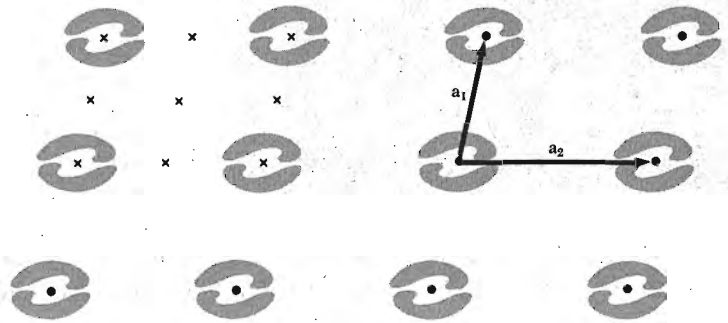

Figure 3 Similar to Fig. 2, but with protein molecules associated in pairs. The crystal translation vectors are $\mathbf{a}_1$ and $\mathbf{a}_2$. A rotation of π radians about any point marked × will carry the crystal into itself. This occurs also for equivalent points in other cells, but we have marked the points × only within one cell.

the description of symmetry operations. The crystal structure of Fig. 2 is drawn to have only translational symmetry operations. The crystal structure of Fig. 3 allows both translational and point symmetry operations.

Basis and the Crystal Structure

A basis of atoms is attached to every lattice point, with every basis identical in composition, arrangement, and orientation. Figure 4 shows how a crystal structure is formed by adding a basis to every lattice point. The lattice is indicated by dots in Figs. 2 and 3, but in Fig. 4c the dots are omitted.

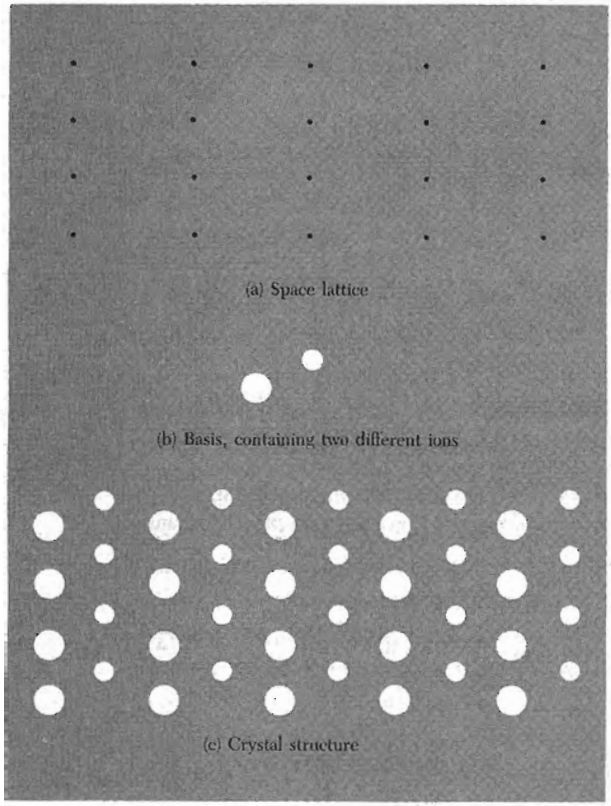

Figure 4 The crystal structure is formed by the addition of the basis (b) to every lattice point of the lattice (a). By looking at (c), you can recognize the basis and then you can abstract the space lattice. It does not matter where the basis is put in relation to a lattice point.

The number of atoms in the basis may be one, or it may be more than one. The position of the center of an atom j of the basis relative to the associated lattice point is

$$\mathbf{r}_j = x_j\mathbf{a}_1 + y_j\mathbf{a}_2 + z_j\mathbf{a}_3 \ . \tag{4}$$

We may arrange the origin, which we have called the associated lattice point, so that $0 \leq x_j,\ y_j,\ z_j \leq 1$.

Primitive Lattice Cell

The parallelepiped defined by primitive axes $\mathbf{a}_1$, $\mathbf{a}_2$, $\mathbf{a}_3$ is called a **primitive cell** (Fig. 5b). A primitive cell is a type of cell or unit cell. (The adjective unit is superfluous and not needed.) A cell will fill all space by the repetition of suitable crystal translation operations. A primitive cell is a minimum-volume cell.

There are many ways of choosing the primitive axes and primitive cell for a given lattice. The number of atoms in a primitive cell or primitive basis is always the same for a given crystal structure.

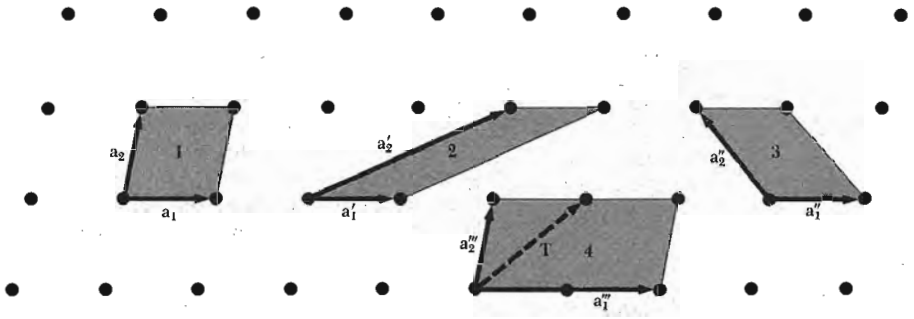

(a)

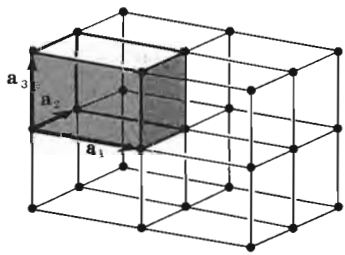

(b)

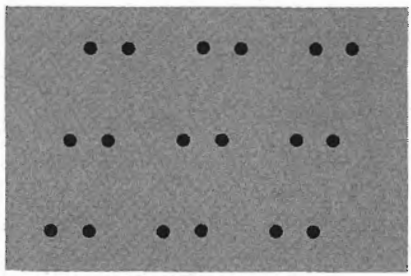

(c)

Figure 5a Lattice points of a space lattice in two dimensions. All pairs of vectors $\mathbf{a}_1$, $\mathbf{a}_2$ are translation vectors of the lattice. But $\mathbf{a}_1'''$, $\mathbf{a}_2'''$ are not primitive translation vectors because we cannot form the lattice translation $\mathbf{T}$ from integral combinations of $\mathbf{a}_1'''$ and $\mathbf{a}_2'''$. All other pairs shown of $\mathbf{a}_1$ and $\mathbf{a}_2$ may be taken as the primitive translation vectors of the lattice. The parallelograms 1, 2, 3 are equal in area and any of them could be taken as the primitive cell. The parallelogram 4 has twice the area of a primitive cell.

Figure 5b Primitive cell of a space lattice in three dimensions.

Figure 5c Suppose these points are identical atoms: sketch in on the figure a set of lattice points, a choice of primitive axes, a primitive cell, and the basis of atoms associated with a lattice point.

There is always one lattice point per primitive cell. If the primitive cell is a parallelepiped with lattice points at each of the eight corners, each lattice point is shared among eight cells, so that the total number of lattice points in the cell is one: $8 \times \frac{1}{8} = 1$.

The volume of a parallelepiped with axes $\mathbf{a}_1$, $\mathbf{a}_2$, $\mathbf{a}_3$ is

$$V_c = |\mathbf{a}_1 \cdot \mathbf{a}_2 \times \mathbf{a}_3| \ , \tag{5}$$

by elementary vector analysis. The basis associated with a primitive cell is called a primitive basis. No basis contains fewer atoms than a primitive basis contains.

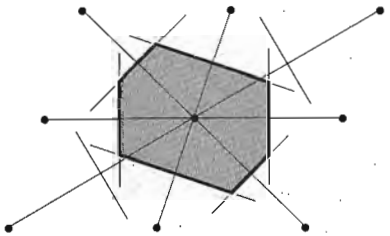

Figure 6 A primitive cell may also be chosen following this procedure: (1) draw lines to connect a given lattice point to all nearby lattice points; (2) at the midpoint and normal to these lines, draw new lines or planes. The smallest volume enclosed in this way is the Wigner-Seitz primitive cell. All space may be filled by these cells, just as by the cells of Fig. 5.

Another way of choosing a primitive cell is shown in Fig. 6. This is known to physicists as a **Wigner-Seitz cell**.

FUNDAMENTAL TYPES OF LATTICES

Crystal lattices can be carried or mapped into themselves by the lattice translations $\mathbf{T}$ and by various other symmetry operations. A typical symmetry operation is that of rotation about an axis that passes through a lattice point. Lattices can be found such that one-, two-, three-, four-, and sixfold rotation axes carry the lattice into itself, corresponding to rotations by 2π, $2\pi/2$, $2\pi/3$, $2\pi/4$, and $2\pi/6$ radians and by integral multiples of these rotations. The rotation axes are denoted by the symbols 1, 2, 3, 4, and 6.

We cannot find a lattice that goes into itself under other rotations, such as by $2\pi/7$ radians or $2\pi/5$ radians. A single molecule properly designed can have any degree of rotational symmetry, but an infinite periodic lattice cannot. We can make a crystal from molecules that individually have a fivefold rotation axis, but we should not expect the lattice to have a fivefold rotation axis. In Fig. 7 we show what happens if we try to construct a periodic lattice having fivefold symmetry: the pentagons do not fit together to fill all space, showing that we cannot combine fivefold point symmetry with the required translational periodicity.

By lattice point group we mean the collection of symmetry operations which, applied about a lattice point, carry the lattice into itself. The possible rotations have been listed. We can have mirror reflections m about a plane through a lattice point. The inversion operation is composed of a rotation of π followed by reflection in a plane normal to the rotation axis; the total effect is to replace $\mathbf{r}$ by $-\mathbf{r}$. The symmetry axes and symmetry planes of a cube are shown in Fig. 8.

Two-Dimensional Lattice Types

There is an unlimited number of possible lattices because there is no natural restriction on the lengths of the lattice translation vectors or on the angle φ between them. The lattice in Fig. 5a was drawn for arbitrary $\mathbf{a}_1$ and $\mathbf{a}_2$. A general lattice such as this is known as an **oblique lattice** and is invariant only under rotation of π and 2π about any lattice point.

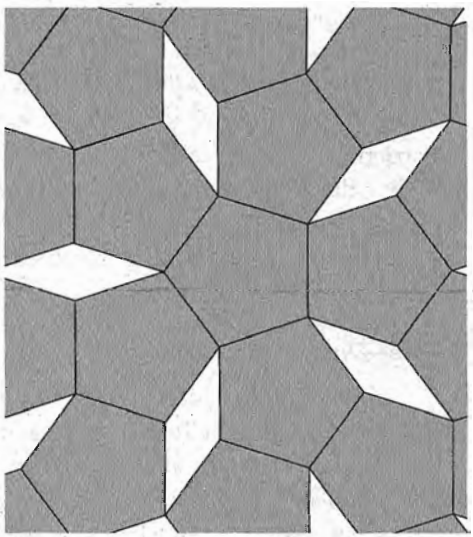

Figure 7 A fivefold axis of symmetry cannot exist in a periodic lattice because it is not possible to fill the area of a plane with a connected array of pentagons. We can, however, fill all the area of a plane with just two distinct designs of "tiles" or elementary polygons. A quasicrystal is a quasiperiodic nonrandom assembly of two types of figures. Quasicrystals are discussed at the end of Chapter 2.

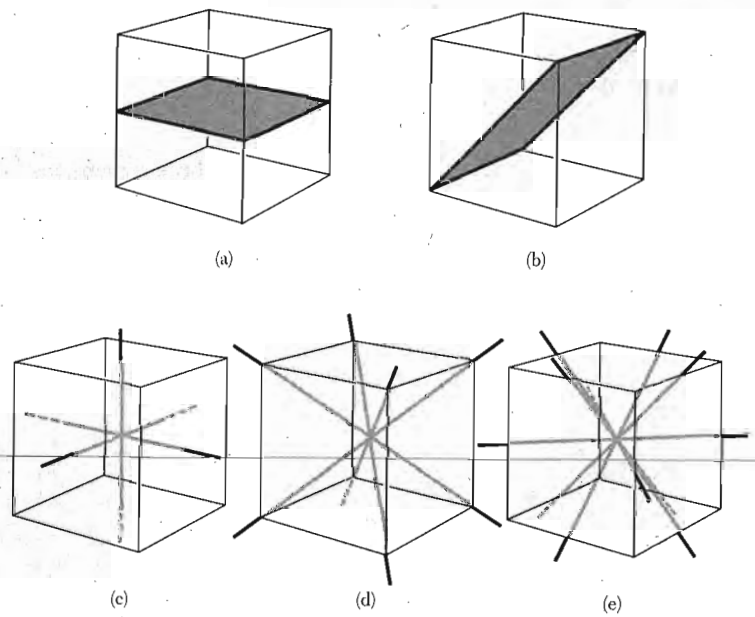

Figure 8 (a) A plane of symmetry parallel to the faces of a cube. (b) A diagonal plane of symmetry in a cube. (c) The three tetrad axes of a cube. (d) The four triad axes of a cube. (e) The six diad axes of a cube.

But special lattices of the oblique type can be invariant under rotation of $2\pi/3$, $2\pi/4$, or $2\pi/6$, or under mirror reflection. We must impose restrictive conditions on $\mathbf{a}_1$ and $\mathbf{a}_2$ if we want to construct a lattice that will be invariant under one or more of these new operations. There are four distinct types of restriction, and each leads to what we may call a **special lattice type**. Thus there are five distinct lattice types in two dimensions, the oblique lattice and the four special lattices shown in Fig. 9. **Bravais lattice** is the common phrase for a distinct lattice type; we say that there are five Bravais lattices or nets in two dimensions.

Three-Dimensional Lattice Types

The point symmetry groups in three dimensions require the 14 different lattice types listed in Table 1. The general lattice is triclinic, and there are 13 special lattices. These are grouped for convenience into systems classified according to seven types of cells, which are triclinic, monoclinic, orthorhombic, tetragonal, cubic, trigonal, and hexagonal. The division into systems is expressed in the table in terms of the axial relations that describe the cells.

The cells in Fig. 10 are conventional cells; of these only the sc is a primitive cell. Often a nonprimitive cell has a more obvious relation with the point symmetry operations than has a primitive cell.

Table 1 The 14 lattice types in three dimensions

System	Number of lattices	Restrictions on conventional cell axes and angles
Triclinic	1	$a_1 \neq a_2 \neq a_3$ $\alpha \neq \beta \neq \gamma$
Monoclinic	2	$a_1 \neq a_2 \neq a_3$ $\alpha = \gamma = 90° \neq \beta$
Orthorhombic	4	$a_1 \neq a_2 \neq a_3$ $\alpha = \beta = \gamma = 90°$
Tetragonal	2	$a_1 = a_2 \neq a_3$ $\alpha = \beta = \gamma = 90°$
Cubic	3	$a_1 = a_2 = a_3$ $\alpha = \beta = \gamma = 90°$
Trigonal	1	$a_1 = a_2 = a_3$ $\alpha = \beta = \gamma < 120°, \neq 90°$
Hexagonal	1	$a_1 = a_2 \neq a_3$ $\alpha = \beta = 90°$ $\gamma = 120°$

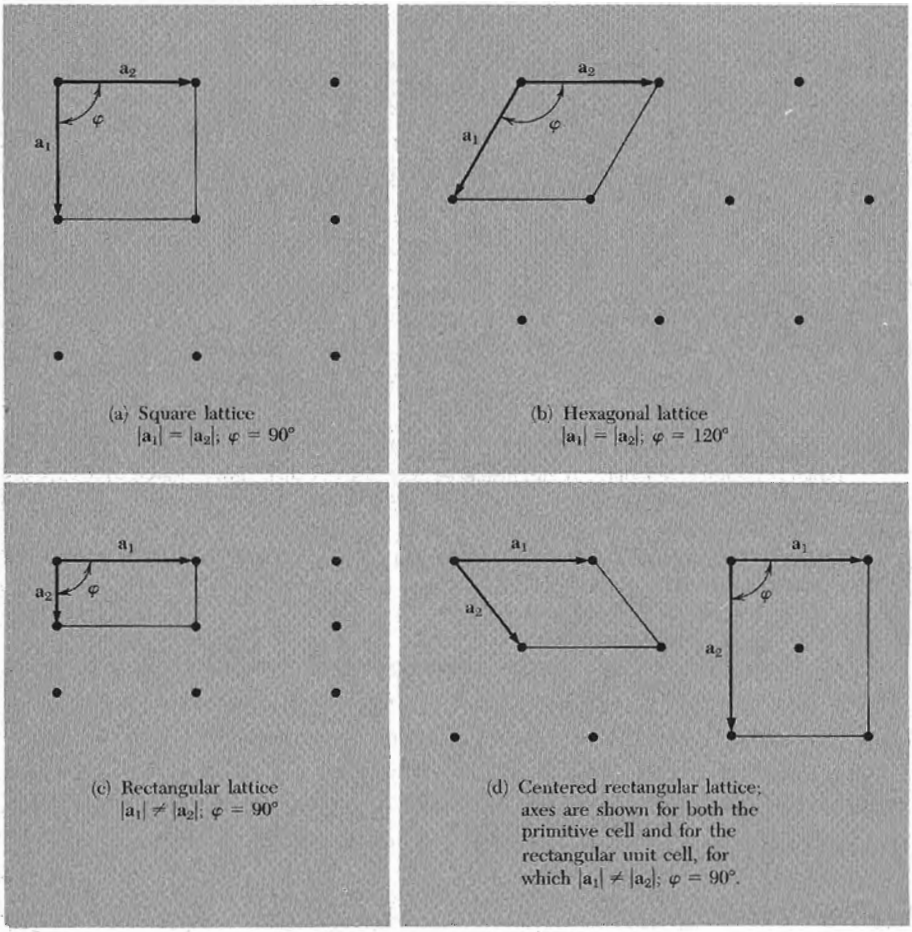

Figure 9

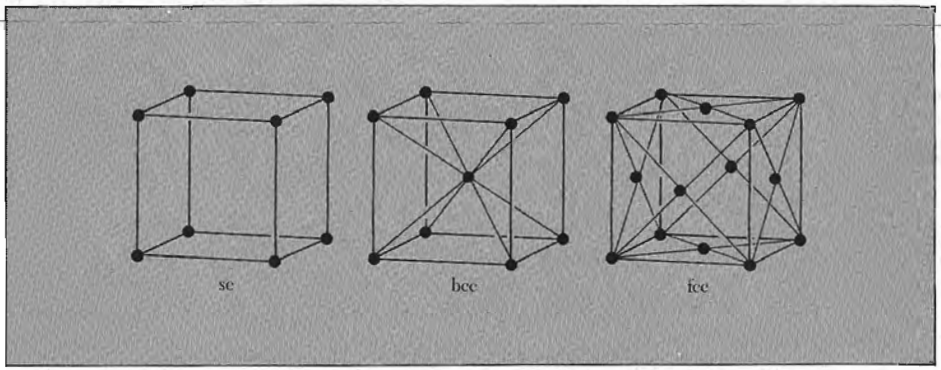

Figure 10 The cubic space lattices. The cells shown are the conventional cells.

Table 2. Characteristics of cubic lattices[a]

	Simple	Body-centered	Face-centered
Volume, conventional cell	a^3	a^3	a^3
Lattice points per cell	1	2	4
Volume, primitive cell	a^3	$\frac{1}{2}a^3$	$\frac{1}{4}a^3$
Lattice points per unit volume	$1/a^3$	$2/a^3$	$4/a^3$
Number of nearest neighbors[a]	6	8	12
Nearest-neighbor distance	a	$3^{1/2}a/2 = 0.866a$	$a/2^{1/2} = 0.707a$
Number of second neighbors	12	6	6
Second neighbor distance	$2^{1/2}a$	a	a
Packing fraction[b]	$\frac{1}{6}\pi$ $=0.524$	$\frac{1}{8}\pi\sqrt{3}$ $=0.680$	$\frac{1}{6}\pi\sqrt{2}$ $=0.740$

[a]Tables of numbers of neighbors and distances in sc, bcc, fcc, hcp, and diamond structures are given on pp. 1037–1039 of J. Hirschfelder, C. F. Curtis and R. B. Bird, *Molecular theory of gases and liquids*, Wiley, 1964.

[b]The packing fraction is the maximum proportion of the available volume that can be filled with hard spheres.

There are three lattices in the cubic system: the simple cubic (sc) lattice, the body-centered cubic (bcc) lattice, and the face-centered cubic (fcc) lattice. The characteristics of the three cubic lattices are summarized in Table 2.

A primitive cell of the bcc lattice is shown in Fig. 11, and the primitive translation vectors are shown in Fig. 12. The primitive translation vectors of the fcc lattice are shown in Fig. 13. Primitive cells by definition contain only one lattice point, but the conventional bcc cell contains two lattice points, and the fcc cell contains four lattice points.

The position of a point in a cell is specified by (4) in terms of the atomic coordinates x, y, z. Here each coordinate is a fraction of the axial length a_1, a_2, a_3 in the direction of the coordinate axis, with the origin taken at one corner of the cell. Thus the coordinates of the body center of a cell are $\frac{1}{2}\frac{1}{2}\frac{1}{2}$, and the face centers include $\frac{1}{2}\frac{1}{2}0$, $0\frac{1}{2}\frac{1}{2}$; $\frac{1}{2}0\frac{1}{2}$.

In the hexagonal system the primitive cell is a right prism based on a rhombus with an included angle of 120°. Figure 14 shows the relationship of the rhombic cell to a hexagonal prism.

INDEX SYSTEM FOR CRYSTAL PLANES

The orientation of a crystal plane is determined by three points in the plane, provided they are not collinear. If each point lay on a different crystal axis, the plane could be specified by giving the coordinates of the points in terms of the lattice constants a_1, a_2, a_3.

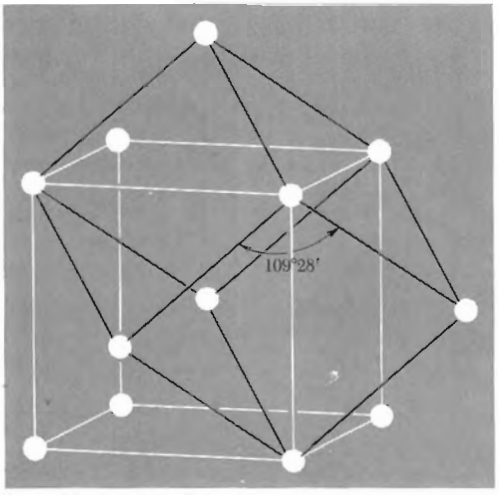

Figure 11 Body-centered cubic lattice, showing a primitive cell. The primitive cell shown is a rhombohedron of edge $\frac{1}{2}\sqrt{3}\,a$, and the angle between adjacent edges is 109°28′.

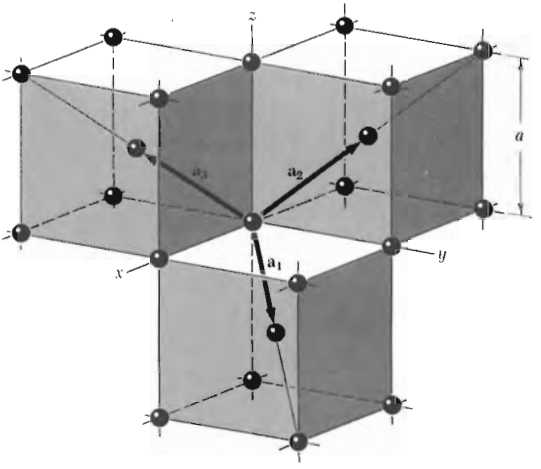

Figure 12 Primitive translation vectors of the body-centered cubic lattice; these vectors connect the lattice point at the origin to lattice points at the body centers. The primitive cell is obtained on completing the rhombohedron. In terms of the cube edge a the primitive translation vectors are

$$\mathbf{a}_1 = \tfrac{1}{2}a(\hat{\mathbf{x}} + \hat{\mathbf{y}} - \hat{\mathbf{z}}) \; ; \qquad \mathbf{a}_2 = \tfrac{1}{2}a(-\hat{\mathbf{x}} + \hat{\mathbf{y}} + \hat{\mathbf{z}}) \; ;$$

$$\mathbf{a}_3 = \tfrac{1}{2}a(\hat{\mathbf{x}} - \hat{\mathbf{y}} + \hat{\mathbf{z}}) \; .$$

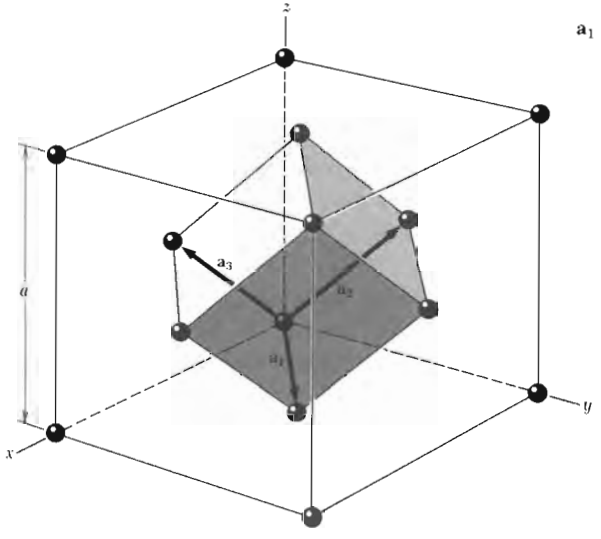

Figure 13 The rhombohedral primitive cell of the face-centered cubic crystal. The primitive translation vectors $\mathbf{a}_1$, $\mathbf{a}_2$, $\mathbf{a}_3$ connect the lattice point at the origin with lattice points at the face centers. As drawn, the primitive vectors are:

$$\mathbf{a}_1 = \tfrac{1}{2}a(\hat{\mathbf{x}} + \hat{\mathbf{y}}) \; ; \qquad \mathbf{a}_2 = \tfrac{1}{2}a(\hat{\mathbf{y}} + \hat{\mathbf{z}}) \; ; \qquad \mathbf{a}_3 = \tfrac{1}{2}a(\hat{\mathbf{z}} + \hat{\mathbf{x}}) \; .$$

The angles between the axes are 60°. Here $\hat{\mathbf{x}}$, $\hat{\mathbf{y}}$, $\hat{\mathbf{z}}$ are the Cartesian unit vectors.

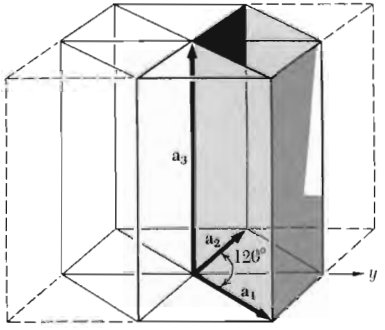

Figure 14 Relation of the primitive cell in the hexagonal system (heavy lines) to a prism of hexagonal symmetry. Here $a_1 = a_2 \neq a_3$.

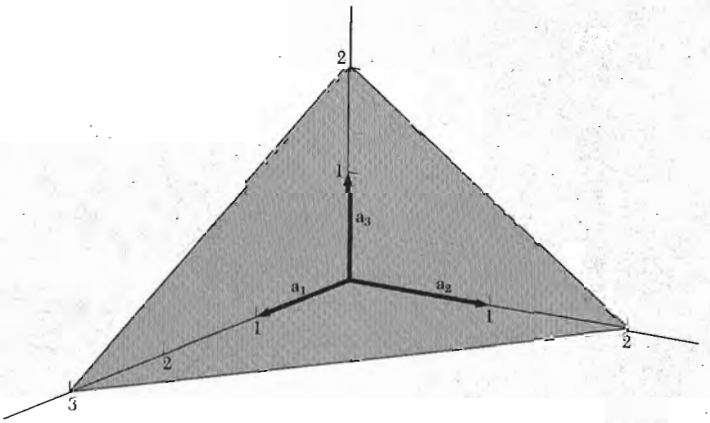

Figure 15 This plane intercepts the $\mathbf{a}_1$, $\mathbf{a}_2$, $\mathbf{a}_3$ axes at $3\mathbf{a}_1$, $2\mathbf{a}_2$, $2\mathbf{a}_3$. The reciprocals of these numbers are $\frac{1}{3}$, $\frac{1}{2}$, $\frac{1}{2}$. The smallest three integers having the same ratio are 2, 3, 3, and thus the indices of the plane are (233).

However, it turns out to be more useful for structure analysis to specify the orientation of a plane by the indices determined by the following rules (Fig. 15).

- Find the intercepts on the axes in terms of the lattice constants a_1, a_2, a_3. The axes may be those of a primitive or nonprimitive cell.
- Take the reciprocals of these numbers and then reduce to three integers having the same ratio, usually the smallest three integers. The result, enclosed in parentheses (hkl), is called the index of the plane.

For the plane whose intercepts are 4, 1, 2, the reciprocals are $\frac{1}{4}$, 1, and $\frac{1}{2}$; the smallest three integers having the same ratio are (142). For an intercept at infinity, the corresponding index is zero. The indices of some important planes in a cubic crystal are illustrated by Fig. 16.

The indices (hkl) may denote a single plane or a set of parallel planes. If a plane cuts an axis on the negative side of the origin, the corresponding index is negative, indicated by placing a minus sign above the index: ($h\bar{k}l$). The cube faces of a cubic crystal are (100), (010), (001), ($\bar{1}00$), ($0\bar{1}0$), and ($00\bar{1}$). Planes equivalent by symmetry may be denoted by curly brackets (braces) around indices; the set of cube faces is {100}. When we speak of the (200) plane we mean a plane parallel to (100) but cutting the $\mathbf{a}_1$ axis at $\frac{1}{2}a$.

The indices [uvw] of a direction in a crystal are the set of the smallest integers that have the ratio of the components of a vector in the desired direction, referred to the axes. The $\mathbf{a}_1$ axis is the [100] direction; the $-\mathbf{a}_2$ axis is the

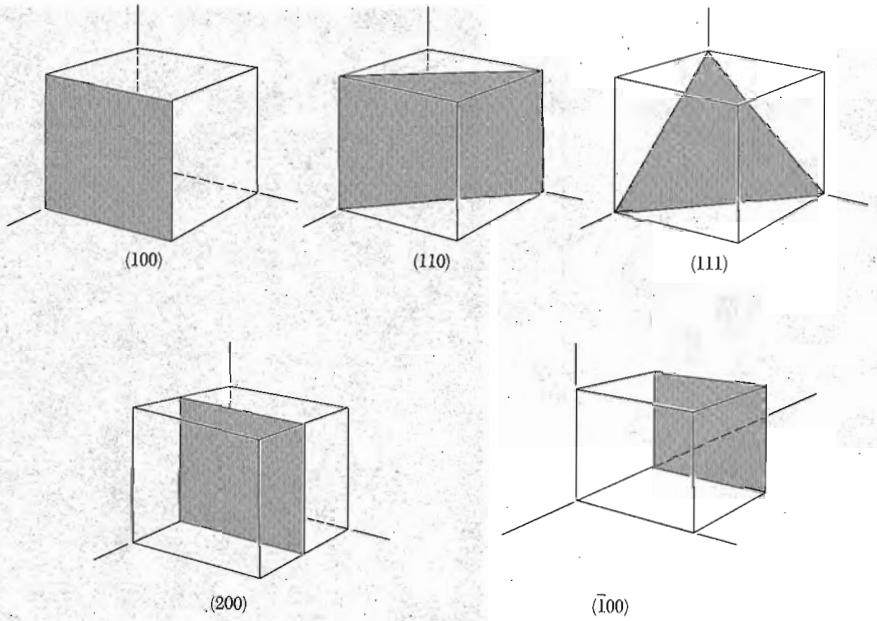

Figure 16 Indices of important planes in a cubic crystal. The plane (200) is parallel to (100) and to ($\bar{1}$00).

[0$\bar{1}$0] direction. In cubic crystals the direction [*hkl*] is perpendicular to a plane (*hkl*) having the same indices, but this is not generally true in other crystal systems.

SIMPLE CRYSTAL STRUCTURES

We discuss simple crystal structures of general interest: the sodium chloride, cesium chloride, hexagonal close-packed, diamond, and cubic zinc sulfide structures.

Sodium Chloride Structure

The sodium chloride, NaCl, structure is shown in Figs. 17 and 18. The lattice is face-centered cubic; the basis consists of one Na atom and one Cl atom separated by one-half the body diagonal of a unit cube. There are four units of NaCl in each unit cube, with atoms in the positions

Cl:	000 ;	$\frac{1}{2}\frac{1}{2}0$;	$\frac{1}{2}0\frac{1}{2}$;	$0\frac{1}{2}\frac{1}{2}$.
Na:	$\frac{1}{2}\frac{1}{2}\frac{1}{2}$;	$00\frac{1}{2}$;	$0\frac{1}{2}0$;	$\frac{1}{2}00$.

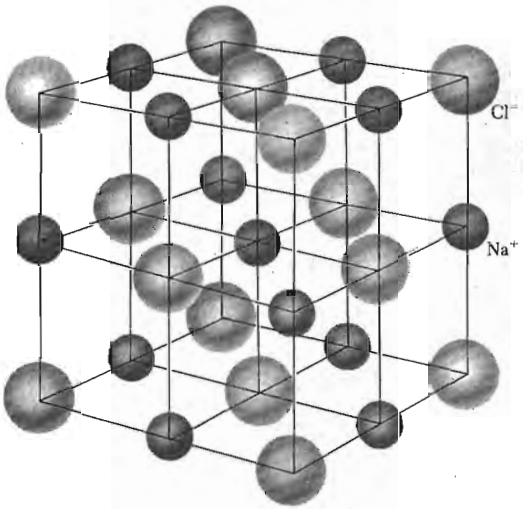

Figure 17 We may construct the sodium chloride crystal structure by arranging Na^+ and Cl^- ions alternately at the lattice points of a simple cubic lattice. In the crystal each ion is surrounded by six nearest neighbors of the opposite charge. The space lattice is fcc, and the basis has one Cl^- ion at 000 and one Na^+ ion at $\frac{111}{222}$. The figure shows one conventional cubic cell. The ionic diameters here are reduced in relation to the cell in order to clarify the spatial arrangement.

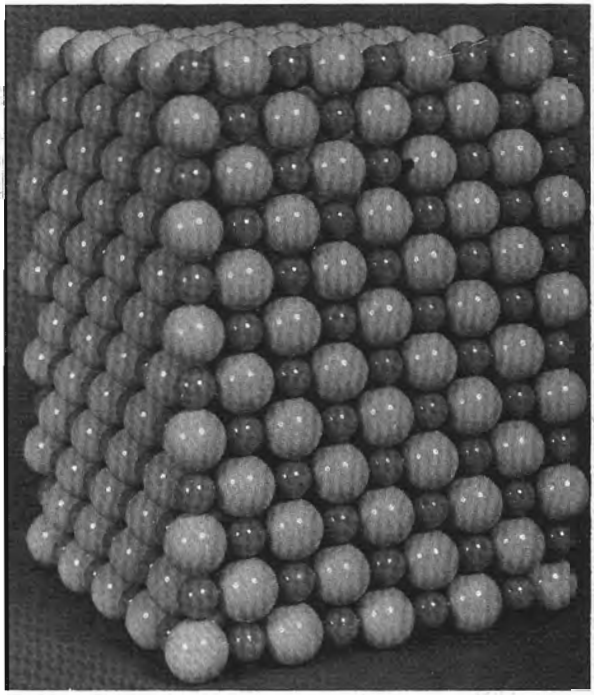

Figure 18 Model of sodium chloride. The sodium ions are smaller than the chlorine ions. (Courtesy of A. N. Holden and P. Singer.)

Figure 19 Natural crystals of lead sulfide, PbS, which has the NaCl crystal structure. (Photograph by B. Burleson.)

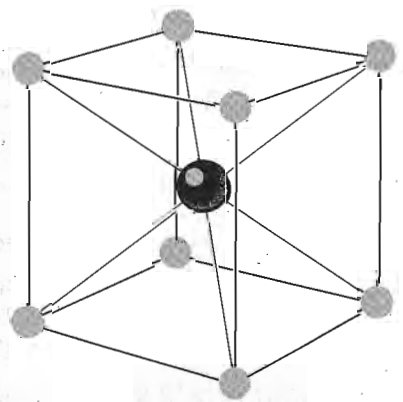

Figure 20 The cesium chloride crystal structure. The space lattice is simple cubic, and the basis has one Cs^+ ion at 000 and one Cl^- ion at $\frac{111}{222}$.

Each atom has as nearest neighbors six atoms of the opposite kind. Representative crystals having the NaCl arrangement include those in the following table. The cube edge a is given in angstroms; 1 Å $\equiv 10^{-8}$ cm $\equiv 10^{-10}$ m $\equiv 0.1$ nm.

Crystal	a	Crystal	a
LiH	4.08 Å	AgBr	5.77 Å
MgO	4.20	PbS	5.92
MnO	4.43	KCl	6.29
NaCl	5.63	KBr	6.59

Figure 19 is a photograph of crystals of lead sulfide (PbS) from Joplin, Missouri. The Joplin specimens form in beautiful cubes.

Cesium Chloride Structure

The cesium chloride structure is shown in Fig. 20. There is one molecule per primitive cell, with atoms at the corners 000 and body-centered positions $\frac{1}{2}\frac{1}{2}\frac{1}{2}$ of the simple cubic space lattice. Each atom may be viewed as at the center of a cube of atoms of the opposite kind, so that the number of nearest neighbors or coordination number is eight.

Crystal	a	Crystal	a
BeCu	2.70 Å	LiHg	3.29 Å
AlNi	2.88	NH_4Cl	3.87
CuZn (β-brass)	2.94	TlBr	3.97
CuPd	2.99	CsCl	4.11
AgMg	3.28	TlI	4.20

Hexagonal Close-packed Structure (hcp)

There are an infinite number of ways of arranging identical spheres in a regular array that maximizes the packing fraction (Fig. 21). One is the face-centered cubic structure; another is the hexagonal close-packed structure (Fig. 22). The fraction of the total volume occupied by the spheres is 0.74 for both structures. No structure, regular or not, has denser packing.

Spheres are arranged in a single closest-packed layer A by placing each sphere in contact with six others. This layer may serve as either the basal plane of an hcp structure or the (111) plane of the fcc structure. A second similar layer B may be added by placing each sphere of B in contact with three spheres of the bottom layer, as in Fig. 21. A third layer C may be added in two ways. We obtain the fcc structure if the spheres of the third layer are added over the holes in the first layer that are not occupied by B. We obtain the hcp structure when the spheres in the third layer are placed directly over the centers of the spheres in the first layer.

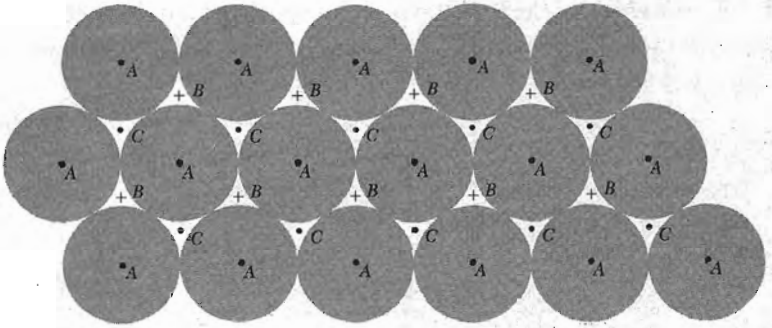

Figure 21 A close-packed layer of spheres is shown, with centers at points marked *A*. A second and identical layer of spheres can be placed on top of this, above and parallel to the plane of the drawing, with centers over the points marked *B*. There are two choices for a third layer. It can go in over *A* or over *C*. If it goes in over *A* the sequence is *ABABAB*. . . and the structure is hexagonal close-packed. If the third layer goes in over *C* the sequence is *ABCABCABC*. . . and the structure is face-centered cubic.

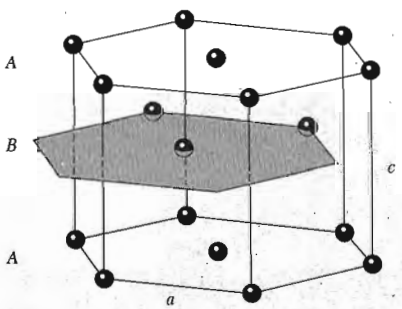

Figure 22 The hexagonal close-packed structure. The atom positions in this structure do not constitute a space lattice. The space lattice is simple hexagonal with a basis of two identical atoms associated with each lattice point. The lattice parameters a and c are indicated, where a is in the basal plane and c is the magnitude of the axis $\mathbf{a}_3$ of Fig. 14.

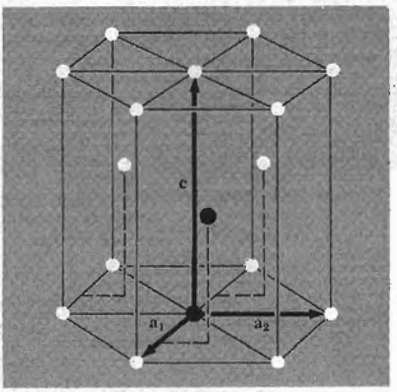

Figure 23 The primitive cell has $a_1 = a_2$, with an included angle of 120°. The c axis (or $\mathbf{a}_3$) is normal to the plane of $\mathbf{a}_1$ and $\mathbf{a}_2$. The ideal hcp structure has $c = 1.633\ a$. The two atoms of one basis are shown as solid circles. One atom of the basis is at the origin; the other atom is at $\frac{2}{3}\frac{1}{3}\frac{1}{2}$, which means at the position $\mathbf{r} = \frac{2}{3}\mathbf{a}_1 + \frac{1}{3}\mathbf{a}_2 + \frac{1}{2}\mathbf{a}_3$.

The hcp structure has the primitive cell of the hexagonal lattice, but with a basis of two atoms (Fig. 23). The fcc primitive cell has a basis of one atom (Fig. 13).

The ratio c/a (or a_3/a_1) for hexagonal closest-packing of spheres has the value $(\frac{8}{3})^{1/2} = 1.633$, as in Problem 3. It is usual to refer to crystals as hcp even if the actual c/a ratio departs somewhat from this theoretical value.

The number of nearest-neighbor atoms is 12 for both hcp and fcc structures. If the binding energy (or free energy) depended only on the number of

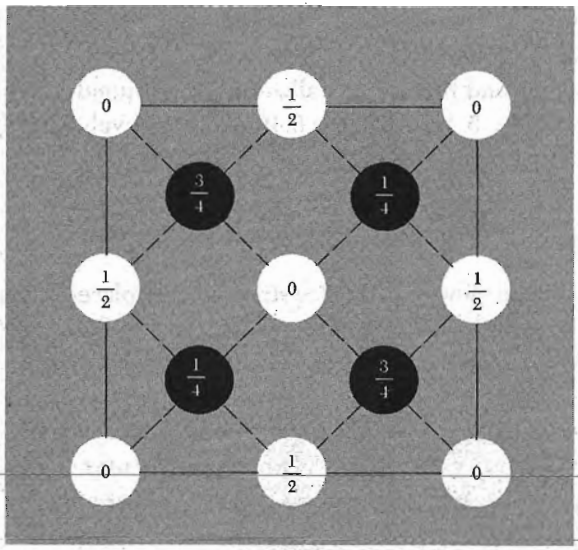

Figure 24 Atomic positions in the cubic cell of the diamond structure projected on a cube face; fractions denote height above the base in units of a cube edge. The points at 0 and $\frac{1}{2}$ are on the fcc lattice; those at $\frac{1}{4}$ and $\frac{3}{4}$ are on a similar lattice displaced along the body diagonal by one-fourth of its length. With a fcc space lattice, the basis consists of two identical atoms at 000; $\frac{1}{4}\frac{1}{4}\frac{1}{4}$.

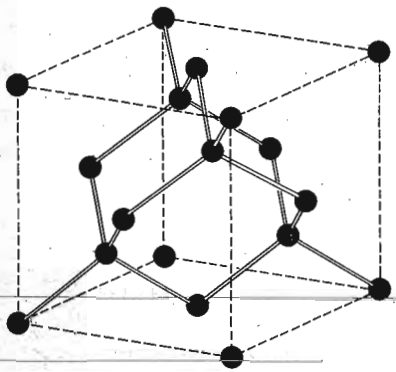

Figure 25 Crystal structure of diamond, showing the tetrahedral bond arrangement.

nearest-neighbor bonds per atom, there would be no difference in energy between the fcc and hcp structures.

Crystal	c/a	Crystal	c/a	Crystal	c/a
He	1.633	Zn	1.861	Zr	1.594
Be	1.581	Cd	1.886	Gd	1.592
Mg	1.623	Co	1.622	Lu	1.586
Ti	1.586	Y	1.570		

Diamond Structure

The space lattice of diamond is fcc. The primitive basis has two identical atoms at 000; $\frac{1}{4}\frac{1}{4}\frac{1}{4}$ associated with each point of the fcc lattice, as in Fig. 24. Thus the conventional unit cube contains eight atoms. There is no way to choose the primitive cell such that the basis of diamond contains only one atom.

The tetrahedral bonding characteristic of the diamond structure is shown in Fig. 25. Each atom has 4 nearest neighbors and 12 next nearest neighbors. The diamond structure is relatively empty: the maximum proportion of the available volume which may be filled by hard spheres is only 0.34, which is 46 percent of the filling factor for a closest-packed structure such as fcc or hcp. The

diamond structure is an example of the directional covalent bonding found in column IV of the periodic table of elements.

Carbon, silicon, germanium, and tin can crystallize in the diamond structure, with lattice constants $a = 3.56$, 5.43, 5.65, and 6.46 Å, respectively. Here a is the edge of the conventional cubic cell.

Cubic Zinc Sulfide Structure

The diamond structure may be viewed as two fcc structures displaced from each other by one-quarter of a body diagonal. The cubic zinc sulfide (zinc blende) structure results when Zn atoms are placed on one fcc lattice and S atoms on the other fcc lattice, as in Fig. 26. The conventional cell is a cube. The coordinates of the Zn atoms are 000; $0\frac{1}{2}\frac{1}{2}$; $\frac{1}{2}0\frac{1}{2}$; $\frac{1}{2}\frac{1}{2}0$; the coordinates of the S atoms are $\frac{1}{4}\frac{1}{4}\frac{1}{4}$; $\frac{1}{4}\frac{3}{4}\frac{3}{4}$; $\frac{3}{4}\frac{1}{4}\frac{3}{4}$; $\frac{3}{4}\frac{3}{4}\frac{1}{4}$. The lattice is fcc. There are four molecules of ZnS per conventional cell. About each atom there are four equally distant atoms of the opposite kind arranged at the corners of a regular tetrahedron.

The diamond structure allows a center-of-inversion symmetry operation at the midpoint of every line between nearest-neighbor atoms. The inversion operation carries an atom at $\mathbf{r}$ into an atom at $-\mathbf{r}$. The cubic ZnS structure does not have inversion symmetry. Examples of the cubic zinc sulfide structure are

Crystal	a	Crystal	a
CuF	4.26 Å	ZnSe	5.65 Å
SiC	4.35	GaAs	5.65
CuCl	5.41	AlAs	5.66
ZnS	5.41	CdS	5.82
AlP	5.45	InSb	6.46
GaP	5.45	AgI	6.47

The close equality of several pairs, notably (Al,Ga)P and (Al,Ga)As, makes possible the construction of semiconductor heterojunctions (Chapter 19).

DIRECT IMAGING OF ATOMIC STRUCTURE

Direct images of crystal structure have been produced by transmission electron microscopy. Perhaps the most beautiful images are produced by scanning tunneling microscopy; in STM (Chapter 19) one exploits the large variations in quantum tunneling as a function of the height of a fine metal tip above the surface of a crystal. The image of Figure 27 was produced in this way; see also Figures 12.19 and 19.21. An STM method has been developed that will assemble single atoms into an organized layer nanometer structure on a crystal substrate: see the electron corral in Figure 19.21.

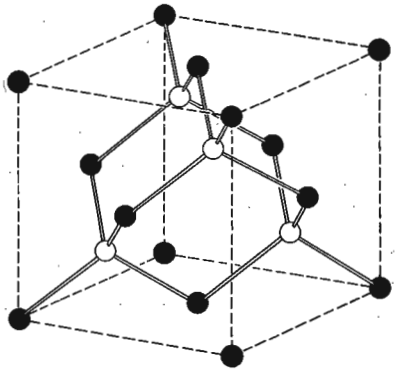

Figure 26 Crystal structure of cubic zinc sulfide.

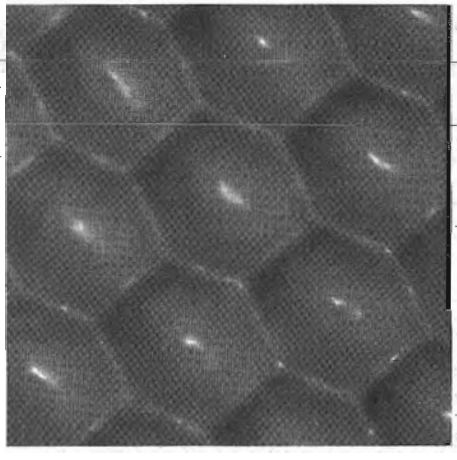

Figure 27 A scanning tunneling microscope image of atoms on a (111) surface of platinum at 4 K. The nearest neighbor spacing is 2.78 Å. (Photo courtesy of D. M. Eigler, IBM Research Division.)

NONIDEAL CRYSTAL STRUCTURES

The ideal crystal of classical crystallographers is formed by the periodic repetition of identical units in space. But no general proof has been given that the ideal crystal is the state of minimum energy of identical atoms at absolute zero. At finite temperatures this is not likely to be true—see the discussion of lattice defects in Chapter 18. Further, it is not always possible for a structure to attain the equilibrium state in a reasonable time—see the discussion of glasses in Chapter 17. Many structures that occur in nature are not entirely periodic; see the quasicrystals treated at the end of Chapter 2. We give some examples here that supplement those in the chapters just cited.

Random Stacking and Polytypism

The fcc and hcp structures are made up of close-packed planes of atoms. The structures differ in the stacking sequence of the planes, fcc having the sequence *ABCABC* . . . and hcp having the sequence *ABABAB* . . . . Structures are known in which the stacking sequence of close-packed planes is random. This is known as **random stacking** and may be thought of as crystalline in two dimensions and noncrystalline or glasslike in the third.

Polytypism is characterized by a stacking sequence with a long repeat unit along the stacking axis. The best known example is zinc sulfide, ZnS, in which more than 150 polytypes have been identified, with the longest periodicity being 360 layers. Another example is silicon carbide, SiC, which occurs with more than 45 stacking sequences of the close-packed layers. The polytype of SiC known as 393R has a primitive cell with $a = 3.079$ Å and $c = 989.6$ Å. The longest primitive cell observed for SiC has a repeat distance of 594 layers. A given sequence is repeated many times within a single crystal. The mechanism that induces such long-range crystallographic order is not a long-range force as such, but is associated with the presence of spiral steps due to dislocations in the growth nucleus (Chapter 20).

CRYSTAL STRUCTURE DATA

In Table 3 we list the more common crystal structures and lattice structures of the elements. Values of the atomic concentration and the density are given in Table 4.

Many elements occur in several crystal structures and transform from one to the other as the temperature or pressure is varied. Sometimes two structures coexist at the same temperature and pressure, although one may be slightly more stable.

The reader who wishes to look up the crystal structure of a substance may consult the excellent compilation by Wyckoff listed in the references at the end of the chapter. *Structure Reports* and the journals Acta Crystallographica and Zeitschrift für Kristallographie are valuable aids.

Table 3 Crystal structures of the elements

The data given are at room temperature for the most common form, or at the stated temperature in deg K. For further descriptions of the elements see Wyckoff, Vol. 1, Chap. 2. Structures labeled complex are described there.

H^1 4K																	He^4 2K
hcp																	hcp
3.75																	3.57
6.12																	5.83
Li 78K	Be											B	C	N 20K	O	F	Ne 4K
bcc	hcp											rhomb.	diamond	cubic	complex		fcc
3.491	2.27												3.567	5.66	(O_2)		4.46
	3.59													(N_2)			
Na 5K	Mg											Al	Si	P	S	Cl	Ar 4K
bcc	hcp	← Crystal structure →										fcc	diamond	complex	complex	complex	fcc
4.225	3.21	← a lattice parameter, in Å →										4.05	5.430			(Cl_2)	5.31
	5.21	← c lattice parameter, in Å →															
K 5K	Ca	Sc	Ti	V	Cr	Mn	Fe	Co	Ni	Cu	Zn	Ga	Ge	As	Se	Br	Kr 4K
bcc	fcc	hcp	hcp	bcc	bcc	cubic	bcc	hcp	fcc	fcc	hcp	complex	diamond	rhomb.	hex.	complex	fcc
5.225	5.58	3.31	2.95	3.03	2.88	complex	2.87	2.51	3.52	3.61	2.66		5.658		chains	(Br_2)	5.64
		5.27	4.68					4.07			4.95						
Rb 5K	Sr	Y	Zr	Nb	Mo	Tc	Ru	Rh	Pd	Ag	Cd	In	Sn (α)	Sb	Te	I	Xe 4K
bcc	fcc	hcp	hcp	bcc	bcc	hcp	hcp	fcc	fcc	fcc	hcp	tetr.	diamond	rhomb.	hex.	complex	fcc
5.585	6.08	3.65	3.23	3.30	3.15	2.74	2.71	3.80	3.89	4.09	2.98	3.25	6.49		chains	(I_2)	6.13
		5.73	5.15			4.40	4.28				5.62	4.95					
Cs 5K	Ba	La	Hf	Ta	W	Re	Os	Ir	Pt	Au	Hg	Tl	Pb	Bi	Po	At	Rn
bcc	bcc	hex.	hcp	bcc	bcc	hcp	hcp	fcc	fcc	fcc	rhomb.	hcp	fcc	rhomb.	sc		
6.045	5.02	3.77	3.19	3.30	3.16	2.76	2.74	3.84	3.92	4.08		3.46	4.95		3.34	—	—
		ABAC	5.05			4.46	4.32					5.52					
Fr	Ra	Ac															
		fcc															
—	—	5.31															

Ce	Pr	Nd	Pm	Sm	Eu	Gd	Tb	Dy	Ho	Er	Tm	Yb	Lu	
fcc	hex.	hex.		complex	bcc	hcp	hcp	hcp	hcp	hcp	hcp	fcc	hcp	
5.16	3.67	3.66	—		4.58	3.63	3.60	3.59	3.58	3.56	3.54	5.48	3.50	
	ABAC					5.78	5.70	5.65	5.62	5.59	5.56		5.55	
Th	Pa	U	Np	Pu	Am	Cm	Bk	Cf	Es	Fm	Md	No	Lr	
fcc	tetr.	complex	complex	complex	hex.									
5.08	3.92				3.64	—	—	—	—	—	—	—	—	
	3.24				ABAC									

Table 4 Density and atomic concentration

The data are given at atmospheric pressure and room temperature, or at the stated temperature in deg K. (Crystal modifications as for Table 3.)

H 4K																	**He** 2K
0.088																	0.205 (at 37 atm)
Li 78K	**Be**											**B**	**C**	**N** 20K	**O**	**F**	**Ne** 4K
0.542	1.82											2.47	3.516	1.03			1.51
4.700	12.1											13.0	17.6				4.36
3.023	2.22												1.54			1.44	3.16
Na 5K	**Mg**											**Al**	**Si**	**P**	**S**	**Cl** 93K	**Ar** 4K
1.013	1.74	← Density in g cm^{-3} (10^3kg m^{-3}) →										2.70	2.33			2.03	1.77
2.652	4.30	← Concentration in 10^{22} cm^{-3} (10^{28} m^{-3}) →										6.02	5.00				2.66
3.659	3.20	← Nearest-neighbor distance, in Å (10^{-10}m) →										2.86	2.35			2.02	3.76
K 5K	**Ca**	**Sc**	**Ti**	**V**	**Cr**	**Mn**	**Fe**	**Co**	**Ni**	**Cu**	**Zn**	**Ga**	**Ge**	**As**	**Se**	**Br** 123K	**Kr** 4K
0.910	1.53	2.99	4.51	6.09	7.19	7.47	7.87	8.9	8.91	8.93	7.13	5.91	5.32	5.77	4.81	4.05	3.09
1.402	2.30	4.27	5.66	7.22	8.33	8.18	8.50	8.97	9.14	8.45	6.55	5.10	4.42	4.65	3.67	2.36	2.17
4.525	3.95	3.25	2.89	2.62	2.50	2.24	2.48	2.50	2.49	2.56	2.66	2.44	2.45	3.16	2.32		4.00
Rb 5K	**Sr**	**Y**	**Zr**	**Nb**	**Mo**	**Tc**	**Ru**	**Rh**	**Pd**	**Ag**	**Cd**	**In**	**Sn**	**Sb**	**Te**	**I**	**Xe** 4K
1.629	2.58	4.48	6.51	8.58	10.22	11.50	12.36	12.42	12.00	10.50	8.65	7.29	5.76	6.69	6.25	4.95	3.78
1.148	1.78	3.02	4.29	5.56	6.42	7.04	7.36	7.26	6.80	5.85	4.64	3.83	2.91	3.31	2.94	2.36	1.64
4.837	4.30	3.55	3.17	2.86	2.72	2.71	2.65	2.69	2.75	2.89	2.98	3.25	2.81	2.91	2.86	3.54	4.34
Cs 5K	**Ba**	**La**	**Hf**	**Ta**	**W**	**Re**	**Os**	**Ir**	**Pt**	**Au**	**Hg** 227	**Tl**	**Pb**	**Bi**	**Po**	**At**	**Rn**
1.997	3.59	6.17	13.20	16.66	19.25	21.03	22.58	22.55	21.47	19.28	14.26	11.87	11.34	9.80	9.31		
0.905	1.60	2.70	4.52	5.55	6.30	6.80	7.14	7.06	6.62	5.90	4.26	3.50	3.30	2.82	2.67	—	—
5.235	4.35	3.73	3.13	2.86	2.74	2.74	2.68	2.71	2.77	2.88	3.01	3.46	3.50	3.07	3.34		
Fr	**Ra**	**Ac**															
		10.07															
—	—	2.66															
		3.76															

Ce	**Pr**	**Nd**	**Pm**	**Sm**	**Eu**	**Gd**	**Tb**	**Dy**	**Ho**	**Er**	**Tm**	**Yb**	**Lu**
6.77	6.78	7.00		7.54	5.25	7.89	8.27	8.53	8.80	9.04	9.32	6.97	9.84
2.91	2.92	2.93	—	3.03	2.04	3.02	3.22	3.17	3.22	3.26	3.32	3.02	3.39
3.65	3.63	3.66		3.59	3.96	3.58	3.52	3.51	3.49	3.47	3.54	3.88	3.43
Th	**Pa**	**U**	**Np**	**Pu**	**Am**	**Cm**	**Bk**	**Cf**	**Es**	**Fm**	**Md**	**No**	**Lr**
11.72	15.37	19.05	20.45	19.81	11.87								
3.04	4.01	4.80	5.20	4.26	2.96	—	—	—	—	—	—	—	—
3.60	3.21	2.75	2.62	3.1	3.61								

SUMMARY

- A lattice is an array of points related by the lattice translation operator $\mathbf{T} = u_1\mathbf{a}_1 + u_2\mathbf{a}_2 + u_3\mathbf{a}_3$, where u_1, u_2, u_3 are integers and $\mathbf{a}_1$, $\mathbf{a}_2$, $\mathbf{a}_3$ are the crystal axes.
- To form a crystal we attach to every lattice point an identical basis composed of s atoms at the positions $\mathbf{r}_j = x_j\mathbf{a}_1 + y_j\mathbf{a}_2 + z_j\mathbf{a}_3$, with $j = 1, 2, \ldots, s$. Here x, y, z may be selected to have values between 0 and 1.
- The axes $\mathbf{a}_1$, $\mathbf{a}_2$, $\mathbf{a}_3$ are primitive for the minimum cell volume $|\mathbf{a}_1 \cdot \mathbf{a}_2 \times \mathbf{a}_3|$ for which the crystal can be constructed from a lattice translation operator $\mathbf{T}$ and a basis at every lattice point.

Problems

1. ***Tetrahedral angles.*** The angles between the tetrahedral bonds of diamond are the same as the angles between the body diagonals of a cube, as in Fig. 12. Use elementary vector analysis to find the value of the angle.

2. ***Indices of planes.*** Consider the planes with indices (100) and (001); the lattice is fcc, and the indices refer to the conventional cubic cell. What are the indices of these planes when referred to the primitive axes of Fig. 13?

3. ***Hcp structure.*** Show that the c/a ratio for an ideal hexagonal close-packed structure is $(\frac{8}{3})^{1/2} = 1.633$. If c/a is significantly larger than this value, the crystal structure may be thought of as composed of planes of closely packed atoms, the planes being loosely stacked.

References

ELEMENTARY

W. B. Pearson, *Crystal chemistry and physics of metals and alloys*, Wiley, 1972.
H. D. Megaw, *Crystal structures: a working approach*, Saunders, 1973.

CRYSTALLOGRAPHY

M. J. Buerger, *Introduction to crystal geometry*, McGraw-Hill, 1971.
G. Burns and A. M. Glaser, *Space groups for solid state physicists*, Academic, 1978.
F. C. Phillips, *An introduction to crystallography*, 4th ed., Wiley, 1971. A good place to begin.
H. J. Juretscke, *Crystal physics: macroscopic physics of anisotropic solids*, Benjamin, 1974.
B. K. Vainshtein, *Modern crystallography*, Springer, 1981.
J. F. Nye, *Physical properties of crystals*, Oxford, 1985.

CRYSTAL GROWTH

W. G. Pfann, *Zone melting*, Krieger, 1978, 1966c.
A. W. Vere, *Crystal growth: principles and progress*, Plenum, 1987.
J. C. Brice, *Crystal growth processes*, Halsted, 1986.
S. H. Liu, "Fractals and their application in condensed matter physics," Solid state physics 39, 207 (1986).

Series: Journal of Crystal Growth, includes proceedings of the International Conferences on Crystal Growth.

Springer Series: Crystals—Growth, Properties, and Applications.

CLASSICAL TABLES AND HANDBOOKS

International tables for x-ray crystallography, Kynoch Press, 4 volumes, Birmingham, 1952–1974.

J. F. Nye; *Physical properties of crystals: their representation by tensors and matrices,* Oxford, 1984.

P. Villars and L. D. Calvert, *Pearson's handbook of crystallographic data for intermetallic phases,* Amer. Soc. Metals, 3 vols., 1985.

A. F. Wells, *Structural inorganic chemistry,* 5th ed., Oxford University Press, 1990, 1984c.

W. G. Wyckoff, *Crystal structures,* 2nd ed., Krieger, 1981.

2

Reciprocal Lattice

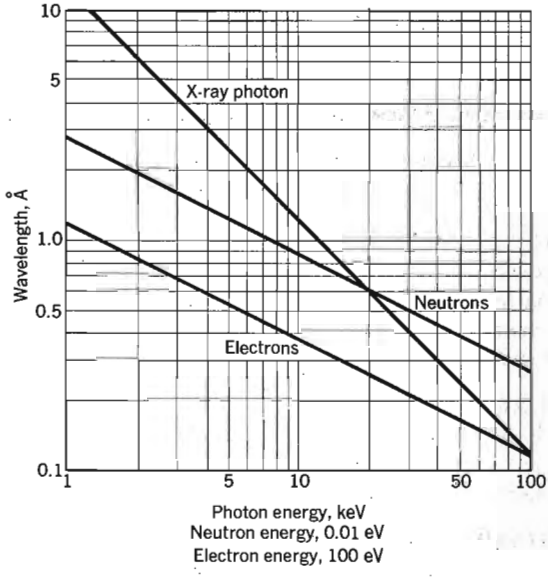

Figure 1 Wavelength versus particle energy, for photons, neutrons, and electrons.

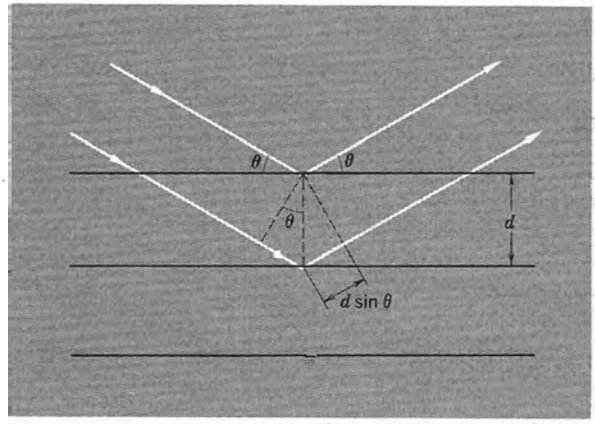

Figure 2 Derivation of the Bragg equation $2d \sin \theta = n\lambda$; here d is the spacing of parallel atomic planes and $2\pi n$ is the difference in phase between reflections from successive planes. The reflecting planes have nothing to do with the surface planes bounding the particular specimen.

DIFFRACTION OF WAVES BY CRYSTALS

Bragg Law

We study crystal structure through the diffraction of photons, neutrons, and electrons (Fig. 1). The diffraction depends on the crystal structure and on the wavelength. At optical wavelengths such as 5000 Å the superposition of the waves scattered elastically by the individual atoms of a crystal results in ordinary optical refraction. When the wavelength of the radiation is comparable with or smaller than the lattice constant, we may find diffracted beams in directions quite different from the incident direction.

W. L. Bragg presented a simple explanation of the diffracted beams from a crystal. The Bragg derivation is simple but is convincing only because it reproduces the correct result. Suppose that the incident waves are reflected specularly from parallel planes of atoms in the crystal, with each plane reflecting only a very small fraction of the radiation, like a lightly silvered mirror. In specular (mirrorlike) reflection the angle of incidence is equal to the angle of reflection. The diffracted beams are found when the reflections from parallel planes of atoms interfere constructively, as in Fig. 2. We treat elastic scattering, in which the energy of the x-ray is not changed on reflection. Inelastic scattering, with excitation of elastic waves, is discussed in Appendix A.

Consider parallel lattice planes spaced d apart. The radiation is incident in the plane of the paper. The path difference for rays reflected from adjacent planes is $2d \sin \theta$, where θ is measured from the plane. Constructive interference of the radiation from successive planes occurs when the path difference is an integral number n of wavelengths λ, so that

$$2d \sin \theta = n\lambda \tag{1}$$

This is the Bragg law. Bragg reflection can occur only for wavelength $\lambda \leq 2d$. This is why we cannot use visible light.

Although the reflection from each plane is specular, for only certain values of θ will the reflections from all parallel planes add up in phase to give a strong reflected beam. If each plane were perfectly reflecting, only the first plane of a parallel set would see the radiation, and any wavelength would be reflected. But each plane reflects 10^{-3} to 10^{-5} of the incident radiation, so that 10^3 to 10^5 planes may contribute to the formation of the Bragg-reflected beam in a perfect crystal. Reflection by a single plane of atoms is treated in Chapter 19 on surface physics.

The Bragg law is a consequence of the periodicity of the lattice. Notice that the law does not refer to the composition of the basis of atoms associated with every lattice point. We shall see, however, that the composition of the basis

determines the relative intensity of the various orders of diffraction (denoted by n above) from a given set of parallel planes. Experimental results for Bragg reflection from single crystals are shown in Figs. 3 and 4, for rotation about a fixed axis.

SCATTERED WAVE AMPLITUDE

The Bragg derivation of the diffraction condition (1) gives a neat statement of the condition for the constructive interference of waves scattered from the lattice points. We need a deeper analysis to determine the scattering intensity from the basis of atoms, which means from the spatial distribution of electrons within each cell.

From (1.3), a crystal is invariant under any translation of the form $\mathbf{T} = u_1\mathbf{a}_1 + u_2\mathbf{a}_2 + u_3\mathbf{a}_3$, where u_1, u_2, u_3 are integers and $\mathbf{a}_1$, $\mathbf{a}_2$, $\mathbf{a}_3$ are the crystal axes. Any local physical property of the crystal is invariant under $\mathbf{T}$, such as the charge concentration, electron number density, or magnetic moment density.

Fourier Analysis

What is most important to us here is that the electron number density $n(\mathbf{r})$ is a periodic function of $\mathbf{r}$, with periods $\mathbf{a}_1$, $\mathbf{a}_2$, $\mathbf{a}_3$ in the directions of the three crystal axes. Thus

$$n(\mathbf{r} + \mathbf{T}) = n(\mathbf{r}) \ . \tag{2}$$

Such periodicity creates an ideal situation for Fourier analysis. The most interesting properties of crystals are directly related to the Fourier components of the electron density.

We consider first a function $n(x)$ with period a in the direction x, in one dimension. We expand $n(x)$ in a Fourier series of sines and cosines:

$$n(x) = n_0 + \sum_{p>0} [C_p \cos(2\pi px/a) + S_p \sin(2\pi px/a)] \ , \tag{3}$$

where the p's are positive integers and C_p, S_p are real constants, called the Fourier coefficients of the expansion. The factor $2\pi/a$ in the arguments ensures that $n(x)$ has the period a:

$$\begin{aligned} n(x + a) &= n_0 + \Sigma[C_p \cos(2\pi px/a + 2\pi p) + S_p \sin(2\pi px/a + 2\pi p)] \\ &= n_0 + \Sigma[C_p \cos(2\pi px/a) + S_p \sin(2\pi px/a)] = n(x) \ . \end{aligned} \tag{4}$$

We say that $2\pi p/a$ is a point in the reciprocal lattice or Fourier space of the crystal. In one dimension these points lie on a line. The reciprocal lattice points tell us the allowed terms in the Fourier series (4) or (5). A term is allowed if it is consistent with the periodicity of the crystal, as in Fig. 5; other points in the reciprocal space are not allowed in the Fourier expansion of a periodic function.

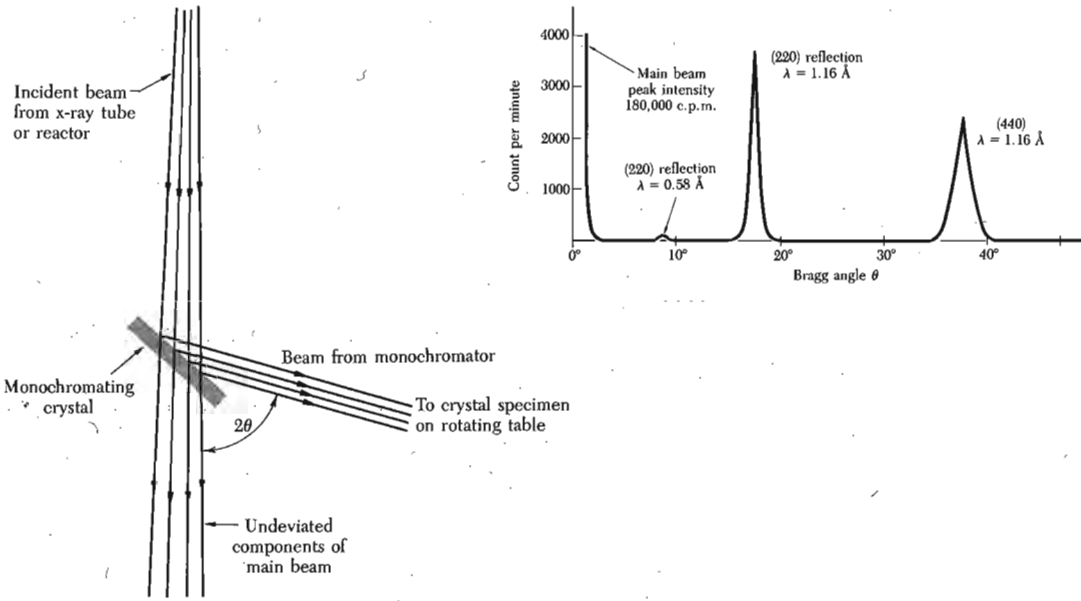

Figure 3 Sketch of a monochromator which by Bragg reflection selects a narrow spectrum of x-ray or neutron wavelengths from a broad spectrum incident beam. The upper part of the figure shows the analysis (obtained by reflection from a second crystal) of the purity of a 1.16 Å beam of neutrons from a calcium fluoride crystal monochromator. The main beam is that not reflected from the second crystal. (After G. Bacon.)

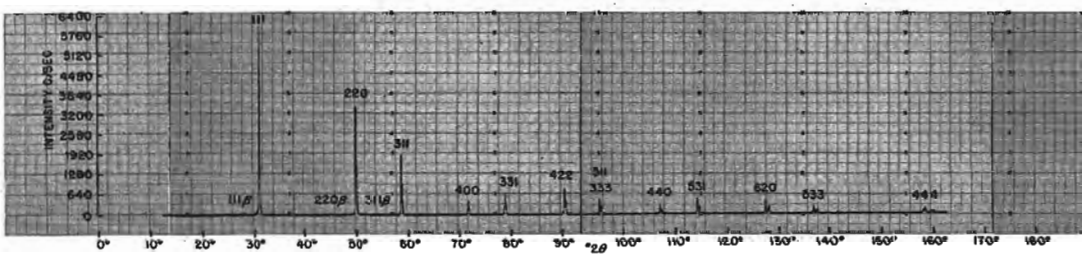

Figure 4 X-ray diffractometer recording of powdered silicon, showing a counter recording of the diffracted beams. (Courtesy of W. Parrish.)

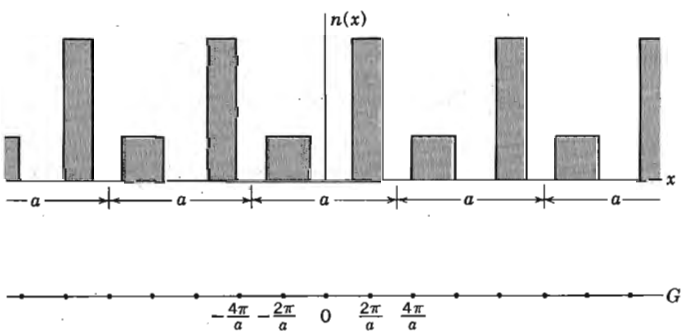

Figure 5 A periodic function $n(x)$ of period a, and the terms $2\pi p/a$ that may appear in the Fourier transform $n(x) = \Sigma\, n_p \exp(i2\pi px/a)$. The magnitudes of the individual terms n_p are not plotted.

It is a great convenience to write the series (4) in the compact form

$$n(x) = \sum_p n_p \exp(i2\pi px/a) \ , \tag{5}$$

where the sum is over all integers p: positive, negative, and zero. The coefficients n_p now are complex numbers. To ensure that $n(x)$ is a real function, we require

$$n^*_{-p} = n_p \ , \tag{6}$$

for then the sum of the terms in p and $-p$ is real. The asterisk on n^*_{-p} denotes the complex conjugate of n_{-p}.

With $\varphi = 2\pi px/a$, the sum of the terms in p and $-p$ in (5) can be shown to be real if (6) is satisfied. The sum is

$$\begin{aligned} n_p(\cos\varphi + i\sin\varphi) + n_{-p}(\cos\varphi - i\sin\varphi) \\ = (n_p + n_{-p})\cos\varphi + i(n_p - n_{-p})\sin\varphi \ , \end{aligned} \tag{7}$$

which in turn is equal to the real function

$$2\mathrm{Re}\{n_p\}\cos\varphi - 2\mathrm{Im}\{n_p\}\sin\varphi \ , \tag{8}$$

if (6) is satisfied. Here $\mathrm{Re}\{n_p\}$ and $\mathrm{Im}\{n_p\}$ denote the real and imaginary parts of n_p. Thus the number density $n(x)$ is a real function, as desired.

The extension of the Fourier analysis to periodic functions $n(\mathbf{r})$ in three dimensions is straightforward. We must find a set of vectors $\mathbf{G}$ such that

$$n(\mathbf{r}) = \sum_{\mathbf{G}} n_{\mathbf{G}} \exp(i\mathbf{G}\cdot\mathbf{r}) \tag{9}$$

is invariant under all crystal translations $\mathbf{T}$ that leave the crystal invariant. It will be shown below that the set of Fourier coefficients $n_{\mathbf{G}}$ determines the x-ray scattering amplitude.

Inversion of Fourier Series. We now show that the Fourier coefficient n_p in the series (5) is given by

$$n_p = a^{-1}\int_0^a dx\, n(x)\exp(-i2\pi px/a) \ . \tag{10}$$

Substitute (5) in (10) to obtain

$$n_p = a^{-1}\sum_{p'} n_{p'}\int_0^a dx\, \exp[i2\pi(p' - p)x/a] \ . \tag{11}$$

If $p' \neq p$ the value of the integral is

$$\frac{a}{i2\pi(p' - p)}(e^{i2\pi(p'-p)} - 1) = 0 \ ,$$

because $p' - p$ is an integer and $\exp[i2\pi(\text{integer})] = 1$. For the term $p' = p$ the integrand is $\exp(i0) = 1$, and the value of the integral is a, so that $n_p = a^{-1}n_p a = n_p$, which is an identity, so that (10) is an identity.

Similarly, the inversion of (9) gives

$$n_{\mathbf{G}} = V_c^{-1} \int_{\text{cell}} dV\, n(\mathbf{r}) \exp(-i\mathbf{G} \cdot \mathbf{r}) \ . \tag{12}$$

Here V_c is the volume of a cell of the crystal.

Reciprocal Lattice Vectors

To proceed further with the Fourier analysis of the electron concentration we must find the vectors $\mathbf{G}$ of the Fourier sum $\Sigma n_{\mathbf{G}} \exp(i\mathbf{G} \cdot \mathbf{r})$ as in (9). There is a powerful, somewhat abstract procedure for doing this. The procedure forms the theoretical basis for much of solid state physics, where Fourier analysis is the order of the day.

We construct the axis vectors $\mathbf{b}_1$, $\mathbf{b}_2$, $\mathbf{b}_3$ of the reciprocal lattice:

$$\mathbf{b}_1 = 2\pi \frac{\mathbf{a}_2 \times \mathbf{a}_3}{\mathbf{a}_1 \cdot \mathbf{a}_2 \times \mathbf{a}_3} \ ; \quad \mathbf{b}_2 = 2\pi \frac{\mathbf{a}_3 \times \mathbf{a}_1}{\mathbf{a}_1 \cdot \mathbf{a}_2 \times \mathbf{a}_3} \ ; \quad \mathbf{b}_3 = 2\pi \frac{\mathbf{a}_1 \times \mathbf{a}_2}{\mathbf{a}_1 \cdot \mathbf{a}_2 \times \mathbf{a}_3} \ . \tag{13}$$

The factors 2π are not used by crystallographers but are convenient in solid state physics.

If $\mathbf{a}_1$, $\mathbf{a}_2$, $\mathbf{a}_3$ are primitive vectors of the crystal lattice, then $\mathbf{b}_1$, $\mathbf{b}_2$, $\mathbf{b}_3$ are primitive vectors of the reciprocal lattice. Each vector defined by (13) is orthogonal to two axis vectors of the crystal lattice. Thus $\mathbf{b}_1$, $\mathbf{b}_2$, $\mathbf{b}_3$ have the property

$$\mathbf{b}_i \cdot \mathbf{a}_j = 2\pi\delta_{ij} \ , \tag{14}$$

where $\delta_{ij} = 1$ if $i = j$ and $\delta_{ij} = 0$ if $i \neq j$.

Points in the reciprocal lattice are mapped by the set of vectors

$$\mathbf{G} = v_1\mathbf{b}_1 + v_2\mathbf{b}_2 + v_3\mathbf{b}_3 \ , \tag{15}$$

where v_1, v_2, v_3 are integers. A vector $\mathbf{G}$ of this form is a **reciprocal lattice vector**.

Every crystal structure has two lattices associated with it, the crystal lattice and the reciprocal lattice. A diffraction pattern of a crystal is, as we shall show, a map of the reciprocal lattice of the crystal. A microscope image, if it could be resolved on a fine enough scale, is a map of the crystal structure in real space. The two lattices are related by the definitions (13). Thus when we rotate a crystal in a holder, we rotate both the direct lattice and the reciprocal lattice.

Vectors in the direct lattice have the dimensions of [length]; vectors in the reciprocal lattice have the dimensions of [1/length]. The reciprocal lattice is a lattice in the Fourier space associated with the crystal. The term is motivated

below. Wavevectors are always drawn in Fourier space, so that every position in Fourier space may have a meaning as a description of a wave, but there is a special significance to the points defined by the set of **G**'s associated with a crystal structure.

The vectors **G** in the Fourier series (9) are just the reciprocal lattice vectors (15), for then the Fourier series representation of the electron density has the desired invariance under any crystal translation $\mathbf{T} = u_1\mathbf{a}_1 + u_2\mathbf{a}_2 + u_3\mathbf{a}_3$ as defined by (1.3). From (9),

$$n(\mathbf{r} + \mathbf{T}) = \sum_{\mathbf{G}} n_{\mathbf{G}} \exp(i\mathbf{G} \cdot \mathbf{r}) \exp(i\mathbf{G} \cdot \mathbf{T}) \ . \tag{16}$$

But $\exp(i\mathbf{G} \cdot \mathbf{T}) = 1$, because

$$\begin{aligned} \exp(i\mathbf{G} \cdot \mathbf{T}) &= \exp[i(v_1\mathbf{b}_1 + v_2\mathbf{b}_2 + v_3\mathbf{b}_3) \cdot (u_1\mathbf{a}_1 + u_2\mathbf{a}_2 + u_3\mathbf{a}_3)] \\ &= \exp[i2\pi(v_1u_1 + v_2u_2 + v_3u_3)] \ . \end{aligned} \tag{17}$$

The argument of the exponential has the form $2\pi i$ times an integer, because $v_1u_1 + v_2u_2 + v_3u_3$ is an integer, being the sum of products of integers. Thus by (9) we have the desired invariance, $n(\mathbf{r} + \mathbf{T}) = n(\mathbf{r})$.

This result proves that the Fourier representation of a function periodic in the crystal lattice can contain components $n_{\mathbf{G}} \exp(i\mathbf{G} \cdot \mathbf{r})$ only at the reciprocal lattice vectors **G** as defined by (15).

Diffraction Conditions

Theorem. The set of reciprocal lattice vectors **G** determines the possible x-ray reflections.

We see in Fig. 6 that the difference in phase factors is $\exp[i(\mathbf{k} - \mathbf{k}') \cdot \mathbf{r}]$ between beams scattered from volume elements **r** apart. The wavevectors of the incoming and outgoing beams are **k** and **k′**. The amplitude of the wave scattered from a volume element is proportional to the local electron concentration $n(\mathbf{r})$. The total amplitude of the scattered wave in the direction of **k′** is proportional to the integral over the crystal of $n(\mathbf{r})\, dV$ times the phase factor $\exp[i(\mathbf{k} - \mathbf{k}') \cdot \mathbf{r}]$.

In other words, the amplitude of the electric or magnetic field vectors in the scattered electromagnetic wave is proportional to the following integral which defines the quantity F that we call the scattering amplitude:

$$F = \int dV\, n(\mathbf{r}) \exp[i(\mathbf{k} - \mathbf{k}') \cdot \mathbf{r}] = \int dV\, n(\mathbf{r}) \exp(-i\Delta\mathbf{k} \cdot \mathbf{r}) \ , \tag{18}$$

where

$$\mathbf{k} + \Delta\mathbf{k} = \mathbf{k}' \ . \tag{19}$$

Here $\Delta\mathbf{k}$ measures the change in wavevector and is called the scattering vector (Fig. 7). We add $\Delta\mathbf{k}$ to **k** to obtain **k′**, the wavevector of the scattered beam.

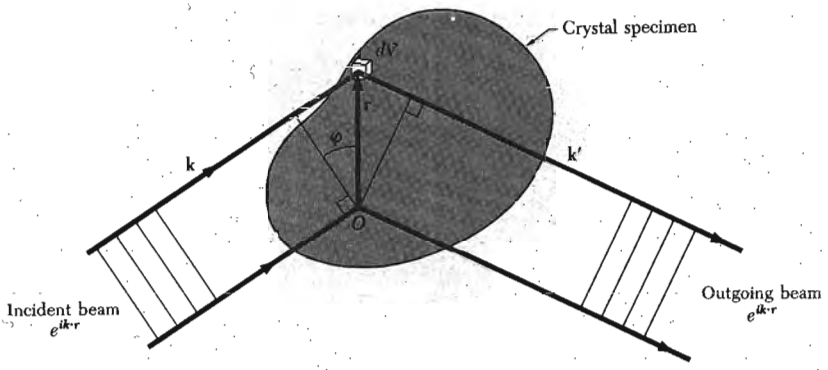

Figure 6 The difference in path length of the incident wave $\mathbf{k}$ at the points O, $\mathbf{r}$ is $r \sin \varphi$, and the difference in phase angle is $(2\pi r \sin \varphi)/\lambda$, which is equal to $\mathbf{k} \cdot \mathbf{r}$. For the diffracted wave the difference in phase angle is $-\mathbf{k}' \cdot \mathbf{r}$. The total difference in phase angle is $(\mathbf{k} - \mathbf{k}') \cdot \mathbf{r}$, and the wave scattered from dV at $\mathbf{r}$ has the phase factor $\exp[i(\mathbf{k} - \mathbf{k}') \cdot \mathbf{r}]$ relative to the wave scattered from a volume element at the origin O.

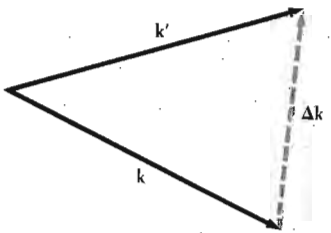

Figure 7 Definition of the scattering vector $\Delta\mathbf{k}$ such that $\mathbf{k} + \Delta\mathbf{k} = \mathbf{k}'$. In elastic scattering the magnitudes satisfy $k' = k$. Further, in Bragg scattering from a periodic lattice any allowed $\Delta\mathbf{k}$ must equal some reciprocal lattice vector $\mathbf{G}$.

We introduce into (18) the Fourier components (9) of $n(\mathbf{r})$ to obtain for the scattering amplitude

$$F = \sum_{\mathbf{G}} \int dV \, n_{\mathbf{G}} \exp[i(\mathbf{G} - \Delta\mathbf{k}) \cdot \mathbf{r}] \, . \tag{20}$$

When the scattering vector $\Delta\mathbf{k}$ is equal to a particular reciprocal lattice vector,

$$\Delta\mathbf{k} = \mathbf{G} \, , \tag{21}$$

the argument of the exponential vanishes and $F = Vn_{\mathbf{G}}$. It is a simple exercise (Problem 4) to show that F is negligibly small when $\Delta\mathbf{k}$ differs significantly from any reciprocal lattice vector.

In elastic scattering of a photon its energy $\hbar\omega$ is conserved, so that the frequency $\omega' = ck'$ of the emergent beam is equal to the frequency of the incident beam. Thus the magnitudes k and k' are equal, and $k^2 = k'^2$, a result that holds also for electron and neutron beams. From (21) we found $\Delta\mathbf{k} = \mathbf{G}$ or

$\mathbf{k} + \mathbf{G} = \mathbf{k}'$, so that the diffraction condition is written as $(\mathbf{k} + \mathbf{G})^2 = k^2$, or

$$2\mathbf{k} \cdot \mathbf{G} + G^2 = 0 \ . \tag{22}$$

This is the central result of the theory of elastic scattering of waves in a periodic lattice. If $\mathbf{G}$ is a reciprocal lattice vector, so is $-\mathbf{G}$, and with this substitution we can write (22) as

$$2\mathbf{k} \cdot \mathbf{G} = G^2 \ . \tag{23}$$

This particular expression is often used as the condition for diffraction.

Equation (23) is another statement of the Bragg condition (1). The result of Problem 1 is that the spacing $d(hkl)$ between parallel lattice planes that are normal to the direction $\mathbf{G} = h\mathbf{b}_1 + k\mathbf{b}_2 + l\mathbf{b}_3$ is $d(hkl) = 2\pi/|\mathbf{G}|$. Thus the result $2\mathbf{k} \cdot \mathbf{G} = G^2$ may be written as

$$2(2\pi/\lambda) \sin \theta = 2\pi/d(hkl) \ ,$$

or $2d(hkl) \sin \theta = \lambda$. Here θ is the angle between the incident beam and the crystal plane.

The integers hkl that define $\mathbf{G}$ are not necessarily identical with the indices of an actual crystal plane, because the hkl may contain a common factor n, whereas in the definition of the indices in Chapter 1 the common factor has been eliminated. We thus obtain the Bragg result:

$$2d \sin \theta = n\lambda \ , \tag{24}$$

where d is the spacing between adjacent parallel planes with indices h/n, k/n, l/n.

Laue Equations

The original result (21) of diffraction theory, namely that $\Delta\mathbf{k} = \mathbf{G}$, may be expressed in another way to give what are called the Laue equations. These are valuable because of their geometrical representation (see Chapter 19).

Take the scalar product of both $\Delta\mathbf{k}$ and $\mathbf{G}$ successively with $\mathbf{a}_1$, $\mathbf{a}_2$, $\mathbf{a}_3$. From (14) and (15) we get

$$\mathbf{a}_1 \cdot \Delta\mathbf{k} = 2\pi v_1 \ ; \qquad \mathbf{a}_2 \cdot \Delta\mathbf{k} = 2\pi v_2 \ ; \qquad \mathbf{a}_3 \cdot \Delta\mathbf{k} = 2\pi v_3 \ . \tag{25}$$

These equations have a simple geometrical interpretation. The first equation $\mathbf{a}_1 \cdot \Delta\mathbf{k} = 2\pi v_1$ tells us that $\Delta\mathbf{k}$ lies on a certain cone about the direction of $\mathbf{a}_1$. The second equation tells us that $\Delta\mathbf{k}$ lies on a cone about $\mathbf{a}_2$ as well, and the third equation requires that $\Delta\mathbf{k}$ lies on a cone about $\mathbf{a}_3$.

Thus, at a reflection $\Delta\mathbf{k}$ must satisfy all three equations; it must lie at the common line of intersection of three cones, which is a severe condition that can be satisfied only by systematic sweeping or searching in wavelength or crystal orientation—or else by sheer accident.

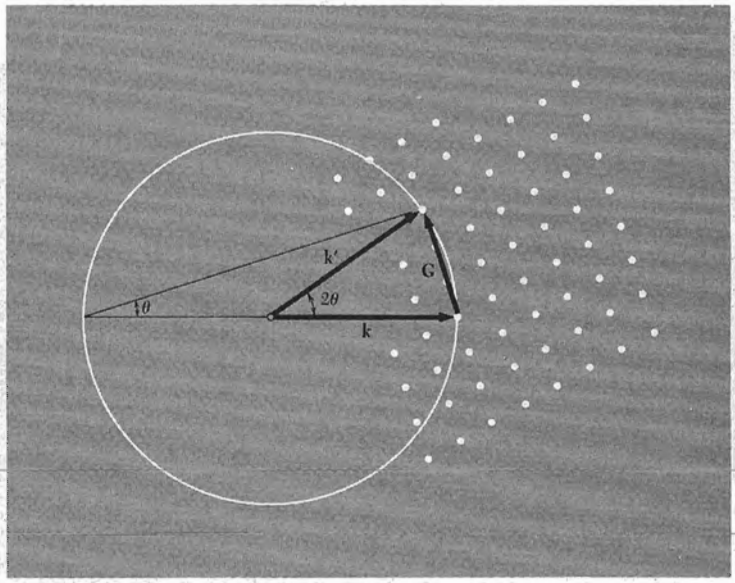

Figure 8 The points on the right-hand side are reciprocal lattice points of the crystal. The vector $\mathbf{k}$ is drawn in the direction of the incident x-ray beam, and the origin is chosen such that $\mathbf{k}$ terminates at any reciprocal lattice point. We draw a sphere of radius $k = 2\pi/\lambda$ about the origin of $\mathbf{k}$. A diffracted beam will be formed if this sphere intersects any other point in the reciprocal lattice. The sphere as drawn intercepts a point connected with the end of $\mathbf{k}$ by a reciprocal lattice vector $\mathbf{G}$. The diffracted x-ray beam is in the direction $\mathbf{k}' = \mathbf{k} + \mathbf{G}$. The angle θ is the Bragg angle of Fig. 2. This construction is due to P. P. Ewald.

A beautiful construction, the Ewald construction, is exhibited in Fig. 8. This helps us visualize the nature of the accident that must occur in order to satisfy the diffraction condition in three dimensions. The condition in two dimensions (diffraction from a surface layer) is treated in Chapter 19.

Reflection from a single plane of atoms takes place in the directions of the lines of intersection of two cones, for example the cones defined by the first two of the Laue equations (25). Now two cones will in general intercept each other provided the wavevector of the particles in the incident beam exceeds some threshold value determined by the first two Laue equations. No accidental coincidence is required, unlike the problem of diffraction in 3D. This matter is of prime importance in the diffraction of low energy electrons from the surface of a crystal.

BRILLOUIN ZONES

Brillouin gave the statement of the diffraction condition that is most widely used in solid state physics, which means in the description of electron energy band theory and of the elementary excitations of other kinds.

Elements of X-Ray Diffraction

THIRD EDITION

B. D. Cullity
Late, Formerly of the Department of Metallurgical Engineering and Materials Science, University of Notre Dame

S. R. Stock
Georgia Institute of Technology

Prentice Hall
Upper Saddle River, NJ 07458

Table of Contents

Chapter 1

Properties of X-Rays

1-1 INTRODUCTION

X-rays were discovered in 1895 by the German physicist Röntgen [1-1][1] and were so named because their nature was unknown at the time. Unlike ordinary light, these rays were invisible, but they traveled in straight lines and affected photographic film in the same way as light. On the other hand, they were much more penetrating than light and could easily pass through the human body, wood, quite thick pieces of metal, and other "opaque" objects.

It is not always necessary to understand a thing in order to use it, and x-rays were almost immediately put to use by physicians and, somewhat later, by engineers, who wished to study the internal structure of opaque objects. By placing a source of x-rays on one side of the object and photographic film on the other, a shadow picture, or *radiograph*, could be made, the less dense portions of the object allowing a greater proportion of the x-radiation to pass through than the more dense. In this way the point of fracture in a broken bone or the position of a crack in a metal casting could be located.

Radiography was thus initiated without any precise understanding of the radiation used, because it was not until 1912 that the exact nature of x-rays was established. In that year the phenomenon of x-ray *diffraction* by crystals was discovered, and this discovery simultaneously proved the wave nature of x-rays and provided a new method for investigating the fine structure of matter. Although radiography is a very important tool in itself and has a wide field of applicability, it is ordinarily limited in the internal detail it can resolve, or disclose, to sizes of the order of 10^{-3} mm. Diffraction, on the other hand, can indirectly reveal details of internal structure of the order of 10^{-7} mm in size, and it is with this phenomenon, and its applications to materials problems, that this book is concerned. The properties of x-rays and the internal structure of crystals are here described in the first two chap-

[1] Numbers in square brackets relate to the references at the end of the book which are organized in two parts: general references ("G" numbers) and specialized references collected by chapter.

ters as necessary preliminaries to the discussion of the diffraction of x-rays by crystals which follows.

1-2 ELECTROMAGNETIC RADIATION

Today it is clear that x-rays are electromagnetic radiation of exactly the same nature as light but of very much shorter wavelength. The unit of measurement in the x-ray region is the angstrom (Å), equal to 10^{-10} m, and x-rays used in diffraction have wavelengths lying approximately in the range 0.5-2.5 Å, whereas the wavelength of visible light is of the order of 6000 Å. X-rays therefore occupy the region between gamma and ultraviolet rays in the complete electromagnetic spectrum (Fig. 1-1). Other units sometimes used to measure x-ray wavelength are the X unit (XU) and the kilo X unit (kX = 1000 XU). The kX unit, whose origin will be described in Sec. 3-7, is only slightly larger than the angstrom. The approved SI unit for wavelengths in the x-ray region is the nanometer:

$$1 \text{ nanometer} = 10^{-9} \text{ m} = 10 \text{ Å}.$$

This unit has not become popular in x-ray diffraction.

It is worthwhile to review briefly some properties of electromagnetic waves. Suppose a monochromatic beam of x-rays, i.e., x-rays of a single wavelength, is traveling in the x direction (Fig. 1-2). Then it has associated with it an electric field **E** in, say, the y direction and, at right angles to this, a magnetic field **H** in the z direction. If the electric field is confined to the xy-plane as the wave travels along, the wave is said to be plane-polarized. (In a completely unpolarized wave, the electric field vector **E** and hence the magnetic field vector **H** can assume all directions in the yz-plane.)

In the plane-polarized wave considered, **E** is not constant with time but varies from a maximum in the $+y$ direction through zero to a maximum in the $-y$ direction and back again, at any particular point in space, say $x = 0$. At any instant of time, say $t = 0$, **E** varies in the same fashion with distance along the x-axis. If both variations are assumed to be sinusoidal, they may be expressed in the one equation

$$\mathbf{E} = A \sin 2\pi\left(\frac{x}{\lambda} - \nu t\right), \tag{1-1}$$

where A = amplitude of the wave, λ = wavelength, and ν = frequency. The variation of **E** is not necessarily sinusoidal, but the exact form of the wave matters little; the important feature is its periodicity. Figure 1-3 shows the variation of **E** graphically. The wavelength and frequency are connected by the relation

$$\lambda = \frac{c}{\nu}, \tag{1-2}$$

where c = velocity of light = 3.00×10^8 m/sec.

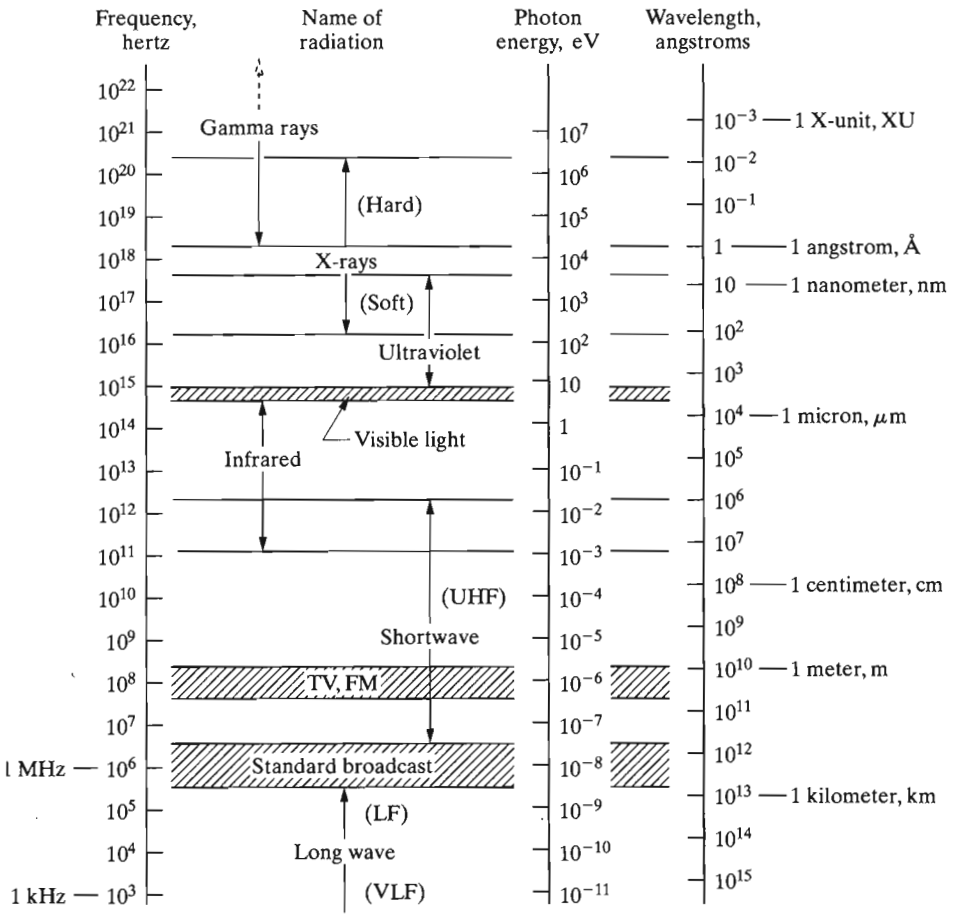

Figure 1-1 The electromagnetic spectrum. The boundaries between regions are arbitrary, since no sharp upper or lower limits can be assigned. (H. A. Enge, M. R. Wehr, J. A. Richards, *Introduction to Atomic Physics, Addison-Wesley Publishing Company, Reading*, MA, 1972.)

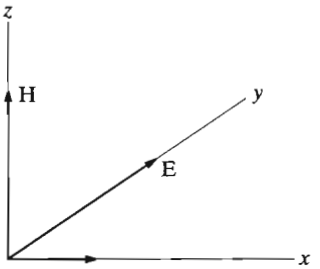

Figure 1-2 Electric and magnetic fields associated with a wave moving in the x-direction.

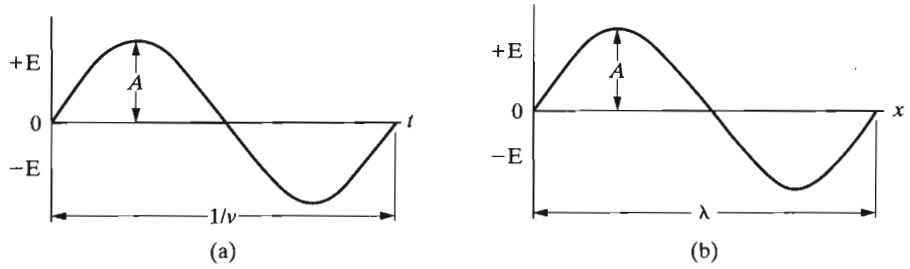

Figure 1-3 The variation of **E**, (a) with t at a fixed value of x and (b) with x at a fixed value of t.

Electromagnetic radiation, such as a beam of x-rays, carries energy, and the rate of flow of this energy through unit area perpendicular to the direction of motion of the wave is called the *intensity I*. The average value of the intensity is proportional to the square of the amplitude of the wave, i.e., proportional to A^2. In absolute units, intensity is measured in joules/m^2/sec, but this measurement is a difficult one and is seldom carried out; most x-ray intensity measurements are made by counting the number of photons incident on a detector or by measuring the degree of blackening of photographic film exposed to the x-ray beam.

An accelerated electric charge radiates energy. The acceleration may, of course, be either positive or negative, and thus a charge continuously oscillating about some mean position acts as an excellent source of electromagnetic radiation. Radio waves, for example, are produced by the oscillation of charge back and forth in the broadcasting antenna, and visible light by oscillating electrons in the atoms of the substance emitting the light. In each case, the frequency of the radiation is the same as the frequency of the oscillator which produces it.

Thus far electromagnetic radiation has been considered as *wave* motion in accordance with classical theory. According to quantum theory, however, electromagnetic radiation can also be considered as a stream of *particles* called quanta or photons. Each photon has associated with it an amount of energy $h\nu$, where h is Planck's constant (6.63×10^{-34} joule · sec). A link is thus provided between the two viewpoints, because the frequency of the wave motion can be calculated from the energy of the photon and vice versa. Radiation thus has a dual wave-particle character, and sometimes one concept, sometimes the other will be used to explain various phenomena, giving preference in general to the classical wave theory whenever it is applicable.

1-3 THE CONTINUOUS SPECTRUM

X-rays are produced when any electrically charged particle of sufficient kinetic energy rapidly decelerates. Electrons are usually used for this purpose, the radiation being produced in an *x-ray tube* which contains a source of electrons and two metal electrodes. The high voltage maintained across these electrodes, some tens of

thousands of volts, rapidly draws the electrons to the anode, or *target*, which they strike with very high velocity. X-rays are produced at the point of impact and radiate in all directions. If e is the charge on the electron (1.60×10^{-19} coulomb) and V the voltage across the electrodes, then the kinetic energy (in joules) of the electrons on impact is given by the equation

$$\text{KE} = eV = \frac{1}{2}mv^2, \tag{1-3}$$

where m is the mass of the electron (9.11×10^{-31} kg) and v its velocity in m/sec just before impact. At a tube voltage of 30,000 volts, this velocity is about one-third that of light. Most of the kinetic energy of the electrons striking the target is converted into heat, less than 1 percent being transformed into x-rays.

When the rays coming from the target are analyzed, they are found to consist of a mixture of different wavelengths, and the variation of intensity with wavelength is found to depend on the tube voltage. Figure 1-4 shows the kind of curves obtained. The intensity is zero up to a certain wavelength, called the *short-wavelength limit* (λ_{SWL}), increases rapidly to a maximum and then decreases, with no sharp limit on the long wavelength side. When the tube voltage is raised, the intensity of all wavelengths increases, and both the short-wavelength limit and the position of the maximum shift to shorter wavelengths. Consider the smooth curves in Fig. 1-4, which correspond to applied voltages of 20 kV or less in the case of a molybdenum target. The radiation represented by such curves is called *polychro-*

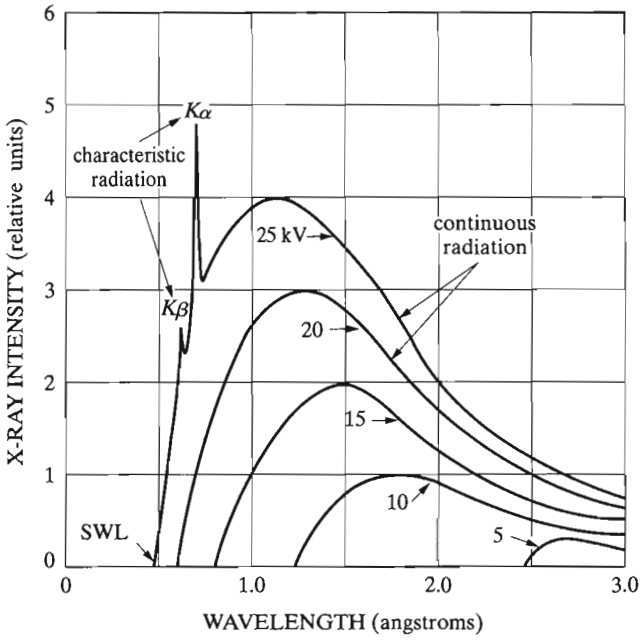

Figure 1-4 X-ray spectrum of molybdenum as a function of applied voltage (schematic). Line widths not to scale.

matic, continuous, or *white* radiation, since it is made up, like white light, of rays of many wavelengths. White radiation is also called *Bremsstrahlung*, German for "braking radiation," because it is caused by electron deceleration.

The continuous spectrum results from the rapid deceleration of the electrons hitting the target since, as mentioned above, any decelerated charge emits energy. Not every electron decelerates in the same way, however; some stop in one impact and release all their energy at once, while others a deflect this way and that by the atoms of the target, successively losing fractions of their total kinetic energy until it is all spent. Those electrons which are stopped in one impact produce photons of maximum energy, i.e., x-rays of minimum wavelength. Such electrons transfer all their energy eV into photon energy so that

$$eV = h\nu_{max}$$

$$\lambda_{SWL} = \lambda_{min} = \frac{c}{\nu_{max}} = \frac{hc}{eV}$$

$$\lambda_{SWL} = \frac{(6.626 \times 10^{-34})(2.998 \times 10^{3})}{(1.602 \times 10^{-19})V} \text{ meter},$$

$$\lambda_{SWL} = \frac{12.40 \times 10^{3}}{V}. \tag{1-4}$$

This equation gives the short-wavelength limit (in angstroms) as a function of the applied voltage V. If an electron is not completely stopped in one encounter but undergoes a glancing impact which only partially decreases its velocity, then only a fraction of its energy eV is emitted as radiation and the photon produced has energy less than $h\nu_{max}$. In terms of wave motion, the corresponding x-ray has a frequency lower than ν_{max} and a wavelength longer than λ_{SWL}. The totality of these wavelengths, ranging upward from λ_{SWL}, constitutes the continuous spectrum. The curves of Fig. 1-4 become higher and shift to the left as the applied voltage is increased, therefore, because the number of photons produced per second and the average energy per photon are both increasing. The total x-ray energy emitted per second, which is proportional to the area under one of the curves of Fig. 1-4, also depends on the atomic number Z of the target and on the tube current i, the latter being a measure of the number of electrons per second striking the target. This total x-ray intensity is given by

$$I_{\text{cont. spectrum}} = AiZV^{m}, \tag{1-5}$$

where A is a proportionality constant and m is a constant with a value of about 2 (see [1-2] for a discussion of this equation; note that a somewhat different form is quoted elsewhere e.g. [G.1]). Where large amounts of white radiation are desired, it is therefore necessary to use a heavy metal like tungsten ($Z = 74$) as a target and as

high a voltage as possible. Note that the material of the target affects the intensity but not the wavelength distribution of the continuous spectrum.

1-4 THE CHARACTERISTIC SPECTRUM

When the voltage on an x-ray tube is raised above a certain critical value, characteristic of the target metal, sharp intensity maxima appear at certain wavelengths, superimposed on the continuous spectrum. Since they are so narrow and since their wavelengths are characteristic of the target metal used, they are called *characteristic lines*. These lines fall into several sets, referred to as *K, L, M*, etc., in the order of increasing wavelength, all the lines together forming the *characteristic spectrum* of the metal used as the target. For a molybdenum target the *K* lines have wavelengths of about 0.7 Å, the *L* lines about 5 Å, and the *M* lines still longer wavelengths. Ordinarily only the *K* lines are useful in x-ray diffraction, the longer-wavelength lines being too easily absorbed. There are several lines in the *K* set, but only the three strongest are observed in normal diffraction work. These are the $K\alpha_1$, $K\alpha_2$, and $K\beta_2$, and for molybdenum their wavelengths are approximately:

$K\alpha_1$: 0.709 Å
$K\alpha_2$: 0.71
$K\beta_2$: 0.632

The α_1 and α_2 components have wavelengths so close together that they are not always resolved as separate lines; if resolved, they are called the *Kα doublet* and, if not resolved, simply the *Kα line*.[2] Similarly, $K\beta_1$ is usually referred to as the *Kβ line*, with the subscript dropped. $K\alpha_1$ is always about twice as strong as $K\alpha_2$, while the intensity ratio of $K\alpha_1$ to $K\beta_1$ depends on atomic number but averages about 5/1.

These characteristic lines may be seen in the uppermost curve of Fig. 1-4. Since the critical *K excitation voltage*, i.e., the voltage necessary to excite *K* characteristic radiation, is 20.01 kV for molybdenum, the *K* lines do not appear in the lower curves of Fig. 1-4. An increase in voltage above the critical voltage increases the intensities of the characteristic lines relative to the continuous spectrum but *does not change their wavelengths*. Figure 1-5 shows the spectrum of molybdenum at 35 kV on a compressed vertical scale relative to that of Fig. 1-4; the increased voltage has shifted the continuous spectrum to still shorter wavelengths and increased the intensities of the *K* lines relative to the continuous spectrum but has not changed their wavelengths.

The intensity of any characteristic line, measured above the continuous spectrum, depends both on the tube current *i* and the amount by which the applied volt-

[2] The wavelength of an unresolved $K\alpha$ doublet is usually taken as the weighted average of the wavelengths of its components, $K\alpha_1$ being given twice the weight of $K\alpha_2$, since it is twice as strong. Thus the wavelength of the unresolved Mo $K\alpha$ line is

$$\tfrac{1}{2}(2 \times 0.709 + 0.714) = 0.711\text{Å}$$

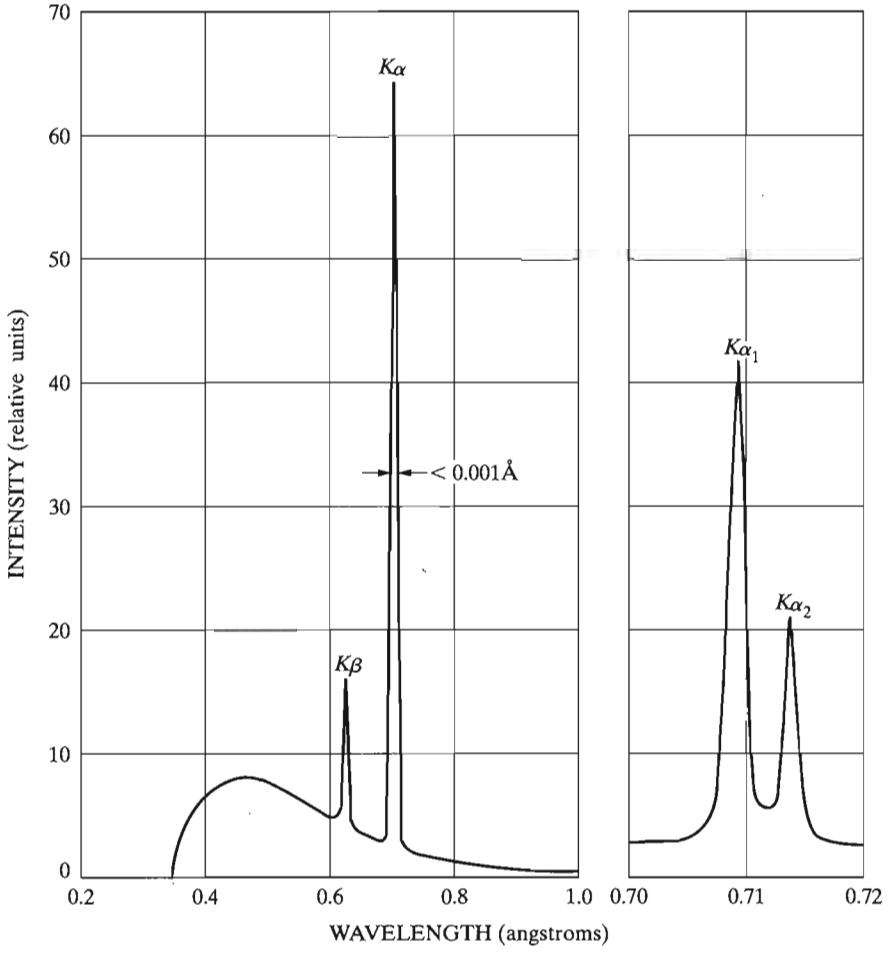

Figure 1-5 Spectrum of Mo at 35 kV (schematic). Line widths not to scale. Resolved $K\alpha$ doublet is shown on an expanded wavelength scale at right.

age V exceeds the critical excitation voltage for that line. For a K line, the intensity is given approximately by

$$I_{K\text{line}} = Bi(V - V_K)^n \tag{1-6}$$

where B is a proportionality constant, V_K the K excitation voltage, and n a constant with a value of about 1.5. (Actually, n is not a true constant but depends on V and varies from 1 to 2 and averages about 1.6 for common tube materials [1.3].) The intensity of a characteristic line can be quite large: for example, in the radiation from a copper target operated at 30 kV, the $K\alpha$ line has an intensity about 90 times that of the wavelengths immediately adjacent to it in the continuous spectrum.

Besides being very intense, characteristic lines are also very narrow, most of them less than 0.001 Å wide measured at half their maximum intensity, as indicated in Fig. 1-5. The existence of this strong sharp $K\alpha$ line is what makes a great deal of x-ray diffraction possible, because many diffraction experiments require the use of monochromatic or approximately monochromatic radiation.

The characteristic x-ray lines were discovered by W. H. Bragg [1.4] and systematized by H. G. Moseley [1.5] The latter found that the wavelength of any particular line decreased as the atomic number of the emitter increased. In particular, he found a linear relation (Moseley's law) between the square root of the line frequency ν and the atomic number Z:

$$\sqrt{\nu} = C(Z - \sigma), \tag{1-7}$$

where C and σ are constants. This relation is plotted in Fig. 1-6 for the $K\alpha_1$ and $L\alpha_1$ lines, the latter being the strongest line in the L series. These curves show, incidentally, that L lines are not always of long wavelength: the $L\alpha_1$ line of a heavy metal like tungsten, for example, has about the same wavelength as the $K\alpha_1$ line of copper, namely about 1.5 Å. The wavelengths of the characteristic x-ray lines of almost

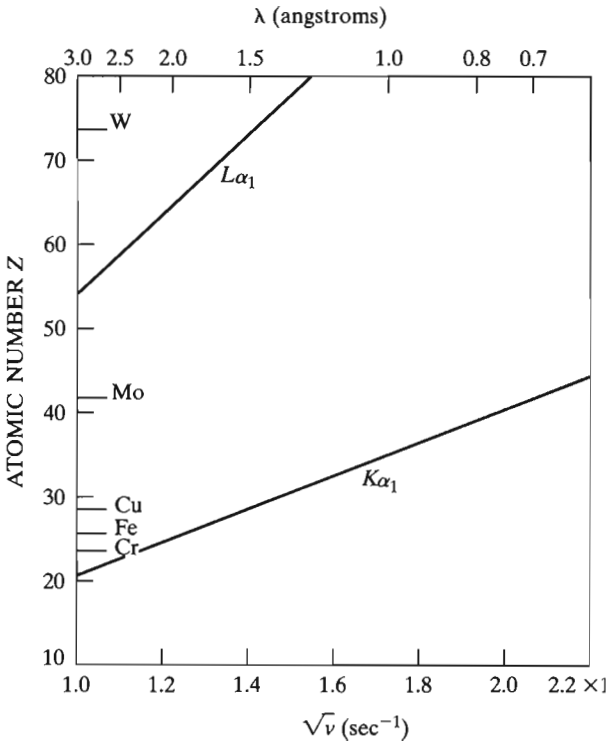

Figure 1-6 Moseley's relation between, $\sqrt{\nu}$ and Z for two characteristic lines.

all the known elements have been precisely measured, mainly by M. Siegbahn and coworkers and a tabulation of these wavelengths for the strongest lines of the K and L series appear in Appendix 7. Data on weaker lines can be found in Vol. C of the *International Tables for Crystallography* [G.1]

While the continuous spectrum results from the rapid deceleration of electrons by the target, the origin of the characteristic spectrum lies in the atoms of the target material itself. To understand this phenomenon, it is enough to consider an atom as consisting of a central nucleus surrounded by electrons lying in various shells (Fig. 1-7), where the designation K, L, M, ... corresponds to the principal quantum number $n = 1, 2, 3, \ldots$ If one of the electrons bombarding the target has sufficient kinetic energy, it can knock an electron out of the K shell, leaving the atom in an excited, high-energy state. One of the outer electrons immediately falls into the vacancy in the K shell, emitting energy in the process, and the atom is once again in its normal energy state. The energy emitted is in the form of radiation of a definite wavelength and is, in fact, characteristic K radiation.

The K-shell vacancy may be filled by an electron from any one of the outer shells, thus giving rise to a series of K lines; $K\alpha$ and $K\beta$ lines, for example, result from the filling of a K-shell vacancy by an electron from the L or M shells, respectively. It is *possible* to fill a K-shell vacancy from either the L or M shell, so that one atom of the target may be emitting $K\alpha$ radiation while its neighbor is emitting $K\beta$; however, it is more *probable* that a K-shell vacancy will be filled by an L electron than by an M electron, and the result is that the $K\alpha$ line is stronger than the $K\beta$ line. It also follows that it is impossible to excite one K line without exciting all the others. L characteristic lines originate in a similar way: an electron is knocked out of the L shell and the vacancy is filled by an electron from some outer shell.

The existence of a critical excitation voltage for characteristic radiation is related to the sharply defined shells of the atoms being bombarded. K radiation, for example, cannot be excited unless the tube voltage provides the bombarding electrons with enough energy to knock an electron out of the K shell of a target atom.

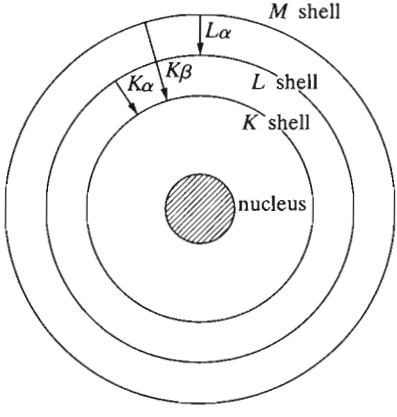

Figure 1-7 Electronic transitions in an atom (schematic). Emission processes indicated by arrows.

If W_K is the work required to remove a K electron, then the necessary kinetic energy of the electrons is given by

$$\frac{1}{2}mv^2 = W_K. \tag{1-8}$$

It requires less energy to remove an L electron than a K electron, since the former is farther from the nucleus; it therefore follows that the L excitation voltage is less than the K and that K characteristic radiation cannot be produced without L, M, etc., radiation accompanying it.

1-5 ABSORPTION

Further understanding of the electronic transitions which can occur in atoms can be gained by considering not only the interaction of electrons and atoms, but also the interaction of x-rays and atoms. When x-rays encounter any form of matter, they are partly transmitted and partly absorbed. Early on Röntgen established that the fractional decrease in the intensity I of an x-ray beam as it passes through any homogeneous substance is proportional to the distance traversed x [1.1]. In differential form,

$$-\frac{dI}{I} = \mu \quad dx \tag{1-9}$$

where the proportionality constant μ is called the *linear absorption coefficient* and is dependent on the substance considered, its density, and the wavelength of the x-rays. Integration of Eq. (1-9) gives

$$I_x = I_0 e^{-\mu x}, \tag{1-10}$$

where I_o = intensity of incident x-ray beam and I_x = intensity of transmitted beam after passing through a thickness x.

The linear absorption coefficient μ is proportional to the density ρ, which means that the quantity μ/ρ is a constant of the material and independent of its physical state (solid, liquid, or gas). This latter quantity, called the *mass absorption coefficient*, is the one usually tabulated. Equation (1-10) may then be rewritten in a more usable form:

$$I_x = I_0 e^{-(\mu/\rho)\rho x}. \tag{1-11}$$

Values of the mass absorption coefficient μ/ρ appear in Appendix 8 for various characteristic wavelengths commonly used in diffraction and in Vol. C of the International Tables for Crystallography [G.1], for other wavelengths.

It is occasionally necessary to know the mass absorption coefficient of a substance containing more than one element. Whether the substance is a mechanical mixture, a solution, or a chemical compound, and whether it is in the solid, liquid,

or gaseous state, its mass absorption coefficient is simply the weighted average of the mass absorption coefficients of its constituent elements. If w_1, w_2, etc., are the weight fractions of elements 1, 2, etc., in the substance and $(\mu/\rho)_1$, $(\mu/\rho)_2$, etc., their mass absorption coefficients, then the mass absorption coefficient of the substance is given by

$$\frac{\mu}{\rho} = w_1\left(\frac{\mu}{\rho}\right)_1 + w_2\left(\frac{\mu}{\rho}\right)_2 + \cdots \tag{1-12}$$

The way in which the absorption coefficient varies with wavelength gives the clue to the interaction of x-rays and atoms. The lower curve of Fig. 1-8 shows this variation for a nickel absorber; it is typical of all materials. The curve consists of two similar branches separated by a sharp discontinuity called an *absorption edge*. Along each branch the absorption coefficient varies with wavelength approximately according to a relation of the form

$$\frac{\mu}{\rho} = k\lambda^3 Z^3, \tag{1-13}$$

where k = a constant, with a different value for each branch of the curve, and Z = atomic number of absorber. Short-wavelength x-rays are therefore highly penetrating and are termed *hard*, while long-wavelength x-rays are easily absorbed and are said to be *soft*.

Matter absorbs x-rays in two distinct ways, by scattering and by true absorption, and these two processes together make up the total absorption measured by the quantity μ/ρ. The *scattering* of x-rays by atoms is similar in many ways to the scattering of visible light by dust particles in the air. It takes place in all directions, and

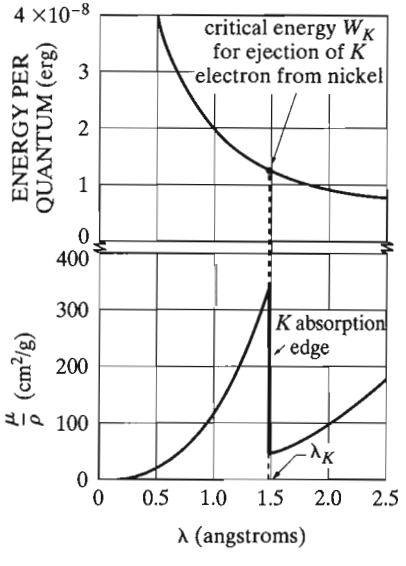

Figure 1-8 Variation with wavelength of the energy per x-ray quantum and of the mass absorption coefficient of nickel.

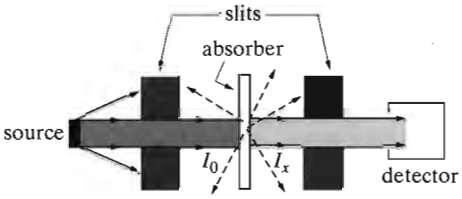

Figure 1-9 Experimental arrangement for measuring absorption. Narrow slits or pinholes define the beam. The detector measures the intensity I_0 of the incident beam when the absorber is removed and the intensity I_x of the transmitted beam when the absorber is in place. Although the scattered radiation (dashed lines) does not represent energy absorbed in the specimen, it does constitute energy removed from the beam and accordingly forms part of the total absorption represented by the coefficient μ/ρ.

since the energy in the scattered beams does not appear in the transmitted beam, it is, so far as the transmitted beam is concerned, said to be absorbed (Fig. 1-9). The phenomenon of scattering will be discussed in greater detail in Chap. 4; it is enough to note here that, except for the very light elements, it is responsible for only a small fraction of the total absorption of x-rays with wavelengths in the range normally used in diffraction. *True absorption* is caused by electronic transitions within the atom and is best considered from the viewpoint of quantum theory. Just as an electron of sufficient energy can knock a K electron, for example, out of an atom and thus cause the emission of K characteristic radiation, so also can an incident quantum of x-rays, provided it has the same minimum amount of energy W_K. In the latter case, the ejected electron is called a *photoelectron* and the emitted characteristic radiation is called *fluorescent radiation*. It radiates in all directions and has exactly the same wavelength as the characteristic radiation caused by electron bombardment of a metal target. (In effect, an atom emits the same K radiation no matter how the K-shell vacancy was originally created.) This phenomenon is the x-ray counterpart of the photoelectric effect in the ultraviolet region of the spectrum; there, photo-electrons can be ejected from the outer shells of a metal atom by the action of ultraviolet radiation, provided the latter has a wavelength less than a certain critical value.

To say that the energy of the incoming quanta must exceed a certain value W_K is equivalent to saying that the wavelength must be less than a certain value λ_K, since the energy per quantum is $h\nu$ and wavelength is inversely proportional to frequency. These relations may be written

$$W_K = h\nu_K = \frac{hc}{\lambda_K}, \tag{1-14}$$

where ν_K and λ_K are the frequency and wavelength, respectively, of the K absorption edge. Now consider the absorption curve of Fig. 1-8 in light of the above. Suppose that x-rays of wavelength 2.5 Å are incident on a sheet of nickel and that this wavelength is continuously decreased. At first the absorption coefficient is about 180 cm^2/g, but, as the wavelength decreases, the frequency increases and so

does the energy per quantum, as shown by the upper curve, thus causing the absorption coefficient to decrease, since the greater the energy of a quantum the more easily it passes through an absorber. When the wavelength is reduced just below the critical value λ_K, which is 1.488 Å for nickel, the absorption coefficient suddenly increases about eightfold in value. True K absorption is now occurring and a large fraction of the incident quanta simply disappear, their energy being converted into K fluorescent radiation and the kinetic energy of ejected photoelectrons. Since energy must be conserved in the process, it follows that the energy per quantum of the fluorescent radiation must be less than that of the incident radiation, or that the wavelength λ_K of the K absorption edge must be shorter than that of any K characteristic line of the absorber (The eight-fold increase in μ/ρ mentioned above means a tremendous decrease in transmitted intensity, because of the exponential nature of Eq. (1-11). If the transmission factor I_x/I_o of a particular nickel sheet is 0.1 for a wavelength just longer than λ_K, then it is only 10^{-8} for a wavelength just shorter.)

As the wavelength of the incident beam decreases below λ_K, the absorption coefficient begins to decrease again, even though the production of K fluorescent radiation and photoelectrons still occurs. At a wavelength of 1.0 Å, for example, the incident quanta have more than enough energy to remove an electron from the K shell of nickel. But the more energetic the quanta become, the greater is their probability of passing right through the absorber, with the result that less and less of them take part in the ejection of photoelectrons.

Plotting the absorption curve of nickel for wavelengths longer than 2.5 Å, i.e., beyond the limit of Fig. 1-8, reveals other sharp discontinuities. These are the L, M, N, etc., absorption edges; in fact, there are three closely spaced L edges (L_I, L_{II}, and L_{III}), five M edges, etc. (Fig. 1-10). Each of these discontinuities marks the wavelength of the incident beam whose quanta have just sufficient energy to eject an L,

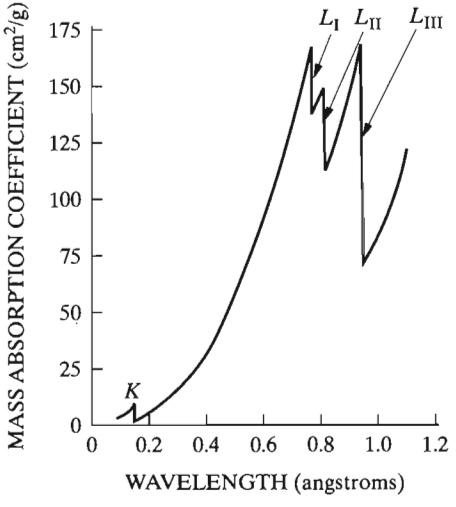

Figure 1-10 Absorption coefficients of lead, showing K and L absorption edges [1.6].

M, N, etc., electron from the atom. The right-hand branch of the curve of Fig. 1-8, for example, lies between the *K* and *L* absorption edges; in this wavelength region incident x-rays have enough energy to remove *L, M*, etc., electrons from nickel but not enough to remove *K* electrons. Absorption-edge wavelengths vary with the atomic number of the absorber in the same way, but not quite as exactly, as characteristic emission wavelengths, that is, according to Moseley's law. Values of the *K* and *L* absorption-edge wavelengths appear in Appendix 7.

The measured values of the absorption edges can be used to construct an energy-level diagram for the atom, which in turn can be used in the calculation of characteristic-line wavelengths. For example, if the energy of the neutral atom is defined as zero, then the energy of an ionized atom (an atom in an excited state) will be some positive quantity, since work must be done to pull an electron away from the positively charged nucleus. If a *K* electron is removed, work equal to W_K must be done and the atom is said to be in the *K* energy state. The energy W_K may be calculated from the wavelength of the *K* absorption edge by the use of Eq. (1-14). Similarly, the energies of the *L, M*, etc., states can be calculated from the wavelengths of the *L, M*, etc., absorption edges and the results plotted in the form of an energy-level diagram for the atom (Fig. 1-11).

Although this diagram is simplified, in that the substructure of all the levels is not shown, it illustrates the main principles. The arrows show the transitions of the *atom*, and their directions are therefore just the opposite of the arrows in Fig. 1-7, which shows the transitions of the *electron*. Thus, if a *K* electron is removed from an atom (whether by an incident electron or x-ray), the atom is raised to the *K* state. If an electron then moves from the *L* to the *K* level to fill the vacancy, the atom undergoes a transition from the *K* to the *L* state. The emission of $K\alpha$ characteristic radiation accompanies this transition, and the arrow indicating $K\alpha$ emission is accordingly drawn *from* the *K* state *to* the *L* state.

Figure 1-11 shows clearly how the wavelengths of characteristic emission lines can be calculated, since the difference in energy between two states will equal $h\nu$, where ν is the frequency of the radiation emitted when the atom goes from one state to the other. Consider the $K\alpha_1$ characteristic line, for example. The "*L* level" of an atom is actually a group of three closely spaced levels (L_I, L_{II}, and L_{III}), and the emission of the $K\alpha_1$ line is due to a $K \rightarrow L_{III}$ transition. The frequency $\nu_{K\alpha_1}$ of this line is therefore given by the equations

$$h\nu_{K\alpha_1} = W_K - W_{L_{III}},$$

$$h\nu_{K\alpha_1} = h\nu_K - h\nu_{L_{III}},$$

$$\frac{1}{\lambda_{K\alpha_1}} = \frac{1}{\lambda_K} - \frac{1}{\lambda_{L_{III}}}, \tag{1-15}$$

where the subscripts *K* and L_{111} refer to absorption edges and the subscript $K\alpha_1$ to the emission line.

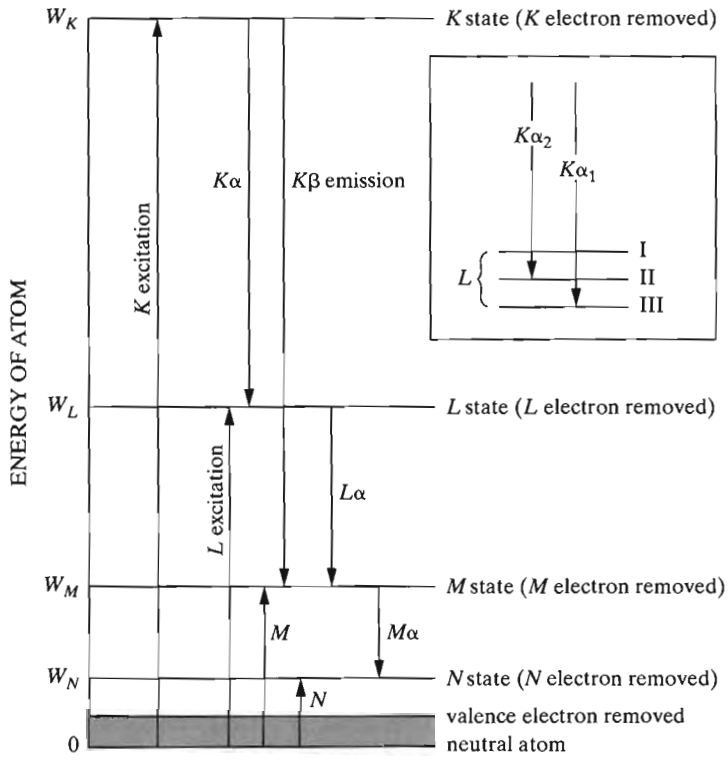

Figure 1-11 Atomic energy levels (schematic). Excitation and emission processes indicated by arrows. The insert at top right shows the fine structure of the *L* state. After Barrett [1.7].

Excitation voltages can be calculated by a relation similar to Eq. (1-4). To excite K radiation, for example, in the target of an x-ray tube, the bombarding electrons must have energy equal to W_K. Therefore

$$eV_K = W_K = h\nu_K = \frac{hc}{\lambda_K},$$

$$V_K = \frac{hc}{e\lambda_K},$$

$$V_K = \frac{12.40 \times 10^3}{\lambda_K}, \tag{1-16}$$

where V_K is the K excitation voltage and λ_K is the K absorption edge wavelength (in angstroms).

Figure 1-12 summarizes some of the relations developed above. This curve gives the short-wavelength limit of the continuous spectrum as a function of applied volt-

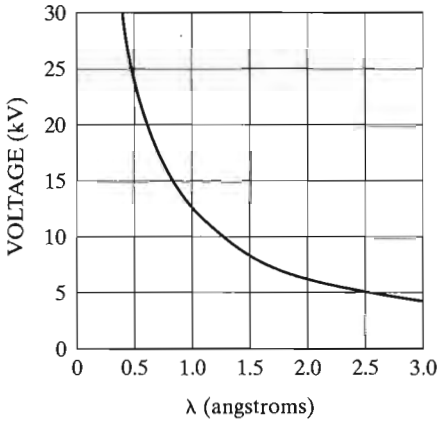

Figure 1-12 Relation between the voltage applied to an x-ray tube and the short-wavelength limit of the continuous spectrum, and between the critical excitation voltage of any metal and the wavelength of its absorption edge.

age. Because of the similarity between Eqs. (1-4) and (1-16), the same curve also allows determination of the critical excitation voltage from the wavelength of an absorption edge.

It might be inferred, from the last two sections, that every atom that has a vacancy in, for example, the K shell will always emit K radiation. That is not so. An atom with a K-shell vacancy is in an ionized, high-energy state. It can lose this excess energy and return to its normal state in two ways: (1) by emitting K radiation ("normal" production of characteristic radiation), or (2) by emitting an electron (*Auger effect* [1.8, 1.9]). In the Auger process a K-shell vacancy is filled from, say, the L_{11} level; the resulting K radiation does not escape from the atom but ejects an electron from, say, the L_{111} level. The ejected electron, called an *Auger electron*, has kinetic energy related to the energy difference between the K and L_{11} states.

The Auger effect is by no means a minor one. In fact, atoms with an atomic number Z less than 31 (gallium) are more likely to eject Auger electrons than to emit x-rays. The likelihood of the Auger process can be found from the fluorescence yield ω, which is defined, for the K shell, by

$$\omega_K = \frac{\text{number of atoms that emit } K \text{ radiation}}{\text{number of atoms with a } K\text{–shell vacancy}}. \tag{1-17}$$

(This quantity is called the *fluorescence* yield, whether the vacancy is caused by incident x-rays or by electrons.) Some values of ω_K are 0.03 for Mg (Z = 12), 0.41 for Cu (Z = 29), and 0.77 for Mo (Z = 42) [G.2, p. 131]. The probability of the Auger process occurring is $(1 - \omega_K)$, which amounts to some 97 percent for Mg and 23 percent for Mo.

Electrons of moderate energy like Auger electrons cannot travel very far in a solid, and an Auger electron emitted by one atom in a solid specimen cannot escape from the specimen unless the atom is situated within about 10 Å of the surface. The electrons that do escape have kinetic energies related to the differences between energy levels of the parent atom, i.e., their energies are characteristic of that atom.

Means are available for measuring these energies, providing a method for chemical analysis of very thin surface layers, called *Auger electron spectroscopy*, used in studies of catalysts, corrosion, impurity segregation at surfaces, etc.

1-6 FILTERS

Many x-ray diffraction experiments require radiation which is as closely monochromatic as possible. However, the beam from an x-ray tube operated at a voltage above V_K contains not only the strong $K\alpha$ line but also the weaker $K\beta$ line and the continuous spectrum. The intensity of these undesirable components can be decreased relative to the intensity of the $K\alpha$ line by passing the beam through a *filter* made of a material whose K absorption edge lies between the $K\alpha$ and $K\beta$ wavelengths of the target metal. Such a material will have an atomic number one less than that of the target metal, for metals with Z near 30.

A filter so chosen will absorb the $K\beta$ component much more strongly than the $K\alpha$ component, because of the abrupt change in its absorption coefficient between these two wavelengths. The effect of filtration is shown in Fig. 1-13, in which the partial spectra of the unfiltered and filtered beams from a copper target ($Z = 29$) are shown superimposed on a plot of the mass absorption coefficient of the nickel filter ($Z = 28$).

The thicker the filter the lower the ratio of intensity of $K\beta$ to $K\alpha$ in the transmitted beam. But filtration is never perfect, of course, no matter how thick the

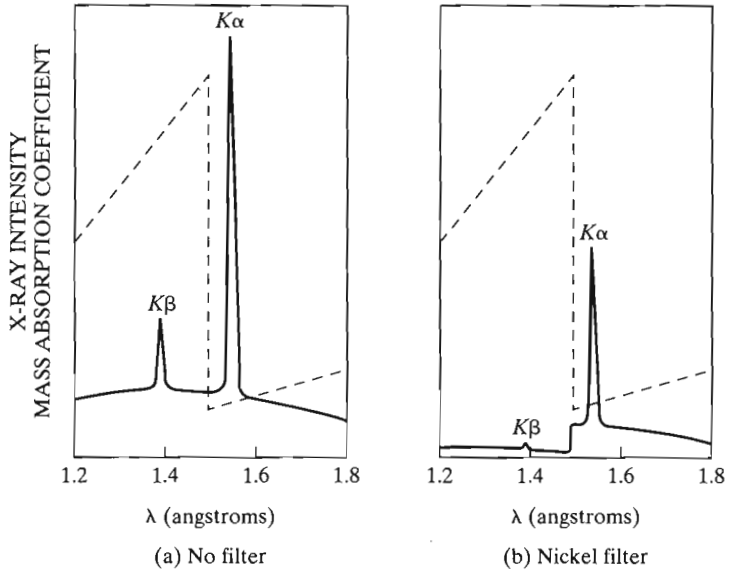

Figure 1-13 Comparison of the spectra of copper radiation (a) before and (b) after passage through a nickel filter (schematic). The dashed line is the mass absorption coefficient of nickel.

filter, and one must compromise between reasonable suppression of the $K\beta$ component and the inevitable weakening of the $K\alpha$ component which accompanies it. In practice, a reduction in the intensity of the $K\alpha$ line to about half its original value decreases the ratio of intensity of $K\beta$ to $K\alpha$ from about 1/9 in the incident beam to about 1/500 in the transmitted beam; this level is sufficiently low for most purposes. Table 1-1 shows the filters used in conjunction with the common target metals, the thicknesses required, and the transmission factors for the $K\alpha$ line. Filter materials are usually used in the form of thin foils. If it is not possible to obtain a given metal in the form of a stable foil, the oxide of the metal may be used. The powdered oxide is mixed with a suitable binder and spread on a paper backing, the required mass of metal per unit area being given in Table 1-1.

1-7 PRODUCTION OF X-RAYS

Since x-rays are produced whenever high-speed electrons collide with a metal target, any x-ray tube must contain (*a*) a source of electrons, (*b*) a high accelerating voltage, and (*c*) a metal target. Furthermore, since most of the kinetic energy of the electrons is converted into heat in the target, the latter is almost always water-cooled to prevent its melting.

All x-ray tubes contain two electrodes, an anode (the metal target) maintained, with few exceptions, at ground potential, and a cathode, maintained at a high negative potential, normally of the order of 30,000 to 50,000 volts for diffraction work. X-ray tubes may be divided into two basic types, according to the way in which electrons are provided: gas tubes, in which electrons are produced by the ionization of a small quantity of gas (residual air in a partly evacuated tube), and filament tubes, in which the source of electrons is a hot filament.

TABLE 1.1 FILTERS FOR SUPPRESSION OF $K\beta$ RADIATION

Target	Filter	Incident beam* $\frac{I(K\alpha)}{I(K\beta)}$	Filter thickness for $\frac{I(K\alpha)}{I(K\beta)} = \frac{500}{1}$ in trans. beam		$\frac{I(K\alpha)\ \text{trans}}{I(K\alpha)\ \text{incident}}$
			mg/cm²	in	
Mo	Zr	5.4	77	0.0046	0.29
Cu	Ni	7.5	18	0.0008	0.42
Co	Fe	9.4	14	0.0007	0.46
Fe	Mn	9.0	12	0.0007	0.48
Cr	V	8.5	10	0.0006	0.49

* This is the intensity ratio *at the target* [G.1]. This ratio outside the x-ray tube will be changed somewhat by the differential absorbtion of $K\alpha$ and $K\beta$ by the tube window, typically beryllium, 0.01 inch (0.25 mm) thick.

TABLE 2.2 CRYSTAL SYSTEMS AND BRAVAIS LATTICES

(The symbol $\neq$ means that equity is not required by symmetry. Accidental equality may occur, as shown by an example in Sec. 2-4.)

System	Axial lengths and angles	Bravais lattice	Lattice symbol
Cubic	Three equal axes at right angles $a = b = c, \quad \alpha = \beta = \gamma = 90°$	Simple Body-centered Face-centered	P I F
Tetragonal	Three axes at right angles, two equal $a = b \neq c, \quad \alpha = \beta = \gamma = 90°$	Simple Body-centered	P I
Orthorhombic	Three unequal axes at right angles $a \neq b \neq c, \quad \alpha = \beta = \gamma = 90°$	Simple Body-centered Base-centered Face-centered	P I C F
Rhombohedral*	Three equal axes, equally inclined $a = b = c, \quad \alpha = \beta = \gamma \neq 90°$	Simple	R
Hexagonal	Two equal coplanar axes at 120°, third axis at right angles $a = b \neq c, \quad \alpha = \beta = 90° \quad (\gamma = 120°)$	Simple	P
Monoclinic	Three unequal axes, one pair not at right angles $a \neq b \neq c, \quad \alpha = \gamma = 90° \neq \beta$	Simple Base-centered	P C
Triclinic	Three unequal axes, unequally inclined and none at right angles $a \neq b \neq c, \quad (\alpha \neq \beta \neq \gamma \neq 90°)$	Simple	P

* Also called trigonal.

point lattices and no more [2.4]; this important result is commemorated by the use of the terms *Bravais lattice* and *point lattice* as synonymous. For example, if a point is placed at the center of each cell of a cubic point lattice, the new array of points also forms a point lattice. Similarly, another point lattice can be based on a cubic unit cell having lattice points at each corner and in the center of each face.

The fourteen Bravais lattices are described in Table 2-2 and illustrated in Fig. 2-10. Some unit cells are *simple*, or *primitive*, cells (symbol P or R), and some are *non-primitive* cells (any other symbol): primitive cells have only one lattice point per cell while nonprimitive have more than one. A lattice point in the interior of a cell "belongs" to that cell, while one in a cell face is shared by two cells and one at a corner is shared by eight. The number of lattice points per cell is therefore given by

$$N = N_i + \frac{N_f}{2} + \frac{N_c}{8}, \tag{2-5}$$

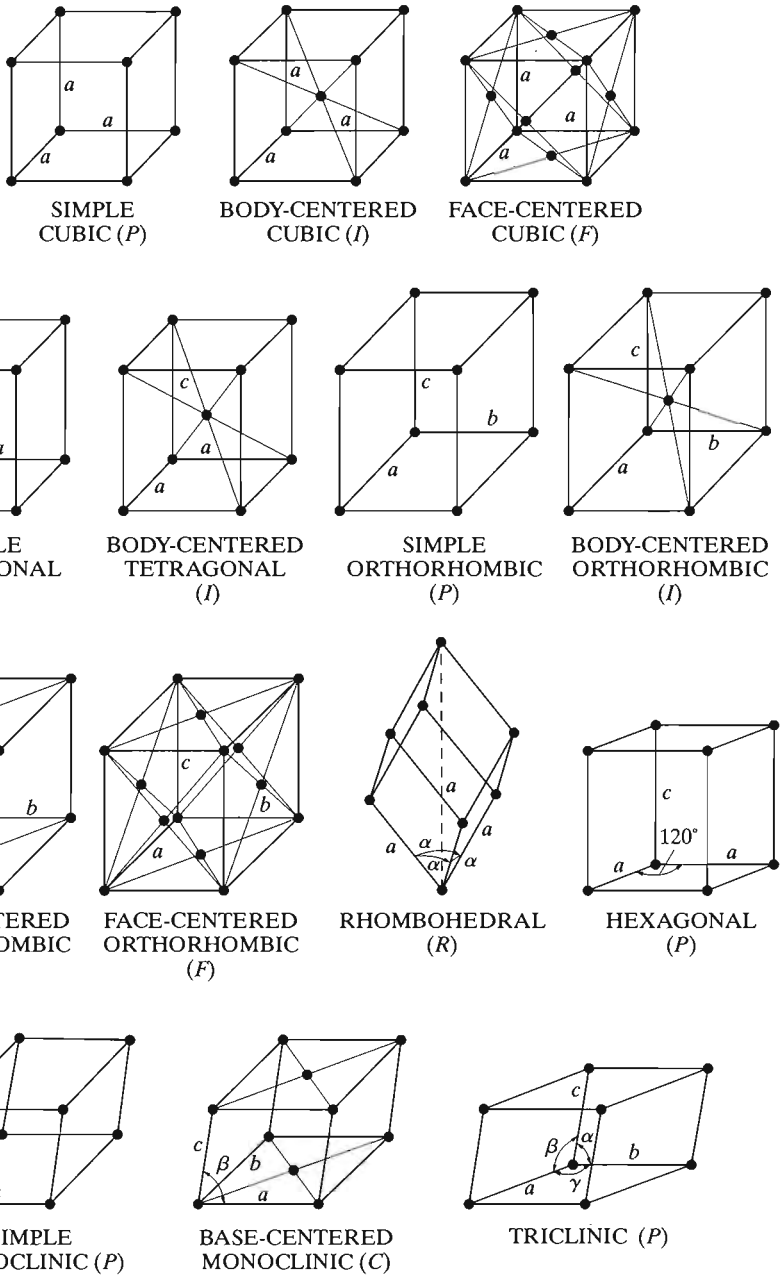

Figure 2-10 The fourteen Bravais lattices.

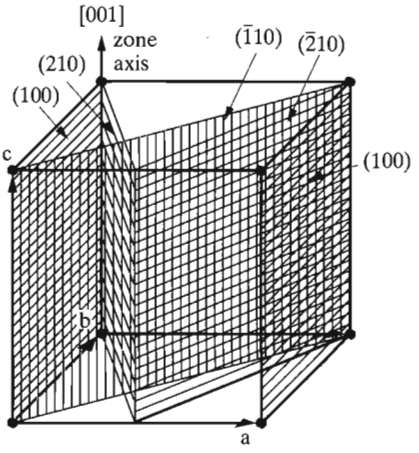

Figure 2-14 All shaded planes in the cubic lattice shown are planes of the zone {001}.

2-8 INDEXING IN THE HEXAGONAL SYSTEM

A slightly different system of plane indexing is used in the hexagonal system. The unit cell of a hexagonal lattice is defined by two equal and coplanar vectors $\mathbf{a}_1$ and $\mathbf{a}_2$, at 120° to one another, and a third axis $\mathbf{c}$ at right angles [Fig. 2-15(a)]. The complete lattice is constructed, as usual, by repeated translations of the points at the unit cell corners by the vectors $\mathbf{a}_1$, $\mathbf{a}_2$, $\mathbf{c}$. Some of the points so generated are shown in the figure, at the ends of dashed lines, in order to exhibit the hexagonal symmetry of the lattice, which has a 6-fold rotation axis parallel to $\mathbf{c}$. The third axis $\mathbf{a}_3$, lying in the basal plane of the hexagonal prism, is so symmetrically related to $\mathbf{a}_1$ and $\mathbf{a}_2$

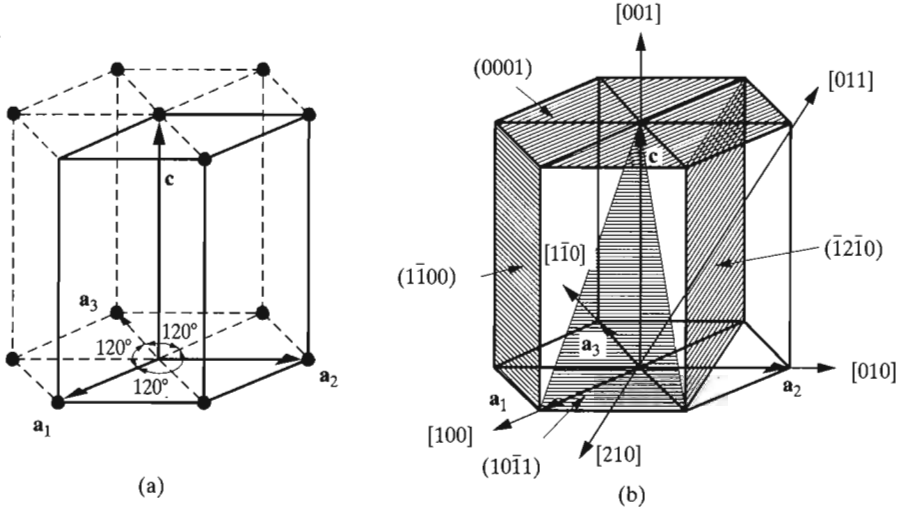

Figure 2-15 (a) The hexagonal unit cell (heavy lines) and (b) indices of planes and directions.

that it is often used in conjunction with the other two. Thus the indices of a plane in the hexagonal system, called Miller-Bravais indices, refer to *four* axes and are written (*hkil*). The index i is the reciprocal of the fractional intercept on the $\mathbf{a}_3$ axis. Since the intercepts of a plane on $\mathbf{a}_1$ and $\mathbf{a}_2$ determine its intercept on $\mathbf{a}_3$, the value of i depends on the values of h and k. The relation is

$$h + k = -i. \tag{2-10}$$

Since i is determined by h and k, it is sometimes replaced by a dot and the plane symbol written $(hk \cdot l)$ Sometimes even the dot is omitted. However, this usage defeats the purpose for which Miller-Bravais indices were devised, namely, to give similar indices to similar planes. For example, the side planes of the hexagonal prism in Fig. 2-15(b) are all similar and symmetrically located, and their relationship is clearly shown in their full Miller-Bravais symbols: $(10\bar{1}0)$, $(01\bar{1}0)$, $(\bar{1}100)$, $(\bar{1}010)$, $(0\bar{1}10)$, $(1\bar{1}00)$. On the other hand, the abbreviated symbols of these planes, $(10 \cdot 0)$, $(01 \cdot 0)$, $(\bar{1}1 \cdot 0)$, $(\bar{1}0 \cdot 0)$, $(0\bar{1} \cdot 0)$, $(1\bar{1} \cdot 0)$ do not immediately suggest this relationship.

Directions in a hexagonal lattice are best expressed in terms of the *three* basic vectors $\mathbf{a}_1$, $\mathbf{a}_2$, and $\mathbf{c}$. Figure 2-15(b) shows several examples of both plane and direction indices. Another system, involving four indices, is sometimes used to designate directions. The required direction is broken up into four component vectors, parallel to $\mathbf{a}_1$, $\mathbf{a}_2$, $\mathbf{a}_3$, and $\mathbf{c}$ and so chosen that the third index is the negative of the sum of the first two. Then, if $[UVW]$ are the indices of a direction referred to three axes and $[uvtw]$ the four-axis indices, the two are related as follows:

$$\begin{aligned} U &= u - t & u &= (2U - V)/3 \\ V &= v - t & v &= (2V - U)/3 \\ W &= w & t &= -(u + v) = -(U + V)/3 \\ & & w &= W. \end{aligned} \tag{2-11}$$

Thus, $[100]$ becomes $[2\bar{1}\bar{1}0]$, $[210]$ becomes $[10\bar{1}0]$, etc.

2-9 CRYSTAL STRUCTURE

So far discussion focused on topics from the field of *mathematical* (*geometrical*) *crystallography* and barely acknowledged actual crystals and the atoms of which they are composed. In fact, all of the above was well known long before the discovery of x-ray diffraction, i.e., long before there was any certain knowledge of the interior arrangements of atoms in crystals.

Chapter 5

Diffraction III: Real Samples

5-1 INTRODUCTION

Before turning to the practical aspects of diffraction from materials, it is valuable to consider how diffraction peaks are altered by the presence of various types of defects. Indeed, knowledge of how diffraction peaks are changed by defects underlies many of the analyses described in the third section of the book. Defects can be small numbers of dislocations in crystals with dimensions of millimeters. At the other extreme, the dislocation density may be so high that it is difficult to imagine the existence of discrete dislocations. Small crystal or grain size can be thought of as another kind of defect and can alter diffraction peak widths. In the limit of 'grain' size approaching that of an atom, as in gases, liquids and amorphous solids such as glasses and many polymers, sharp diffraction peaks no longer exist, and important information about these materials can be gleaned from how they scatter x-rays. At the other limit, that of defect-free crystals with millimeter or greater dimensions, diffracted intensity must be treated in a fashion quite different from the approach in Chap. 4.

5-2 CRYSTALLITE SIZE

In Chap. 4 the discussion of the structure factor revealed that *destructive interference is just as much a consequence of the periodicity of atom arrangement as is constructive interference.* If the path difference between x-rays photons scattered by the first two planes of atoms differs only slightly from an integral number of wavelengths, then the plane of atoms scattering x-rays exactly out of phase with the photons from the first plane will lie deep within the crystal. If the crystal is so small that this plane of atoms does not exist, then complete cancellation of all the scattered x-rays will not result. It follows that there is a connection between the amount of "out-of-phaseness" that can be tolerated and the size of the crystal. The result is that very small crystals cause broadening (a small angular divergence) of the dif-

fracted beam, i.e., diffraction (scattering) at angles near to but not equal to, the exact Bragg angle. Therefore consider the scattering of x-rays incident on the crystal at angles deviating slightly from the exact Bragg angle.

Suppose, for example, that the crystal has a thickness t measured in a direction perpendicular to a particular set of Bragg plane (Fig. 5-1). Let there be $(m + 1)$ planes in this set. Define the Bragg angle θ as a variable and let θ_B be the angle which exactly satisfies Bragg's law for the particular values of λ and d involved, or

$$\lambda = 2d \sin \theta_B.$$

In Fig. 5-1, rays **A**, **D**,..., **M** make exactly this angle θ_B with the diffraction planes. Ray **D**′, scattered by the atoms of the first lattice plane below the surface, is therefore one wavelength out of phase with **A**′; and ray **M**′, scattered by the mth plane of atoms below the surface, is m wavelengths out of phase with **A**′. Thus, at a diffraction angle $2\theta_B$, rays **A**′, **D**′,..., **M**′ are completely in phase and unite to form a diffracted beam of maximum amplitude, i.e., a beam of maximum intensity, since the intensity is proportional to the square of the amplitude.

Incident x-rays that make angles only slightly different from θ_B, produce incomplete destructive interference. Ray **B**, for example, makes a slightly larger angle θ_1, such that ray **L**′ from the mth plane below the surface is $(m + 1)$ wavelengths out of phase with **B**′, the ray from the surface plane. This means that midway in the crystal there is a plane populated by atoms scattering x-rays which are one-half (actually, an integer plus one-half) wavelength out of phase with ray **B**′ from the atoms of the surface plane. These rays cancel one another, and so do the other rays from similar pairs of planes throughout the crystal, the net effect being that rays scattered by the top half of the crystal annul those scattered by the bottom half. The intensity of the beam diffracted at an angle $2\theta_1$ is therefore zero. It is also zero at an angle $2\theta_2$ where θ_2 is such that ray **N**′ from the mth plane below the surface is

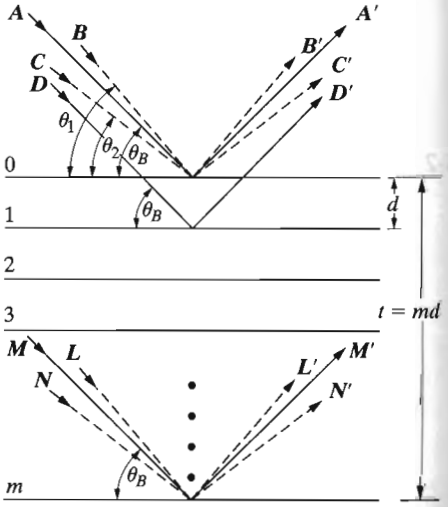

Figure 5-1 Effect of crystal size on diffraction.

$(m - 1)$ wavelengths out of phase with ray $\mathbf{C}'$ from the surface plane. This defines, therefore, the two limiting angles, $2\theta_1$ and $2\theta_2$, at which the diffracted intensity must drop to zero. It follows that the diffracted intensities at angles near $2\theta_B$, but not greater than $2\theta_1$ or less than $2\theta_2$, are *not zero* but have values intermediate between zero and the maximum intensity of the beam diffracted at an angle $2\theta_B$. The curve of diffracted intensity vs. 2θ will thus have the form of Fig. 5-2(a) in contrast to Fig. 5-2(b), which illustrates the hypothetical case of diffraction occurring only at the exact Bragg angle.

The width of the diffraction curve of Fig. 5-2(a) increases as the thickness of the crystal decreases, because the angular range $(2\theta_1 - 2\theta_2)$ increases as m decreases. The width B is usually measured, in radians, at an intensity equal to half the maximum intensity, and this measure of width is termed the full-width at half maximum of FWHM. [Note that B is an angular width, in terms of 2θ (not θ), and not a linear width.] A rough measure of B, is one-half the difference between the two extreme angles at which the intensity is zero, which amounts to assuming that the diffraction line is triangular in shape. Therefore,

$$B = \frac{1}{2}(2\theta_1 - 2\theta_2) = \theta_1 - \theta_2.$$

The path-difference equations for these two angles are similar to Eq. (3-1) but related to the entire thickness of the crystal rather than to the distance between adjacent planes:

$$2t \sin \theta_1 = (m + 1)\lambda,$$

$$2t \sin \theta_2 = (m - 1)\lambda.$$

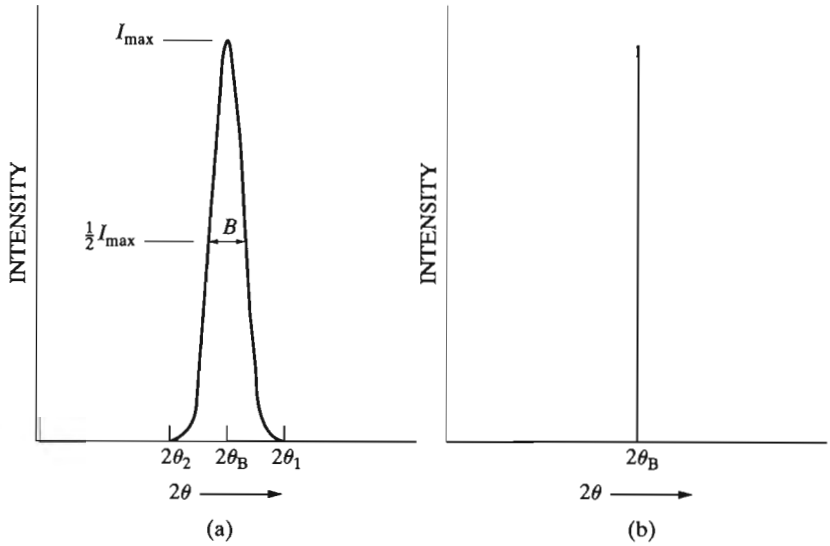

Figure 5-2 Effect of fine crystallite size on diffraction curves (schematic).

By subtraction,

$$t(\sin\theta_1 - \sin\theta_2) = \lambda,$$

$$2t\cos\left(\frac{\theta_1 + \theta_2}{2}\right)\sin\left(\frac{\theta_1 - \theta_2}{2}\right) = \lambda.$$

But θ_1 and θ_2 are both very nearly equal to θ_B, so that

$$\theta_1 + \theta_2 = 2\theta_B \text{ (approx.)}$$

and

$$\sin\left(\frac{\theta_1 - \theta_2}{2}\right) = \left(\frac{\theta_1 - \theta_2}{2}\right) \text{(approx.)}.$$

Therefore

$$2t\left(\frac{\theta_1 - \theta_2}{2}\right)\cos\theta_B = \lambda,$$

$$t = \frac{\lambda}{B\cos\theta_B}. \tag{5-1}$$

A more exact treatment of the problem gives

$$t = \frac{0.9\lambda}{B\cos\theta_B}, \tag{5-2}$$

which is known as Scherrer's formula [5.1]. It is used to estimate the *size* of very small crystals from the measured width of their diffraction curves. Note that whether a value of 0.9 or 1 is used depends on the shape(s) of the crystallites assumed to be in the sample. A detailed discussion appears elsewhere [G.17]. What is the order of magnitude of this effect? Suppose $\lambda = 1.5$ Å, $d = 1.0$ Å, and $\theta = 49°$. Then for a crystal 1 mm in diameter the breadth B, due to the small crystal effect alone, would be about 2×10^{-7} radian (10^{-5} degree), or too small to be observable. Such a crystal would contain some 10^7 parallel lattice planes of the spacing assumed above. However, if the crystal were only 500 Å thick, it would contain only 500 planes, and the diffraction curve would be relatively broad, namely about 4×10^{-3} radian (0.2°), which is easily measurable.

Nonparallel incident rays, such as **B** and **C** in Fig. 5-1, actually exist in any real diffraction experiment, since the "perfectly parallel beam" assumed in Fig. 3-2 is an idealization. As will be shown in Sec. 6-4, any actual beam of x-rays contains divergent and convergent rays as well as parallel rays, so that the phenomenon of diffraction at angles not exactly satisfying Bragg's law actually takes place.

Neither is any real beam ever strictly monochromatic. The usual "monochromatic" beam is simply one containing the strong $K\alpha$ component superimposed on the continuous spectrum. But the $K\alpha$ line itself has a width of about 0.001 Å and

this narrow range of wavelengths in the nominally monochromatic beam is a further cause of line broadening, i.e., of measurable diffraction at angles close, but not equal, to $2\theta_B$, since for each value of λ there is a corresponding value of θ. (Translated into terms of diffraction line width, a range of wavelengths extending over 0.001 Å leads to an increase in line width, for $\lambda = 1.5$ Å and $\theta = 45^o$, of about 0.08^o over the width one would expect if the incident beam were strictly monochromatic.) Line broadening due to this natural "spectral width" is proportional to $\tan\theta$ and becomes quite noticeable as θ approaches 90^o.

5-3 INTERFERENCE FUNCTION

The calculation of the intensity of diffraction peaks in Ch. 4 was for diffraction at the exact Bragg angle θ_B. At this angle, and in the absence of any defects producing displacement of the unit cells of the crystal, the total amplitude diffracted by the N unit cells of the crystal is the sum of the amplitude F_n scattered by each unit cell:

$$A_{TOTAL} = NF_n. \tag{5-3}$$

At deviations from the exact Bragg angle, the individual unit cells will scatter slightly out of phase. Also, the vector $(\mathbf{S} - \mathbf{S_0})/\lambda$ no longer extends from the origin of the reciprocal lattice to a reciprocal lattice point. As was shown in the preceding section, x-rays scattered from an effectively infinite crystal at $\theta \neq \theta_B$ will be out of phase and the diffracted intensity will equal zero. If the crystal is small enough, however, the intensity will not go to zero off the exact Bragg condition, and the calculation which follows shows how diffracted intensity varies with angle as a function of the number of unit cells along the direction of the diffraction vector $(\mathbf{S} - \mathbf{S_0})$, i.e., along the direction *normal* to the Bragg planes.

Figure 5-3 shows the direct space and reciprocal space diagrams, respectively, for diffraction from a crystal at $\theta(1) > \theta_B(1)$ for 001 and at $\theta(2) > \theta_B(2)$ for 002, where "1" and "2" in parenthesis indicate the angle for the first and second order diffraction. If a θ–2θ diffractmeter is used, the portion of the reciprocal lattice sampled during a scan is indicated by the horizontal line from the origin in Fig. 5-3b (i.e., along $\mathbf{b}_3$ in this example). If $\mathbf{H}_{hkl}$ (or $\mathbf{H}$ for short) is the reciprocal lattice vector from the origin of the reciprocal lattice to the reciprocal lattice point hhe, the diffraction off the exact Bragg condition means that $(\mathbf{S} - \mathbf{S_0})/\lambda \neq \mathbf{H}$. The difference between these two vectors *along* the direction of $(\mathbf{S} - \mathbf{S_0})/\lambda$ will be written as δ is often termed the deviation parameter and is shown in Fig. 5-3. In order to calculate the intensity diffracted from the crystal at $\theta \neq \theta_B$, the phase differences for scattering from different unit cells must be included. For the three unit vectors of the crystal $\mathbf{a}_1$, $\mathbf{a}_2$, and $\mathbf{a}_3$:

$$A_{TOTAL} = \sum_{n_1=0}^{N_1-1} \sum_{n_2=0}^{N_2-1} \sum_{n_3=0}^{N_3-1} F \exp \frac{2\pi i}{\lambda}[(\mathbf{S} - \mathbf{S_0}) \cdot (n_1\mathbf{a}_1 + n_2\mathbf{a}_2 + n_3\mathbf{a}_3)], \tag{5-4}$$

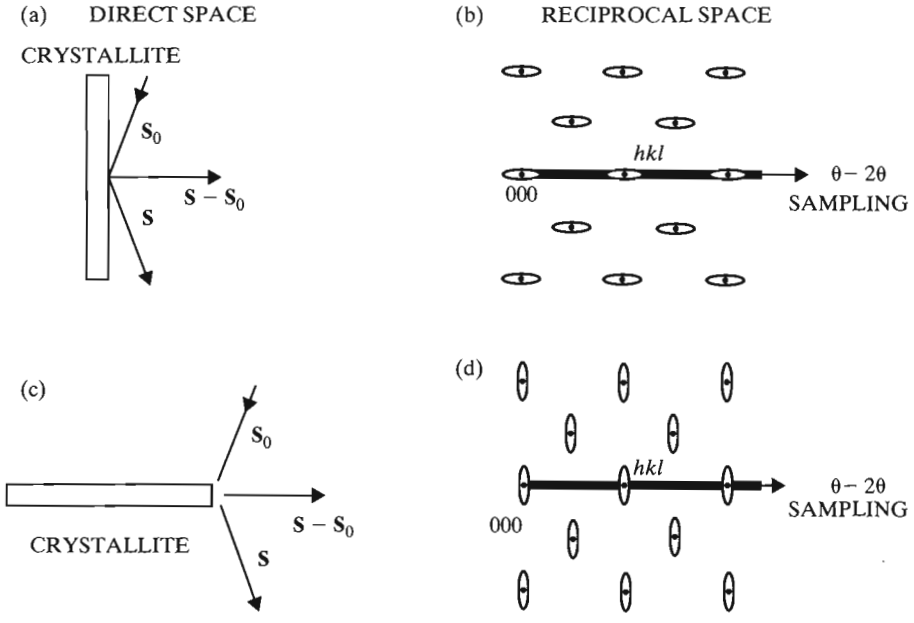

Figure 5-4 Illustration of detectability of diffraction peak broadening for a θ–2θ diffractometer for two crystallite orientations. (a) and (c) show direct space and reciprocal space, respectively, for one crystallite orientation relative to $\mathbf{S} - \mathbf{S}_0$ and (b) and (d) show the two spaces for a second crystallite orientation. The ellipses surrounding the reciprocal lattice points show the eleongation of the rel points into rel rods (due to small crystallite dimensions) and represent contours of constant diffracted intensity. The horizontal, solid bar represents the reciprocal space sampling region (RSSR).

5-4 STRAIN

In the preceeding sections crystal size was seen as a type of defect, i.e., a deviation from the crystal of infinite extent and perfect atomic periodicty assumed in the derivation of Eq. 4-20 or 21. Dislocations and subgrains are another type of defect which have important consequences in diffraction. Before the existence of dislocations was established experimentally, considerable indirect evidence had been gathered showing that all real crystals possess, to a greater or lesser degree, a *mosaic structure* such as is illustrated in a greatly exaggerated fashion in Fig. 5-5.

A crystal with mosaic structure does not have its atoms arranged on a perfectly regular lattice extending from one side of the crystal to the other; instead, the lattice is broken up into a number of tiny blocks, each slightly disoriented one from another. The size of these blocks is of the order of 1000 Å, while the maximum angle of disorientation between them may vary from a very small value to as much as one degree, depending on the crystal. If this angle is ε, then diffraction of a parallel monochromatic beam from a "single" crystal will occur not only at an angle of incidence θ_B but at all angles between θ_B and $\theta_B + \varepsilon$. Another effect of mosaic struc-

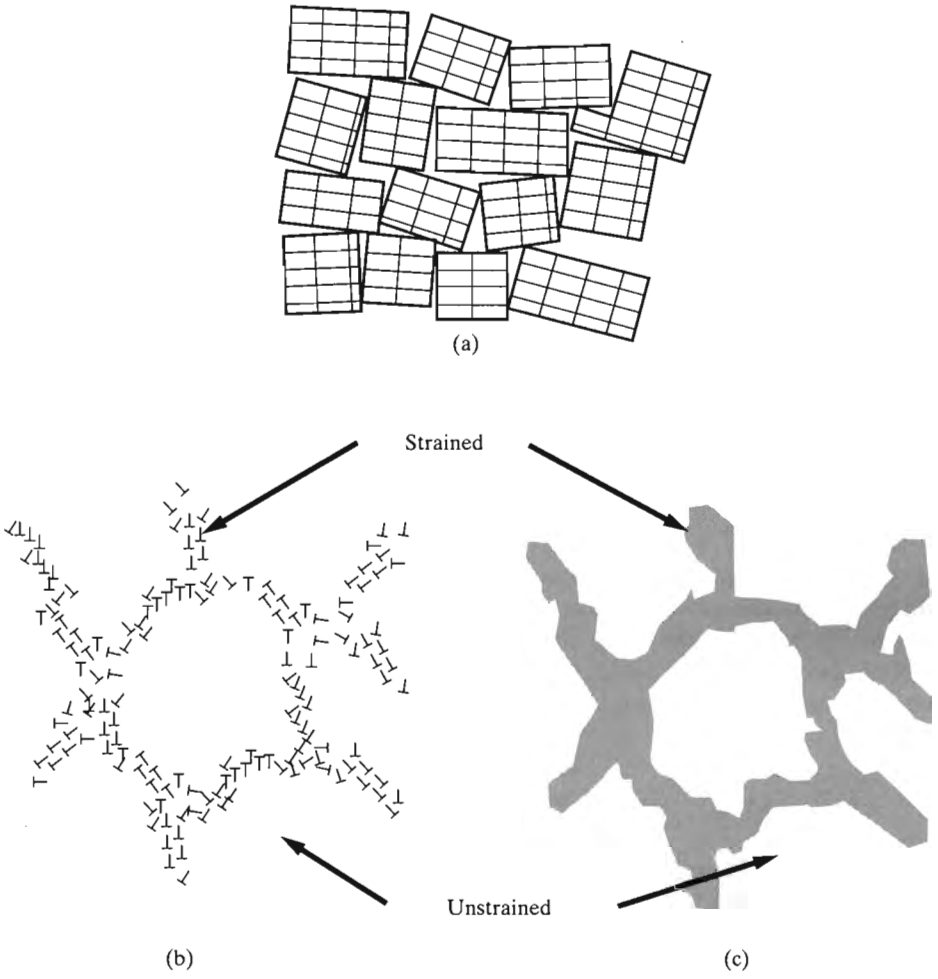

Figure 5-5 Mosaic structure of a real crystal. (a) Rotations between adjacent domains (left), (b) dislocations walls separating different mosaic blocks (middle) and (c) regions corresponding to high dislocation densities in (b) where microstrain is significant. In (b) the symbol ⊥ shows the positions of dislocation lines running through the plane of the drawing.

ture is to increase the integrated intensity of the diffracted beam relative to that theoretically calculated for an ideally perfect crystal (Sec. 5-5).

In the 1960s the TEM provided direct evidence of mosaic structure. It showed that real crystals, whether single crystals or individual grains in a polycrystalline aggregate, had a substructure defined by the dislocations present. The density of these dislocations is not uniform; they tend to group themselves into walls (subgrain boundaries) surrounding small volumes having a low dislocation density (subgrains or cells). Today the term "mosaic structure" is seldom used, but the little

blocks of Fig. 5-5 are identical with sub-grains and the regions between the blocks are the dislocation walls. It is the strains and strain gradients associated with the groups of dislocations that is responsible for the increase in integrated intensity of diffraction not the fact that there are rotated domains.

It is useful at this juncture to consider the effects of strain on diffraction peaks. Two types of stresses can be identified, *microstresses* and *macrostresses*. Microstresses and the corresponding microstrains vary from one grain to another, or from one part of a grain to another part, on a microscopic scale. On the other hand, the stress may be quite uniform over large distances; it is then referred to as *macrostress*.

The effect of strain, both uniform and nonuniform, on the direction of x-ray reflection is illustrated in Fig. 5-6. A portion of an unstrained grain appears in (a) on the left, and the set of transverse diffraction planes shown has everywhere its equilibrium spacing d_0. The diffraction line from these planes appears on the right. If the grain is then given a uniform tensile strain at right angles to the diffraction planes, their spacing becomes larger than d_0, and the corresponding diffraction line shifts to lower angles but does not otherwise change, as shown in (b). This line shift

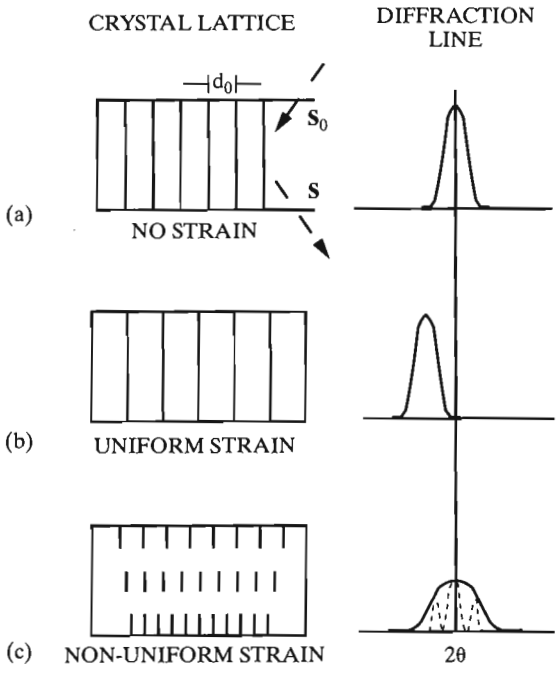

Figure 5-6 Effect of uniform and non-uniform strains (left side of the figure) on diffraction peak position and width (right side of the figure). (a) shows the unstrained sample, (b) shows uniform strain and (c) shows non-uniform strain within the volume sampled by the x-ray beam.

is the basis of the x-ray method for the measurement of macrostress, as will be described in Chap. 15. In (c) the grain is bent and the strain is nonuniform; on the top (tension) side the Bragg plane spacing exceeds d_0, on the bottom (compression) side it is less than d_0, and somewhere in between it equals d_0. Thus, a single grain can be thought of as composed of a number of small regions in each of which the plane spacing is substantially constant but different from the spacing in adjoining regions. These regions cause the various sharp diffraction lines indicated on the right of (c) by the dotted curves. The sum of these sharp lines, each slightly displaced from the other, is the broadened diffraction line shown by the full curve and, of course, the broadened line would normally be the only one experimentally observable. Differentiating Bragg's law yields the relation between the broadening produced and the nonuniformity of the strain:

$$b = \Delta 2\theta = -2\frac{\Delta d}{d}\tan\theta, \tag{5-9}$$

where b is the extra broadening, over and above the instrumental breadth of the line, due to a fractional variation in Bragg plane spacing $\Delta d/d$. This equation allows the variation in strain, $\Delta d/d$, to be calculated from the observed broadening. This value of $\Delta d/d$ however, includes both tensile and compressive microstrain and must be divided by two to obtain the maximum tensile strain alone, or maximum compressive strain alone, if these two are assumed equal. The maximum strain so found can then be multiplied by the elastic modulus E to give the maximum microstress present.

5-5 PERFECT CRYSTALS

Within a few years of the discovery of the diffraction of x-rays by crystals, it was apparent that the approach used in Chap. 4 to calculate diffracted intensities was inadequate to describe diffraction from highly perfect crystals [5.2, 5.3]. Diffracted intensities from perfect crystals were substantially less than those from deformed crystals, i.e., ideally imperfect crystals, and the variation of diffracted intensity with increasing levels of deformation was demonstrated [5.4]. Crystals with greater perfection exhibited diffraction peak widths which were smaller than those of less perfect crystals, but there appeared to be a minimum width of a diffraction peak which depended on the material, the wavelength of x-rays, the reflection and other factors. The assumptions behind the derivation of the *kinematical* diffraction equations outlined in Chap. 4 did not apply to the case of highly perfect crystals with dimensions greater than ~ 1–5 μm.

Explaining the effects described above requires development of *dynamical* diffraction theory, but the origin of the decreased diffracting power of perfect crystals is easy to illustrate (Fig. 5-7). In the discussion which follows it is important to remember that every time a ray is diffracted it undergoes a phase shift of $\pi/2$ relative to the incident beam. If the incident beam with wave vector $\mathbf{K}_0$ enters a crystal at the correct angle θ for *hkl* diffraction, diffracted rays $\mathbf{K}_1$ are produced at angle 2θ

Chapter 10

Determination of Crystal Structure

10-1 INTRODUCTION

Since 1913, when W. L. Bragg solved the structure of NaCl, the structures of many thousands of crystals, organic and inorganic, have been determined. This vast body of knowledge is of fundamental importance in such fields as crystal chemistry, solid-state physics, and the biological sciences because, to a large extent, structure determines properties and the properties of a substance are never fully understood until its structure is known. In metallurgy, a knowledge of crystal structure is a necessary prerequisite to any understanding of such phenomena as plastic deformation, alloy formation, or phase transformations. Crystal structure underlies technologically useful effects such as piezoelectricity, and knowledge of it is required for understanding the nature of point and other atomic-scale defects controlling many materials properties.

The work of structure determination goes on continuously since there is no dearth of unsolved structures. New substances are constantly being synthesized, and the structures of many old ones remain unknown. In themselves, crystal structures vary widely in complexity: the simplest can be solved in a few hours, while the more complex may require months or even years for their complete solution. (Proteins form a notable example of the latter kind; some protein structures are now known, but others still defy solution.) Complex structures require complex methods of solution, and structure determination in its entirety is more properly the subject of a series of books than of a single chapter. Therefore, only some of the principles and their application to the solution of fairly simple structures will be considered here. Because polycrystalline diffraction patterns are the kind most often encountered by the materials scientist/engineer, this chapter will treat only these methods.

The basic principles involved in structure determination have already been introduced in Chaps. 3 and 4. In brief, the crystal structure of a substance determines the diffraction pattern of that substance or, more specifically, the shape and

size of the unit cell determines the angular positions of the diffraction lines, and the arrangement of the atoms within the unit cell determines the relative intensities of the lines. It may be worthwhile to state this again in tabular form:

Crystal structure	Diffraction pattern
Unit cell	Line positions
Atom positions	Line intensities

Since structure determines the diffraction pattern, it should be possible to go in the other direction and deduce the structure from the pattern. It is possible *but not by any direct manner.* Given a structure, its diffraction pattern can be calculated in a very straightforward fashion, and examples of such calculations were given in Sec. 4-13; but the reverse problem, that of directly calculating the structure from the observed pattern, has not yet been solved for the general case (Sec. 10-7). The procedure adopted is essentially one of trial and error. On the basis of an educated guess, a structure is assumed, its diffraction pattern calculated, and the calculated pattern compared with the observed one. If the two agree in all detail, the assumed structure is correct; if not, the process is repeated as often as is necessary to find the correct solution. The problem is not unlike that of deciphering a code, and requires of the crystallographer the same qualities possessed by a good cryptanalyst, namely, knowledge, perseverance, and not a little intuition.

The determination of an unknown structure proceeds in three major steps:

1. The shape and size of the unit cell are deduced from the angular positions of the diffraction lines. An assumption is first made as to which of the seven crystal systems the unknown structure belongs and then, on the basis of this assumption, the correct Miller indices are assigned to each reflection. This step is called "indexing the pattern" and is possible only when the correct choice of crystal system has been made. Once this is done, the shape of the unit cell is known (from the crystal system), and its size is calculable from the positions and Miller indices of the diffraction lines.
2. The number of atoms per unit cell is then computed from the shape and size of the unit cell, the chemical composition of the specimen, and its measured density.
3. Finally, the positions of the atoms within the unit cell are deduced from the relative intensities of the diffraction lines.

Only when these three steps have been accomplished is the structure determination complete. The third step is generally the most difficult, and there are many structures which are known only incompletely, in the sense that this final step has not yet been made. Nevertheless, a knowledge of the shape and size of the unit cell, without any knowledge of atom positions, is in itself of very great value in many applications.

The average materials scientist/engineer is rarely, if ever, called upon to determine an unknown crystal structure. If the structure is at all complex, its determination is a job for a specialist in x-ray crystallography, who can bring special techniques, both experimental and mathematical, to bear on the problem. He or she should, however, know enough about structure determination to unravel any simple structures encountered and, what is more important, to index the powder patterns of substances of *known* structure, as this is a routine problem in almost all diffraction work. The procedures given below for indexing patterns are applicable whether the structure is known or not, but they are of course very much easier to apply if the structure is known beforehand.

Many crystal structures allow substitution of atoms of one element for another. Materials such as GaAs and InSb, both of which have the zinc blende structure, and have lattice parameters 5.653 Å and 6.479 Å, respectively, are isotypes. As such, it is not surprising that considerable In, for example, can replace Ga atoms in the GaAs lattice; this type of alloying, in which the minority atoms are in solid solution, can improve mechanical properties, i.e., resistance to dislocation generation, propagation and multiplication. Whenever there are two types of atoms occupying a lattice or a set of sub-lattice sites, it is possible that the different atoms take up a nonrandom or ordered arrangement. This ordering can be long range or short range, and examining ordering is an important subset of crystal structure determination in materials work. Accordingly, the last three sections of this chapter concern themselves with what can be learned about ordering from diffraction from polycrystalline samples.

10-2 PRELIMINARY TREATMENT OF DATA

The first step in determining the crystal structure of a polycrystalline sample is recording the diffraction pattern over as wide a range of 2θ as possible, normally with diffractometry. Specimen preparation must ensure random orientation of the individual particies of powder, if the observed relative intensities of the diffraction lines are to have any meaning in terms of crystal structure. After the pattern is obtained the value of $\sin^2\theta$ is calculated for each diffraction line; this set of $\sin^2\theta$ values is the raw material for the determination of cell size and shape. Or one can calculate the d value of each line and work from this set of numbers.

Since the problem of structure determination is one of finding a structure which will account for all the lines on the pattern, in both position and intensity, the investigator must make sure at the outset that the observed pattern does not contain any extraneous lines. The ideal pattern contains lines formed by x-rays of a single wavelength, diffracted only by the substance whose structure is to be determined. There are therefore two sources of extraneous lines:

1. *Diffraction of x-rays having wavelengths different from that of the principal component of the radiation.* If filtered radiation is used, then $K\alpha$ radiation is the principal component, and characteristic x-rays of any other wave-

length may produce extraneous lines. The chief offender is $K\beta$ radiation, which is never entirely removed by a filter and may be a source of extraneous lines for reflections with high diffracting power. A quick check for $K\beta$ radiation begins with identification of the most intense line of the pattern, presumably formed with $K\alpha$ radiation. Using $\lambda_{K\alpha}$, d_1 is calculated from $2\theta_\alpha$ via Bragg's law. If $K\beta$ radiation is present, a diffraction peak from d_1 results at a $2\theta_\beta$ different from $2\theta_\alpha$ and the relationship between diffraction angles and wavelengths is

$$\left(\frac{\lambda_{K\alpha}^2}{\lambda_{K\beta}^2}\right)\sin^2\theta_\beta = \sin^2\theta_\alpha, \tag{10-1}$$

where $\lambda_{K\alpha}^2/\lambda_{K\beta}^2$ has a value near 1.2 for most radiations. If it is suspected that a particular line is due to $K\beta$ radiation, multiplication of its $\sin^2\theta$ value by $\lambda_{K\alpha}^2/\lambda_{K\beta}^2$ will give a value equal, or nearly equal, to the value of $\sin^2\theta$ for some $K\alpha$ line on the pattern, unless the product exceeds unity. The $K\beta$ line corresponding to a given $K\alpha$ line is always located at a smaller angle 2θ and has lower intensity. However, since $K\alpha$ and $K\beta$ lines (from different planes) may overlap on the pattern, Eq. (10-1) alone can establish only the possibility that a given line is due to $K\beta$ radiation, but it can never prove that it is. Another possible source of extraneous lines is L characteristic radiation from tungsten contamination on the target of the x-ray tube, particularly if the tube is old. If such contamination is suspected, equations such as (10-1) can be set up to test the possibility that certain lines are due to tungsten radiation.

2. *Diffraction by substances other than the unknown.* Such substances are usually impurities in the specimen but may also include the specimen mount or badly aligned slits. Careful specimen preparation and good experimental technique will eliminate extraneous lines due to these causes.

For reasons to be discussed in Chap. 13, the observed values of $\sin^2\theta$ always contain small systematic errors. These errors are not large enough to cause any difficulty in indexing patterns of cubic crystals, but they can seriously interfere with the determination of some noncubic structures. The best method of removing such errors from the data is to calibrate the camera or diffractometer with a substance of known lattice parameter, mixed with the unknown, i.e., by adding an internal standard. The difference between the observed and calculated values of $\sin^2\theta$ for the standard substance gives the error in $\sin^2\theta$, and this error can be plotted as a function of the observed values of $\sin^2\theta$. Figure 10-1 shows a correction curve of this kind, obtained with a particular specimen and a particular Hull/Debye–Scherrer camera.[1] The errors represented by the ordinates of such a

[1]For the shape of this curve, see Prob. 13-5.

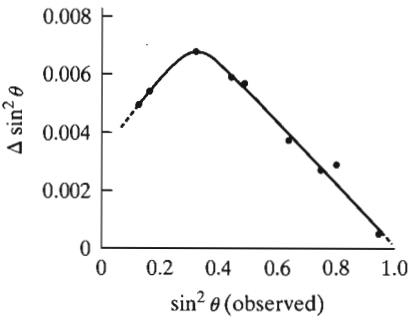

Figure 10-1 An example of a correction curve for $\sin^2\theta$ values.

curve can then be applied to each of the observed values of $\sin^2\theta$ for the diffraction lines of the unknown substance. For the particular determination represented by Fig. 10-1, the errors shown are to be subtracted from the observed values.

10-3 INDEXING PATTERNS OF CUBIC CRYSTALS

A cubic crystal gives diffraction lines whose $\sin^2\theta$ values satisfy the following equation, obtained by combining the Bragg's law with the plane-spacing equation for the cubic system, as in Eq. (3-11):

$$\frac{\sin^2\theta}{(h^2 + k^2 + l^2)} = \frac{\sin^2\theta}{s} = \frac{\lambda^2}{4a^2}. \tag{10-2}$$

Since the sum $s = (h^2 + k^2 + l^2)$ is always integral and $\lambda^2/4a^2$ is a constant for any one pattern, the problem of indexing the pattern of a cubic substance is one of finding a set of integers s which will yield a constant quotient when divided one by one into the observed $\sin^2\theta$ values. (Certain integers, such as 7, 15, 23, 28, 31, etc., are impossible because they cannot be formed by the sum of three squared integers.) Once the proper integers s are found, the indices hkl of each line can be written down by inspection or from the tabulation in Appendix 9.

The proper set of integers s is not hard to find because there are only a few possible sets. Each of the four common cubic lattice types has a characteristic sequence of diffraction lines, described by their sequential s values:

Simple cubic:	1, 2, 3, 4, 5, 6, 8, 9, 10, 11, 12, 13, 14, 16, . . .
Body-centered cubic:	2, 4, 6, 8, 10, 12, 14, 16, . . .
Face-centered cubic:	3, 4, 8, 11, 12, 16, . . .
Diamond cubic:	3, 8, 11, 16, . . .

Each set can be tried in turn. Longer lists can be prepared from Appendix 9. If a set of integers satisfying Eq. (10-2) cannot be found, then the substance involved does not belong to the cubic system, and other possibilities (tetragonal, hexagonal, etc.) must be explored. Note that some s values from the lists shown above may be absent, even though the sample in question properly belongs to one of the three

cubic Bravais lattices. Diamond cubic materials such as Si are FCC, but symmetry, due to presence of two Si atoms per lattice site, dictates that $s = 4, 12$, etc. will be absent.

The following example will illustrate the steps involved in indexing the pattern of a cubic substance and finding its lattice parameter. In this particular example, Cu $K\alpha$ radiation was used and eight diffraction lines were observed. Their $\sin^2\theta$ values are listed in the second column of Table 10-1. Values of $(\sin^2\theta)/s$ for the three cubic Bravais lattices are given in columns 4, 8, and 10 for FCC, simple cubic and BCC, respectively. If the observed lines are from a particular lattice type, the $(\sin^2\theta)/s$ values should be constant. The data in Table 10-1 reveal the material to be fcc. The fifth column lists the lattice parameter calculated from each line position, and the sixth column gives the Miller indices of each line. The systematic error in $\sin^2\theta$ appears as a gradual decrease in the value of $\lambda^2/4a^2$, and a gradual increase in the value of a, as θ increases. As discussed in Chap. 13 that the systematic error in a decreases as θ increases; therefore, the value of a for the highest-angle line, namely, 3.62 Å, is the most accurate of those listed. The analysis of line positions face-centered therefore leads to the conclusion that the substance involved, copper in this case, is cubic in structure with a lattice parameter of 3.62 Å. Certain information about the arrangement of atoms within the unit cell has been obtained, and use of observed line intensities was required in order to obtain this information. In this particular case, the observation consisted simply in noting which lines had zero intensity.

TABLE 10.1

1	2	3	4	5	6	7	8	9	10
			FCC			SC		BCC	
Line	$\sin^2\theta$	$s = (h^2+k^2+l^2)$	$\frac{\sin^2\theta}{s} = \frac{\lambda^2}{4a^2}$	a(Å)	hkl	s	$\frac{\sin^2\theta}{s}$	s	$\frac{\sin^2\theta}{s}$
1	0.140	3	0.0467	3.57	111	1	0.140	2	0.0700
2	0.185	4	0.0463	3.59	200	2	0.093	4	0.0463
3	0.369	8	0.0461	3.59	220	3	0.123	6	0.0615
4	0.503	11	0.0457	3.61	311	4	0.123	8	0.0629
5	0.548	12	0.0457	3.61	222	5	0.110	10	0.0548
6	0.726	16	0.0454	3.62	400	6	0.121	12	0.0605
7	0.861	19	0.0453	3.62	331	8	0.108	14	0.0615
8	0.905	20	0.0453	3.62	420	9	0.101	16	0.0566

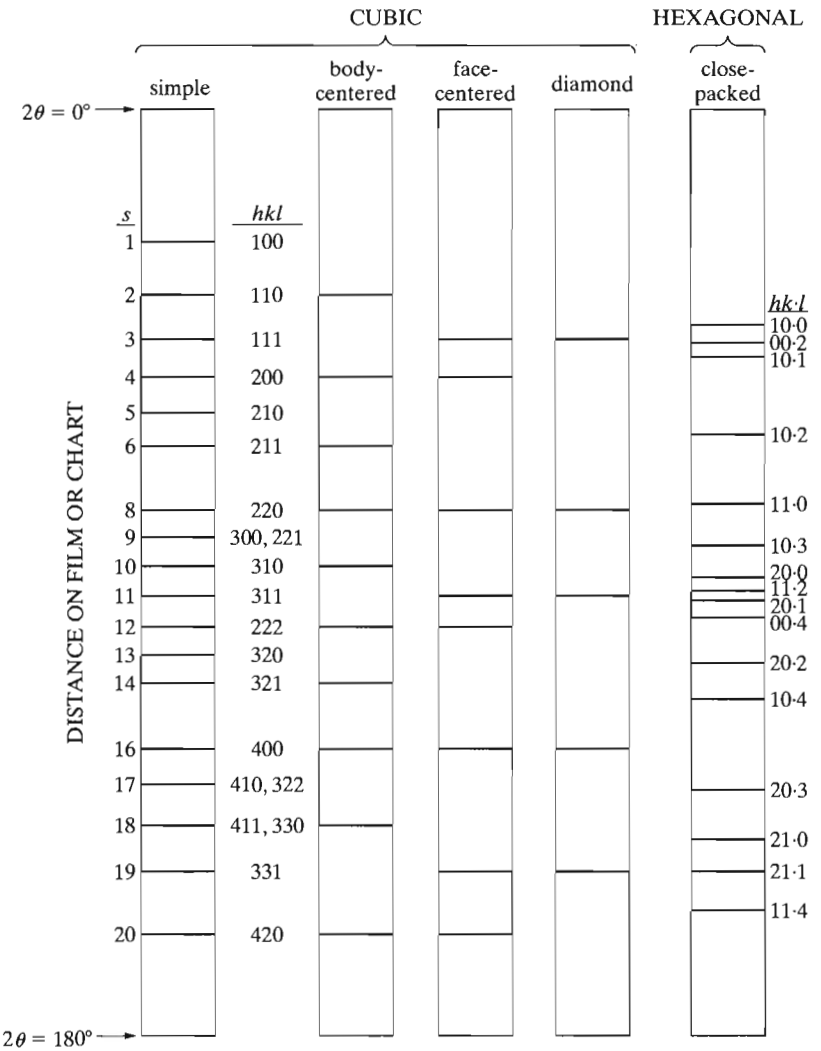

Figure 10-2 Calculated diffraction patterns for various lattices $s = (h^2 + k^2 + l^2)$.

The characteristic line sequences for cubic lattices are shown graphically in Fig. 10-2, in the form of calculated diffraction patterns. The calculations are made for Cu $K\alpha$ radiation and a lattice parameter a of 3.50 Å. The positions of all the diffraction lines which would be formed under these conditions are indicated as they would appear on a film or chart of the length shown. (For comparative purposes, the pattern of a hexagonal close-packed structure is also illustrated, since this structure is frequently encountered. The line positions are calculated for Cu $K\alpha$ radiation, $a = 2.50$ Å, and $c/a = 1.633$, which corresponds to the close packing of spheres.)

Powder patterns of cubic substances can usually be distinguished at a glance from those of noncubic substances, since the latter patterns normally contain many more lines. In addition, the Bravais lattice can usually be identified by inspection: there is an almost regular sequence of lines in simple cubic and body-centered cubic patterns, but the former contains almost twice as many lines, while a face-centered cubic pattern is characterized by a pair of lines, followed by a single line, followed by a pair, another single line, etc.

The problem of indexing a cubic pattern is of course very much simplified if the substance involved is *known* to be cubic and if the lattice parameter is also known. The simplest procedure then is to calculate the value of $\lambda^2/4a^2$ and divide this value into the observed $\sin^2\theta$ values to obtain the value of s for each line.

There is one difficulty that may arise in the interpretation of cubic powder patterns, and that is due to a possible ambiguity between simple cubic and body-centered cubic patterns. There is a regular sequence of lines in both patterns up to the sixth line; the sequence then continues regularly in body-centered cubic patterns, but is interrupted in simple cubic patterns since $s = 7$ is impossible. Therefore, if λ is so large, or a so small, that six lines or less appear on the pattern, the two Bravais lattices are indistinguishable. For example, suppose that the substance involved is actually body-centered cubic but the investigator mistakenly indexes it as simple cubic, assigning the value $s = 1$ to the first lines, $s = 2$ to the second line, etc. He or she thus obtains a value of $\lambda^2/4a^2$ twice as large as the true one, and a value of a which is $1/\sqrt{2}$ times the true one. This mistake becomes apparent when the number of atoms per unit cell is calculated from the measured density of the specimen (Sec. 10-6); the wrong cell size will give a nonintegral value for the number of atoms per cell, and such a value is impossible. The ambiguity in the diffraction pattern itself can be avoided by choosing a wavelength short enough to produce at least seven lines on the pattern.

10-4 INDEXING PATTERNS OF NONCUBIC CRYSTALS

The problem of indexing powder patterns becomes more difficult as the number of unknown parameters increases. There is only one unknown parameter for cubic crystals, the cell edge a, but noncubic crystals have two or more, and special techniques have had to be devlsed in order to index the patterns of such crystals. Graphical methods were the primary method before computers became widespread; availability of spreadsheet programs, for example, allows rapid implementation of routines for indexing diffraction patterns from non-cubic phases. Analytical methods of indexing involve arithmetical manipulation of the observed $\sin^2\theta$ values in an attempt to find certain relationships among them. Since each crystal system is characterised by particular relationships between $\sin^2\theta$ values, recognition of these relationships identifies the crystal system and leads to a solution of the line indices. These analytical methods are due mainly to Hesse and Lipson [10.1, 10.2, G.15, G.32, G.33].

Chapter 13

Precise Parameter Measurements

13-1 INTRODUCTION

Many applications of x-ray diffraction require precise knowledge of the lattice parameter (or parameters) of the material under study. In the main, these applications involve solid solutions; since the lattice parameter of a solid solution varies with the concentration of the solute, the composition of a given solution can be determined from a measurement of its lattice parameter. Thermal expansion coefficients can also be determined, without a dilatometer, by measurements of lattice parameter as a function of temperature in a high-temperature camera or diffractometer. Since, in general, a change in solute concentration or temperature produces only a small change in lattice parameter, rather precise parameter measurements must be made in order to measure these quantities with any accuracy. This chapter concentrates on the methods used to obtain high precision with polycrystalline samples, leaving the various applications to be discussed elsewhere. Cubic substances will be covered first, because they are the simplest, but the general conclusions will also be valid for noncubic materials, which will be discussed in detail later.

The process of measuring a lattice parameter is a very indirect one, and is fortunately of such a nature that high precision is fairly easily obtained. The parameter a of a cubic substance is directly proportional to the spacing d of any particular set of Bragg planes. Measuring the Bragg angle θ for hkl and using Bragg's law to determine d allows calculation of a. But it is sin θ, not θ, which appears in Bragg's law. Precision in d, or a, therefore depends on precision in sin θ, a derived quantity, and not on precision in θ, the measured quantity. This is fortunate because the value of sin θ changes very slowly with θ in the neighborhood of 90°, as inspection of Fig. 13-1 or a table of sines will show. For this reason, a very accurate value of sin θ can be obtained from a measurement of θ which is itself not particularly precise, *provided that* θ *is near* 90°. For example, an error in θ of 1° leads to an error in sin θ

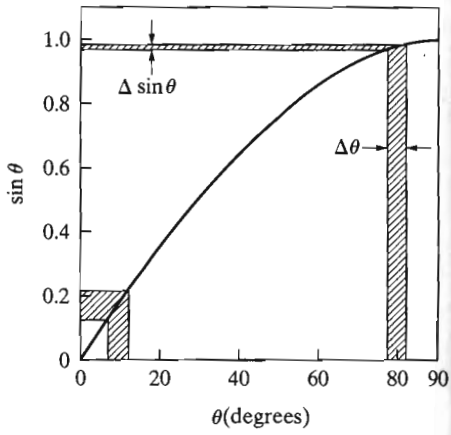

Figure 13-1 The variation of sin θ with θ. The error in sin θ caused by a given error in θ decreases as θ increases ($\Delta\theta$ exaggerated).

of 1.7 percent at $\theta = 45^\circ$ but only 0.15 percent at $\theta = 85^\circ$. Stated in another way, the angular position of a diffracted beam is much more sensitive to a given change in plane spacing when θ is large than when it is small.

The same result follows directly from differentiation of Bragg's law with respect to θ:

$$\frac{\Delta \mathrm{d}}{\mathrm{d}} = \frac{\Delta\lambda}{\lambda} - \cot\theta\Delta\theta. \tag{13-1}$$

Neglecting $\Delta\lambda$ yields

$$\frac{\Delta d}{d} = -\cot\theta\Delta\theta. \tag{13-2}$$

In the cubic system,

$$a = d\sqrt{h^2 + k^2 + l^2}.$$

Therefore

$$\frac{\Delta a}{a} = \frac{\Delta d}{d} = -\cot\theta\Delta\theta. \tag{13-3}$$

Since $\cot\theta$ approaches zero as θ approaches 90°, $\Delta a/a$, the fractional error in a caused by a given error in θ, also approaches zero as θ approaches 90°, or as 2θ approaches 180°. The key to precision in parameter measurements therefore lies in the use of back reflected beams having 2θ values as near to 180° as possible.

Although the parameter error disappears as 2θ approaches 180°, diffracted beams cannot be observed at this angle. Because the values of a calculated for the various lines on the pattern approach the true value more closely as 2θ increases, the true value of a should be found simply by plotting the measured values against 2θ and extrapolating to $2\theta = 180^\circ$. Unfortunately, this curve is not linear and the

extrapolation of a nonlinear curve is not accurate. If the measured values of a are plotted against certain functions of θ, however, rather than against θ or 2θ directly, the resulting curve is a straight line which may be extrapolated with confidence. The bulk of this chapter is devoted to showing how these functions can be derived and used. Because the exact form of the function depends on the geometry of the apparatus used to record the diffraction pattern, the nature and functional dependence of systematic errors must be examined before extrapolation procedures can be discussed.

Prior to developing such a mathematical understanding, it is important to appreciate what sort of precision is possible. Without any extrapolation or any particular attention to good experimental technique, simply by selection of the parameter calculated for the highest-angle line on the pattern, a precision of 0.01 Å usually results. Since the lattice parameters of many engineering materials are in the neighborhood of 3 to 4 Å, this represents a precision of about 0.3 percent. With good experimental technique and the use of the proper extrapolation function, this precision can be increased to 0.001 Å, or 0.03 percent, without much difficulty. Finally, about the best precision that can be expected is 0.0001 Å, or 0.003 percent, but this can be obtained only by the expenditure of considerable effort, both experimental and computational.

In work of high precision it is imperative that the units in which the measured parameter is expressed, kX or Å, be correctly stated. In order to avoid confusion on this point, the reader is advised to review the discussion of these units given in Sec. 3-7. The actual *numerical value* of the wavelength or wavelengths used in the determination of the parameter should be explicitly stated.

Methods of determining lattice parameters with high precision are reviewed by Barrett and Massalski [G.10], Klug and Alexander [G.17], Parrish and Wilson [G.13], Azaroff and Buerger [G.33], and Jenkins and Snyder [G.25]

DIFFRACTOMETERS

The general approach in finding an extrapolation function is to consider the various effects which can lead to errors in the measured values of θ, and to find out how these errors in θ vary with the angle θ itself. The diffractometer is a complex apparatus and therefore subject to misalignment of its component parts. A further difficulty with most commercial diffractometers is the impossibility of observing the same back-reflected cone of radiation on both sides of the incident beam. Thus, the experimenter has no automatic check on the accuracy of the angular scale of the instrument or the precision of its alignment.

When a diffractometer is used to measure d-spacings, the more important sources of systematic error in d are the following:

1. Misalignment of the instrument. In particular, the center of the incident beam must intersect the diffractometer axis and the 0° position of the detector slit.

2. Use of a flat specimen instead of a specimen curved to conform to the focusing circle. This error is minimized, with loss of intensity, by decreasing the irradiated width of the specimen by means of an incident beam of small horizontal divergence.
3. Absorption in the specimen. Specimens of low absorption should be made as thin as possible.
4. Displacement of the specimen from the diffractometer axis (Fig. 13-2) This is usually the largest single source of error. It causes an error in d given by

$$\frac{\Delta d}{d} = -\frac{D \cos^2 \theta}{R \sin \theta}, \tag{13-4}$$

where D is the specimen displacement parallel to the diffraction-plane normal (positive when the displacement is in front of the axis) and R is the diffractometer radius (Problem 13-6).
5. Vertical divergence of the incident beam. This error is minimized, with loss of intensity, by decreasing the vertical opening of the detector slit.

The functional forms of the various systematic errors in peak position are summarized elsewhere [G.26], but no single extrapolation function can be completely satisfactory, because $\Delta d/d$ varies as $\cos^2 \theta$ for errors (2) and (3) but as $\cos^2 \theta / \sin \theta$ for error (4). Often the effect of (5) is included in the extrapolation function so that $\Delta d/d$ varies as $[\cos^2 \theta / \sin \theta + \cos^2 \theta / \theta]$. The sum in the brackets is termed the Nelson-Riley function and is used primarily for data collected with Hull/Debye–Scherrer camera (Sec. 13-3). Extrapolation against $\cos^2 \theta$ is often

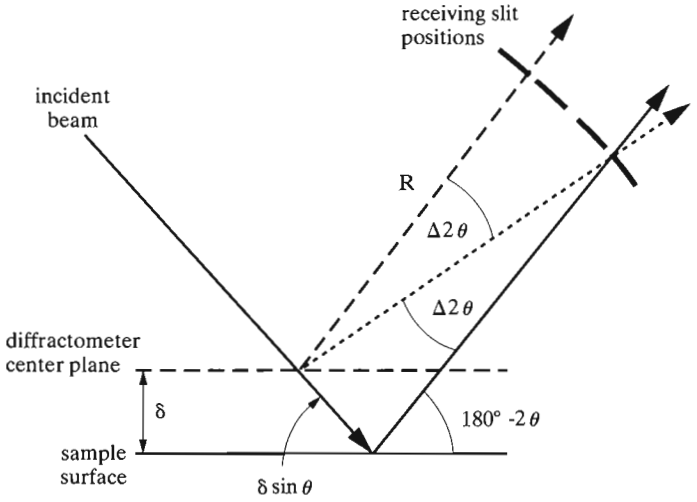

Figure 13-2. Illustration of shift of peak position $\Delta 2\theta$ as a function of sample displacement.

termed the Bradley-Jay method and is valid only for diffraction peaks with $\theta > 60°$. Presumably the function that gives the better straight line will disclose what error is predominant.

The suggested procedure is therefore:

a) Carefully align the component parts of the instrument in accordance with the manufacturer's instructions.
b) Adjust the specimen surface to coincide as closely as possible with the diffractometer axis.
c) Extrapolate the calculated parameters against $\cos^2\theta/\sin\theta$ or $\cos^2\theta$ to a value of $\theta = 90°$.

For a cubic crystal with a lattice parameter a_0 and an extrapolation based on displacement error,

$$\frac{\Delta d}{d} = \frac{\Delta a}{a_0} = \frac{a - a_0}{a_0} = k_1 \frac{\cos^2\theta}{\sin\theta}, \tag{13-5}$$

and, after rearranging terms, the apparent lattice parameter a is

$$a = a_0 + a_0 k_1 \frac{\cos^2\theta}{\sin\theta}. \tag{13-6}$$

If a Nelson-Riley extrapolation function is appropriate,

$$\frac{a - a_0}{a} = k_2 \left[\frac{\cos^2\theta}{\sin\theta} + \frac{\cos^2\theta}{\theta} \right] \tag{13-7}$$

which converts to

$$a = a_0 - a_0 k_2 \left[\frac{\cos^2\theta}{\sin\theta} + \frac{\cos^2\theta}{\theta} \right]. \tag{13-8}$$

A similar equation applies for the Bradley-Jay function. Note that all of these extrapolation functions yield $a = a_0$ at $\theta = 90°$.

Every effort should, of course, be made to measure line positions precisely. To achieve a precision of 3 parts in 100,000, equivalent to ±0.0001 Å in the lattice parameter, Eq. (13-2) shows that the 2θ position of a line at $2\theta = 160°$ must be measured to within 0.02° and lower angle lines even more closely. Recording peaks with ratemeter output and continuous scanning can be problematic, and step scanning should be used. Before computerized diffractometers were available it was customary to take the 2θ value of the peak's maximum intensity as the line position; now peak centroids or more sophisticated methods for establishing peak position (which are standard in the field of stress measurement, see 6-13 for further details) are recommended.

Noncubic crystals present additional difficulties, regardless of the particular extrapolation function chosen. Consider, for example, hexagonal and tetragonal crystals. The difficulty is simply this: the position of a line which has indices *hkl* is determined by two parameters, a and c, and it is impossible to calculate both of them from the observed $\sin^2\theta$ value of that line alone. One way of avoiding this difficulty is to ignore the *hkl* lines and divide the remainder into two groups, those with indices *hk*0 and those with indices 00*l*. A value of a is calculated for each *hk*0 line and a value of c from each 00*l* line; two separate extrapolations are then made to find a_0 and c_0. Since there are usually very few *hk*0 and 00*l* lines in the back-reflection region, the extrapolations necessarily will be less accurate. Instead, it is better to use Cohen's analytical method (Sec. 13-7) for noncubic substances.

Extrapolation should be done with least squares fitting of the data and the extrapolation function chosen to represent the systematic errors. Use of least squares eliminates the variability in how different individuals assign a straight line through the same set of points, and most pocket calculators and computer spreadsheet programs have built-in routines for least squares fitting of data.

It should be noted that the least-squares fitting is not a way of finding the best curve to fit a given set of observations. The investigator must know at the outset, from an understanding of the phenomenon involved, the kind of relation (linear, parabolic, exponential, etc.) the two quantities x and y are supposed to obey. All the least-squares method can do is to give the best values of the constants in the equation selected, but it does this in a quite objective and unbiased manner.

To conclude this section, a few general remarks on the nature of errors may not be amiss. In the measurement of a lattice parameter, as in many other physical observations, two kinds of error are involved, *systematic* and *random*. A systematic error is one which varies in a regular manner with some particular parameter. Further, a systematic error is always of the same sign. Random errors, on the other hand, are the ordinary chance errors involved in any direct observation; they may be positive or negative and do not vary in any regular manner with the 2θ position of the diffraction line.

Systematic errors in a approach zero as θ approaches 90° and may be eliminated by use of the proper extrapolation function. The magnitude of these errors is proportional to the slope of the extrapolation line and, if these errors are small, the line will be quite flat. If the systematic errors were increased on purpose, say, by displacing the sample from the diffractometer axis, the slope of the line will increase but the extrapolated value of a_0 will remain the same. The random errors involved in measuring line positions show up as random errors in a, and are responsible for the deviation of the various points from the extrapolation line. The random errors in a also decrease in magnitude as θ increases, due essentially to the slow variation of $\sin\theta$ with θ at large angles.

These various effects are summarized graphically in Fig. 13-3. In (a) the calculated points conform quite closely to the line, indicating small random errors, but the line itself is quite steep because of large systematic errors. The opposite situation is shown in (b): here the systematic error is small, but the wide scatter of the

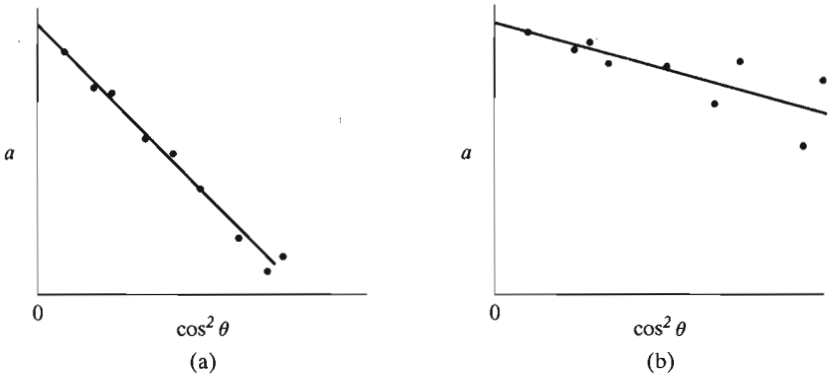

Figure 13-3 Extreme forms of extrapolation curves (schematic): (a) large systematic errors, small random errors; (b) small systematic errors, large random errors.

points shows that large random errors have been made. Inasmuch as the uncertainty in a regression line increases with the degree of scatter, it is obvious that every possible effort should be made to minimize random errors at the start.

13-3 HULL/DEBYE–SCHERRER CAMERAS

Historically, extrapolation methods were developed for the Hull/Debye–Scherrer camera, and, even though this method normally would not be chosen today for lattice parameter measurements, it is instructive to go through some of the geometry leading to the extrapolation functions.

For a Hull/Debye–Scherrer camera, the chief sources of error in θ are the following:

1. Film shrinkage.
2. Incorrect camera radius.
3. Off-centering of specimen.
4. Absorption in specimen.

Since only the back-reflection region is suitable for precise measurements, consider these various errors in terms of the quantities S' and ϕ, defined in Fig. 13-4. S' is the distance on the film between two corresponding back-reflection lines; 2ϕ is the supplement of 2θ, i.e., $\phi = 90^\circ - \theta$. These quantities are related to the camera radius R by the equation

$$\phi = \frac{S'}{4R}. \tag{13-9}$$

Shrinkage of the film, caused by processing and drying, causes an error $\Delta S'$ in the quantity S'. The camera *radius* may also be in error by an amount ΔR. The effects

tion which is highly absorbed, and γ and β small, by using a diffractometer at low values of 2θ. [3] By these means the depth of penetration can often be made surprisingly small. For instance, if a steel specimen is examined in a diffractometer with Cu $K\alpha$ radiation, 95 percent of the information afforded by the lowest angle line of ferrite (the 110 line at $2\theta = 45°$) applies to a depth of only 2 μm. There are limits, of course, to reducing the depth of x-ray penetration, and when information is required from very thin surface films, electron diffraction, glancing angle diffraction, or x-ray reflectivity are far more suitable tools.

Although the diffracted beam in any reflection method comes only from a very thin surface layer, it must not be supposed that the information on a diffraction pattern obtained by a transmission method is truly representative of the entire cross section of the specimen. Calculations such as those given above show that a greater proportion of the total diffracted energy originates in a layer of given thickness on the back side of the specimen (the side from which the transmitted beam leaves) than in a layer of equal thickness on the front side. If the specimen is highly absorbing, a transmission method can be almost as nonrepresentative of the entire specimen as a back-reflection method, in that most of the diffracted energy will originate in a thin surface layer. See Problem 14-5.

14-6 SIZE AND STRAIN SEPARATION

As indicated in Sec. 14-4, separating the different contributions to line broadening, if present, requires use of multiple diffraction peaks and analysis of the peaks' shapes. The quality of the diffraction pattern, or more specifically the diffraction peaks and their tails, must be very high if the somewhat involved Fourier analysis pioneered by Warren is to be worthwhile [e.g., 14.3 - 14.6, Chap. 7 of 6.7, Chap. 9 of G.17, Chap. 13 of G.20, and Chap. 8 of G.35]. Other simpler approaches using peak widths have their place in analyzing size and strain broadening.

It is important to realize that crystallite sizes obtained from peak width measurements give volume-average sizes whereas those from peak shape analysis give number-averages. This can be seen by comparing a histogram of average crystallite diameters observed with TEM (Fig. 14-7) with the average diameter determined from diffractometry and the Scherrer equation (Eq. 5-2) [14.7]. The sample was a dilute mixture of platinum nanoparticles in an amorphous silica matrix, the diffraction pattern of the sample appears in Fig. 14-2 and Table 14-1 lists the crystallite sizes obtained from the x-ray diffraction peaks and Scherrer's equation. The crystallite size averaged 38 Å from TEM and 50 Å from the FWHM of the x-ray diffraction peaks. A small number of very large crystallites were noted during TEM of the samples, and simulation of the diffraction peaks [14.8] produced by a small number of large crystallites mixed with a much larger number of 35-40 Å crystal-

[3] Some of these requirements may be contradictory. For example, in measuring the lattice parameter of a thin surface layer with a diffractometer, a compromise must be found between the low value of θ required for shallow penetration and the high value of θ required for precise parameter measurements.

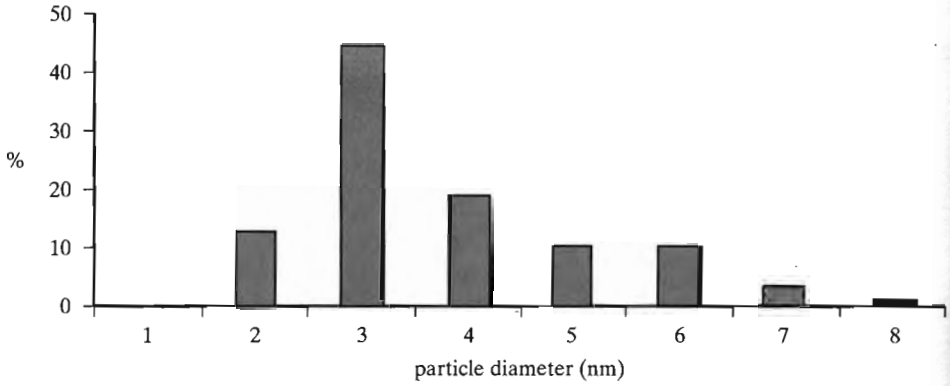

Figure 14-7 Histogram of Pt nanocluster size as observed by TEM in a Pt/silica xerogel nanocomposite [14.10].

lites reveals that this is the probable origin of the difference between TEM and X-ray FWHM sizes.

Contributions from crystallite size, micro strain and instrumental effects can be separated in a straight-forward fashion if the peaks are Lorentzian- or Gaussian-shaped. If

B_{exp} is the experimentally measured FWHM,
B_{size} is the FWHM due to crystallite size,
B_{strain} is the FWHM due to micro strain and
B_{inst} is the FWHM due to the instrument,
then for Lorentzian peaks

$$B_{exp} = B_{size} + B_{strain} + B_{inst} \tag{14-8}$$

and for Gaussian peaks

$$B^2_{exp} = B^2_{size} + B^2_{strain} + B^2_{inst}. \tag{14-9}$$

Correction for the instrumental width in either case can be obtained by recording a diffraction pattern, under identical conditions, of the same substance but in a well-annealed, large-grained condition.

Separation of size and strain components can be done by plotting $B \cos \theta$ as a function of $\sin \theta$ (Fig. 14-8); this type of plot is known as a Williamson-Hall plot [14.9] and implicitly assumes that peak shapes are Lorentzian. Rearranging the terms of Eq. 5-2 produces

$$B \cos \theta = 0.9\lambda/t \tag{14-10}$$

and of Eq. 5-9 yields

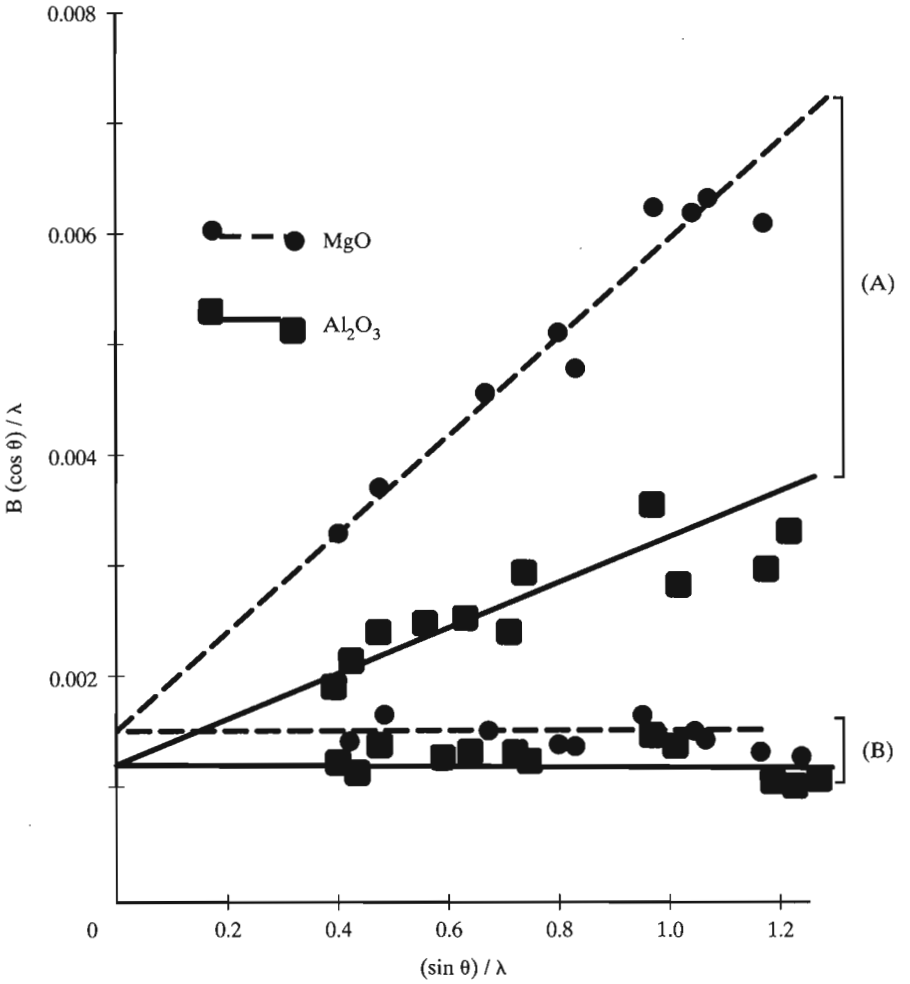

Figure 14-8 Williamson-Hall plot for MgO and Al_2O_3, curves (A) ball milled for 2 hours and (B) ball milled for 2 hours, then annealed for 2 hours at 1350° C. After Lewis and Lindley [14.10].

$$\beta \cos\theta = -2(\Delta d/d) \sin\theta. \tag{14-11}$$

If size broadening is the only significant contribution to peak width, then $B_{exp} \cos\theta$ is a constant for all peaks (i.e., its Williamson-Hall plot is a horizontal line). If strain broadening is the important contribution, $B_{exp} \cos\theta$ is a linear function of $\sin\theta$. Figure 14-8 shows data for two oxide ceramics in two conditions: after ball milling and ball milling followed by annealing at 1350 C for 2 hr [14.10]. As one would expect, ball milling produces less microstrain in Al_2O_3, a substance which is often used to polish solid samples prior to optical microscopy, and the crystallite size of

the two oxides is similar. The crystallite size remained constant after annealing, but virtually all of the strain was relieved.

CRYSTAL ORIENTATION

14-7 GENERAL

Each grain in a polycrystalline aggregate normally has a crystallographic orientation different from that of its neighbors. Considered as a whole, the orientations of all the grains may be randomly distributed in relation to some selected frame of reference, or they may tend to cluster, to a greater or lesser degree, about some particular orientation or orientations. Any aggregate characterized by the latter condition is said to have a *preferred orientation, or texture*, which may be defined simply as a condition in which the distribution of crystal orientations is nonrandom As discussed in Chap. 4 preferred orientation can have a profound effect on diffracted intensities measured by diffractometry.

Preferred orientation is a very common condition. Among metals and alloys it is most evident in wire and sheet, and the kinds of texture found in these products are treated below. The preferred orientation that is produced by the forming process itself (wire drawing or sheet rolling) is called a *deformation texture*. It is due to the tendency of the grains in a polycrystalline aggregate to rotate during plastic deformation; each grain undergoes slip and rotation in a complex way that is determined by the imposed forces and by the slip and rotation of adjoining grains; the result is a preferred, nonrandom orientation. When the cold-worked metal, possessed of a deformation texture, is recrystallized by annealing, the new grain structure usually has a preferred orientation too, often different from that of the cold-worked material. This is called a *recrystallization texture* or *annealing texture*. It is due to the influence which the texture of the cold-worked matrix has on the nucleation and/or growth of the new grains in that matrix.

Preferred orientation is not confined to metallurgical products. It also exists in rocks, in ceramics, in semiconductor thin films and other coatings and in both natural and artificial polymeric fibers and sheets. In fact, preferred orientation is generally the rule, not the exception, and the preparation of an aggregate with completely random crystal orientations is a difficult matter.

The industrial importance of preferred orientation lies in the effect, often very marked, which it has on the overall, macroscopic properties of materials. Given the fact that all single crystals are anisotropic, i.e., have different properties in different directions, it follows that an aggregate having preferred orientation must also have directional properties to a greater or lesser degree. Such properties may or may not be beneficial, depending on the intended use of the material. For example, sheet steel for the cores of small electric motors should have, for magnetic reasons, all grains oriented with their {100} planes parallel to the sheet surface. But this texture would not be satisfactory if the steel were to be formed into a cup by deep drawing: here a texture with {111} planes parallel to the surface would make the steel less

Appendix 3

Lattice Geometry

A3-1 PLANE SPACINGS

The value of d, the distance between adjacent planes in the set (hkl), may be found from the following equations.

Cubic:
$$\frac{1}{d^2} = \frac{h^2 + k^2 + l^2}{a^2}$$

Tetragonal:
$$\frac{1}{d^2} = \frac{h^2 + k^2}{a^2} + \frac{l^2}{c^2}$$

Hexagonal:
$$\frac{1}{d^2} = \frac{4}{3}\left(\frac{h^2 + hk + k^2}{a^2}\right) + \frac{l^2}{c^2}$$

Rhombohedral:
$$\frac{1}{d^2} = \frac{(h^2 + k^2 + l^2)\sin^2\alpha + 2(hk + kl + hl)\cos^2\alpha - \cos\alpha)}{a^2(1 - 3\cos^2\alpha + 2\cos^3\alpha)}$$

Orthorhombic:
$$\frac{1}{d^2} = \frac{h^2}{a^2} + \frac{k^2}{b^2} + \frac{l^2}{c^2}$$

Monoclinic:
$$\frac{1}{d^2} = \frac{1}{\sin^2\beta}\left(\frac{h^2}{a^2} + \frac{k^2\sin^2\beta}{b^2} + \frac{l^2}{c^2} - \frac{2hl\cos\beta}{ac}\right)$$

Triclinic:
$$\frac{1}{d^2} = \frac{1}{V^2}(S_{11}h^2 + S_{22}k^2 + S_{33}l^2 + 2S_{12}hk + 2S_{23}kl + 2S_{13}hl)$$

In the equation for triclinic crystals,

V = volume of unit cell (see below),

$$S_{11} = b^2c^2\sin^2\alpha,$$

$$S_{22} = a^2c^2\sin^2\beta,$$

$$S_{33} = a^2b^2\sin^2\gamma,$$

$$S_{12} = abc^2(\cos\alpha\cos\beta - \cos\gamma),$$

$$S_{23} = a^2bc(\cos\beta\cos\gamma - \cos\alpha),$$

$$S_{13} = ab^2c(\cos\gamma\cos\alpha - \cos\beta).$$

A3-2 CELL VOLUMES

The following equations give the volume V of the unit cell.

Cubic: $V = a^3$

Tetragonal: $V = a^2c$

Hexagonal: $V = \dfrac{\sqrt{3}a^2c}{2} = 0.866a^2c$

Rhombohedral: $V = a^3\sqrt{1 - 3\cos^2\alpha + 2\cos^2\alpha}$

Orthorhombic: $V = abc$

Monoclinic: $V = abc\sin\beta$

Triclinic: $V = abc\sqrt{1 - \cos^2\alpha - \cos^2\beta - \cos^2\gamma + 2\cos\alpha\,\cos\beta\,\cos\gamma}$

A3-3 INTERPLANAR ANGLES

The angle ϕ between the plane $(h_1k_1l_1)$, of spacing d_1, and the plane $(h_2k_2l_2)$, of spacing d_2, may be found from the following equations. (V is the volume of the unit cell.)

Cubic: $$\cos\phi = \frac{h_1h_2 + k_1k_2 + l_1l_2}{\sqrt{(h_1^2 + k_1^2 + l_1^2)(h_2^2 + k_2^2 + l_2^2)}}$$

Tetragonal: $$\cos\phi = \frac{\dfrac{h_1h_2 + k_1k_2}{a^2} + \dfrac{l_1l_2}{c^2}}{\sqrt{\left(\dfrac{h_1^2 + k_1^2}{a^2} + \dfrac{l_1^2}{c^2}\right)\left(\dfrac{h_2^2 + k_2^2}{a^2} + \dfrac{l_2^2}{c^2}\right)}}$$

Hexagonal:

$$\cos\phi = \frac{h_1h_2 + k_1k_2 + \frac{1}{2}(h_1k_2 + h_2k_1) + \dfrac{3a^2}{4c^2}l_1l_2}{\sqrt{\left(h_1^2 + k_1^2 + h_1k_1 + \dfrac{3a^2}{4c^2}l_1^2\right)\left(h_2^2 + k_2^2 + h_2k_2 + \dfrac{3a^2}{4c^2}l_2^2\right)}}$$

Rhombohedral:

$$\cos\phi = \frac{a^4 d_1 d_2}{V^2}\left[\sin^2\alpha(h_1h_2 + k_1k_2 + l_1l_2)\right.$$
$$\left.+(\cos^2\alpha - \cos\alpha)(k_1l_2 + k_2l_1 + l_1h_2 + l_2h_1 + h_1k_2 + h_2k_1)\right]$$

Orthorhombic:
$$\cos\phi = \frac{\dfrac{h_1h_2}{a^2} + \dfrac{k_1k_2}{b^2} + \dfrac{l_1l_2}{c^2}}{\sqrt{\left(\dfrac{h_1^2}{a^2} + \dfrac{k_1^2}{b^2} + \dfrac{l_1^2}{c^2}\right)\left(\dfrac{h_2^2}{a^2} + \dfrac{k_2^2}{b^2} + \dfrac{l_2^2}{c^2}\right)}}$$

Monoclinic:

$$\cos\phi = \frac{d_1d_2}{\sin^2\beta}\left[\frac{h_1h_2}{a^2} + \frac{k_1k_2\sin^2\beta}{b^2} + \frac{l_1l_2}{c^2} - \frac{(l_1h_2 + l_2h_1)\cos\beta}{ac}\right]$$

Triclinic:

$$\cos\phi = \frac{d_1d_2}{V^2}\left[S_{11}h_1h_2 + S_{22}k_1k_2 + S_{33}l_1l_2\right.$$
$$\left.+S_{23}(k_1l_2 + k_2l_1) + S_{13}(l_1h_2 + l_2h_1) + S_{12}(h_1k_2 + h_2k_1)\right]$$

Appendix 9

Quadratic Forms of Miller Indices

	Cubic				Hexagonal	
$h^2+k^2+l^2$	hkl				h^2+hk+k^2	hk
	Simple	Face-centered	Body-centered	Diamond		
1	100				1	10
2	110	. . .	110		2	
3	111	111	. . .	111	3	11
4	200	200	200		4	20
5	210				5	
6	211	. . .	211		6	
7					7	21
8	220	220	220	220	8	
9	300, 221				9	30
10	310	. . .	310		10	
11	311	311	. . .	311	11	
12	222	222	222		12	22
13	320				13	31
14	321	. . .	321		14	
15					15	
16	400	400	400	400	16	40
17	410, 322				17	
18	411, 330	. . .	411, 330		18	
19	331	331	. . .	331	19	32
20	420	420	420		20	
21	421				21	41
22	332	. . .	332		22	
23					23	
24	422	422	422	422	24	
25	500, 430				25	50
26	510, 431	. . .	510, 431		26	
27	511, 333	511, 333	. . .	511, 333	27	33
28					28	42
29	520, 432				29	
30	521	. . .	521		30	
31					31	51
32	440	440	440	440	32	
33	522, 441				33	
34	530, 433	. . .	530, 433		34	
35	531	531	. . .	531	35	
36	600, 442	600, 442	600, 442		36	60
37	610				37	43
38	611, 532	. . .	611, 532		38	
39					39	52
40	620	620	620	620	40	
41	621, 540, 443				41	
42	541	. . .	541		42	
43	533	533	. . .	533	43	61
44	622	622	622		44	
45	630, 542				45	
46	631	. . .	631		46	
47					47	
48	444	444	444	444	48	44
49	700, 632				49	70, 53

	Cubic				Hexagonal	
	hkl					
$h^2 + k^2 + l^2$	Simple	Face-centered	Body-centered	Diamond	$h^2 + hk + k^2$	*hk*
50	710, 550, 543	. . .	710, 550, 543		50	
51	711, 551	711, 551	. . .	711, 551	51	
52	640	640	640		52	62
53	720, 641				53	
54	721, 633, 552	. . .	721, 633, 552		54	
55					55	
56	642	642	642	642	56	
57	722, 544				57	71
58	730	. . .	730		58	
59	731, 553	731, 553	. . .	731, 553	59	

Name and formula

Reference code:	00-010-0173
Mineral name:	Corundum, syn
Compound name:	Aluminum Oxide
Common name:	diamonite
PDF index name:	Aluminum Oxide
Empirical formula:	Al_2O_3
Chemical formula:	Al_2O_3

Crystallographic parameters

Crystal system:	Rhombohedral
Space group:	R-3c
Space group number:	167
a (Å):	4.7580
b (Å):	4.7580
c (Å):	12.9910
Alpha (°):	90.0000
Beta (°):	90.0000
Gamma (°):	120.0000
Calculated density (g/cm^3):	3.99
Measured density (g/cm^3):	4.05
Volume of cell (10^6 pm^3):	254.70
Z:	6.00
RIR:	1.00

Subfiles and quality

Subfiles:	Alloy, metal or intermetalic Cement and Hydration Product Common Phase Corrosion Educational pattern Forensic Inorganic Mineral NBS pattern Superconducting Material
Quality:	Indexed (I)

Comments

Color:	Blue, colorless, yellow purple to violet, green, pink to deep pigeon-blood red
Creation Date:	1/1/1970
Modification Date:	1/1/1970
Optical Data:	A=1.7604, B=1.7686, Sign=-
Melting Point:	2050°
Color:	Blue, colorless, yellow purple to violet, green, pink to deep pigeon-blood red
Sample Preparation:	Sample annealed at 1400 C for four hours in an Al_2O_3 crucible
Analysis:	Spectroscopic analysis showed <0.1% K, Na, Si; <0.01% Ca, Cu, Fe, Mg, Pb; <0.001% B, Cr, Li, Mn, Ni
Temperature of Data Collection:	Pattern taken at 26 C
Common Name:	Also called: ruby. Common Name: Also called: sapphire. Additional Patterns: See ICSD 60419 (PDF 77-2135). Additional Patterns: To replace 43-1484.

References

Primary reference: Natl. Bur. Stand. (U.S.), Circ. 539, **9**, 3, (1960)
Optical data: Dana's System of Mineralogy, 7th Ed., **I**, 520

Peak list

No.	h	k	l	d [A]	2Theta[deg]	I [%]
1	0	1	2	3.47900	25.584	75.0
2	1	0	4	2.55200	35.137	90.0
3	1	1	0	2.37900	37.785	40.0
4	0	0	6	2.16500	41.685	1.0
5	1	1	3	2.08500	43.363	100.0
6	2	0	2	1.96400	46.184	2.0
7	0	2	4	1.74000	52.553	45.0
8	1	1	6	1.60100	57.519	80.0
9	2	1	1	1.54600	59.769	4.0
10	1	2	2	1.51400	61.166	6.0
11	0	1	8	1.51000	61.345	8.0
12	2	1	4	1.40400	66.548	30.0
13	3	0	0	1.37400	68.198	50.0
14	1	2	5	1.33700	70.359	2.0
15	2	0	8	1.27600	74.268	4.0
16	1	0	10	1.23900	76.882	16.0
17	1	1	9	1.23430	77.229	8.0
18	2	2	0	1.18980	80.695	8.0
19	3	0	6	1.16000	83.219	1.0
20	2	2	3	1.14700	84.378	6.0
21	1	3	1	1.13820	85.184	2.0
22	3	1	2	1.12550	86.378	6.0
23	1	2	8	1.12460	86.464	4.0
24	0	2	10	1.09880	89.021	8.0
25	0	0	12	1.08310	90.665	4.0
26	1	3	4	1.07810	91.204	8.0
27	2	2	6	1.04260	95.263	14.0
28	0	4	2	1.01750	98.410	2.0
29	2	1	10	0.99760	101.095	12.0
30	1	1	12	0.98570	102.792	1.0
31	4	0	4	0.98190	103.349	4.0
32	3	2	1	0.94310	109.526	1.0
33	1	2	11	0.94130	109.837	1.0
34	3	1	8	0.93450	111.033	4.0
35	2	2	9	0.91780	114.130	4.0
36	3	2	4	0.90760	116.146	14.0
37	0	1	14	0.90520	116.635	4.0
38	4	1	0	0.89910	117.906	8.0
39	2	3	5	0.88840	120.239	1.0
40	4	1	3	0.88040	122.077	4.0
41	0	4	8	0.86980	124.652	2.0
42	1	3	10	0.85800	127.737	12.0
43	3	0	12	0.85020	129.923	4.0
44	2	0	14	0.84600	131.155	4.0
45	1	4	6	0.83030	136.170	22.0
46	1	1	15	0.81370	142.405	4.0
47	4	0	10	0.80720	145.218	11.0
48	0	5	4	0.79880	149.298	7.0
49	1	0	16	0.79700	150.255	14.0
50	3	3	0	0.79310	152.457	13.0

Stick Pattern

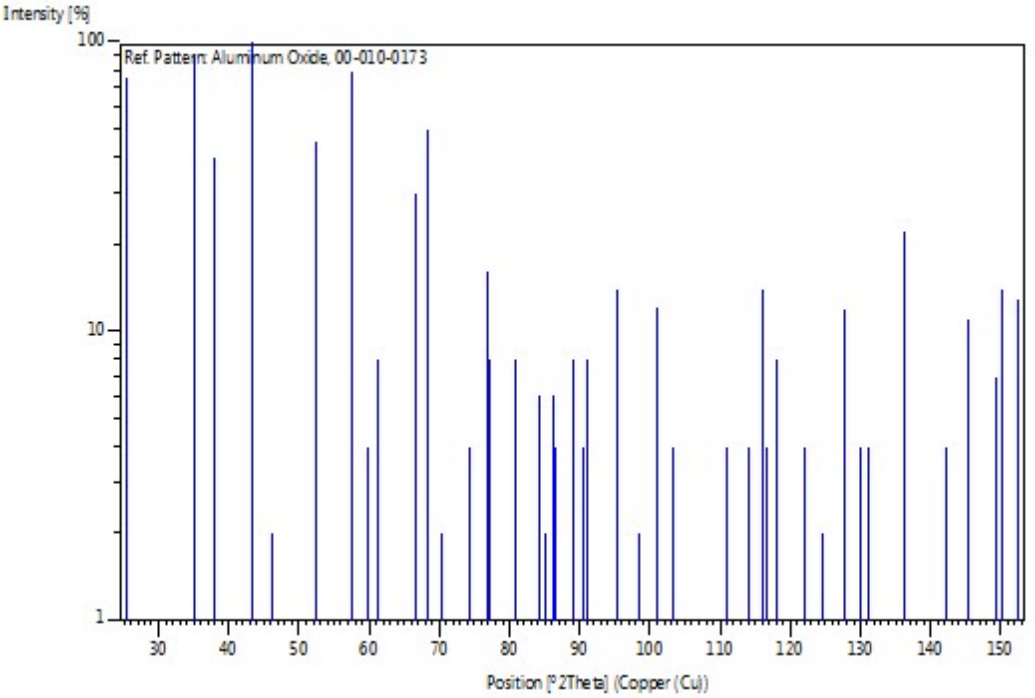

Status Primary **QM:** Star (S) **Pressure/Temperature:** Ambient **Chemical Formula:** Zn O
Empirical Formula: O Zn **Weight %:** O19.66 Zn80.34 **Atomic %:** O50.00 Zn50.00
Compound Name: Zinc Oxide **Mineral Name:** Zincite, syn **Common Name:** zinc white, chinese white

Radiation: CuKá1 **:** 1.5406Å **Filter:** Graph Mono **d-Spacing:** Diff. **Cutoff:** 17.70
Intensity: Diffractometer

SYS: Hexagonal **SPGR:** P63mc (186)
Author's Cell [AuthCell a: 3.24982(9)Å **AuthCell c:** 5.20661(15)Å **AuthCell Vol:** 47.62Å³
AuthCell Z: 2.00 **AuthCell MolVol:** 23.81 **]** **Author's Cell Axial Ratio [c/a:** 1.602 **]** **Dcalc:** 5.675g/cm³
SS/FOM: F(27) = 129.6(0.0072, 29)

Space Group: P63mc (186) **Molecular Weight:** 81.38
Crystal Data [XtlCell a: 3.250Å **XtlCell b:** 3.250Å **XtlCell c:** 5.207Å **XtlCell :** 90.00° **XtlCell :** 90.00°
XtlCell : 120.00° **XtlCell Vol:** 47.62Å³ **XtlCell Z:** 2.00 **]**
Crystal Data Axial Ratio [c/a: 1.602 **a/b:** 1.000 **c/b:** 1.602 **]**
Reduced Cell [RedCell a: 3.250Å **RedCell b:** 3.250Å **RedCell c:** 5.207Å **RedCell :** 90.00°
RedCell : 90.00° **RedCell :** 120.00° **RedCell Vol:** 47.62Å³ **]**

: =2.013 **:** =2.029 **Sign:** =+

Crystal (Symmetry Allowed): Non-centrosymmetric, Pyro / Piezo (p), Piezo (2nd Harm.)

CAS: 1314-13-2 **Pearson:** hP4.00 **Prototype Structure:** Zn O **Prototype Structure (Alpha Order):** O Zn
LPF Prototype Structure: Zn O,hP4,186 **LPF Prototype Structure (Alpha Order):** O Zn
Mineral Classification: Wurtzite (Supergroup), 2H (Group)

Subfile(s): NBS Pattern, Pigment/Dye, Common Phase, Forensic, Educational Pattern, Metals & Alloys, Mineral Related (Mineral , Synthetic), Inorganic, Pharmaceutical, Primary Pattern

Last Modification Date: 01/15/2012

Cross-Ref PDF #'s: 00-005-0664 (Alternate), 01-075-1526 (Alternate), 04-001-7297, 04-003-2106, 04-004-2776, 04-004-4530, 04-004-4531, 04-004-5134, 04-004-6457, 04-004-7538, 04-004-8997, 04-005-4711, 04-005-5072, 04-005-5076, 04-006-1673, 04-006-2543, 04-006-2557, 04-006-9717, 04-007-1614, 04-007-4718, 04-007-5097, 04-007-9627, 04-007-9804, 04-007-9805, 04-008-2750, 04-008-3506, 04-008-4400, 04-008-6994, 04-008-7114, 04-008-8196, 04-008-8197, 04-008-8198, 04-009-7657

References:

Type	Reference
Primary Reference	McMurdie, H., Morris, M., Evans, E., Paretzkin, B., Wong-Ng, W., Ettlinger, L., Hubbard, C. Powder Diffr. 1, 76 (1986).
Additional Pattern	5. Swanson, H., Fuyat, R. Natl. Bur. Stand. (U. S.), Circ. 539 2, 25 (1953).
Optical Data	Dana's System of Mineralogy, 7th Ed. I, 504.
Polymorphism	3. Bates, C., White, W., Roy, R. Science 137, 993 (1962).
Polymorphism	4. Radczewski, O., Schicht, R. Naturwissenschaften 56, 514 (1969).
Structure	1. Bragg, W. Philos. Mag. 39, 647 (1920).
Structure	2. Abrahams, S., Bernstein, J. Acta Crystallogr., Sec. B: Struct. Crystallogr. Cryst. Chem. 25, 1233 (1969).

Database Comments: Additional Patterns: To replace 00-005-0664 (5). See PDF 01-075-1526. Color: Colorless. General Comments: The structure was determined by Bragg (1) and refined by Abrahams, Bernstein (2). Powder Data: References to other early patterns may be found in reference (5). Polymorphism/Phase Transition: A high pressure cubic NaCl-type of ZnO is reported by Bates et al. (3) and a cubic, sphalerite type is reported by Radczewski, Schicht (4). Sample Source or Locality: The sample was obtained from the New Jersey Zinc Co., Bethlehem, Pennsylvania, USA. Temperature of Data Collection: The approximate temperature of data collection was 299 K. Unit Cell Data Source: Powder Diffraction.

d-Spacings (27) - 00-036-1451 (Fixed Slit Intensity) - Cu K1 1.54056Å

2	d(Å)	I	h	k	l	*	2	d(Å)	I	h	k	l	*	2	d(Å)	I	h	k	l	*
31.7694	**2.814300**	57	1	0	0		72.5599	1.301740	2	0	0	4		107.4262	0.955607	1	2	0	4	
34.4211	**2.603320**	44	0	0	2		76.9528	1.238010	4	2	0	2		110.3879	0.938120	3	3	0	0	
36.2521	**2.475920**	100	1	0	1		81.3677	1.181620	1	1	0	4		116.2744	0.906943	8	2	1	3	
47.5376	1.911140	23	1	0	2		89.6045	1.093120	7	2	0	3		121.5669	0.882558	4	3	0	2	
56.6016	1.624720	32	1	1	0		92.7808	1.063840	3	2	1	0		125.1826	0.867681	1	0	0	6	
62.8624	1.477120	29	1	0	3		95.3007	1.042260	6	2	1	1		133.9254	0.837033	3	2	0	5	
66.3782	1.407150	4	2	0	0		98.6092	1.015950	4	1	1	4		136.5130	0.829282	1	1	0	6	
67.9610	1.378180	23	1	1	2		102.9424	0.984641	2	2	1	2		138.5054	0.823695	2	2	1	4	
69.0982	1.358250	11	2	0	1		104.1304	0.976632	5	1	0	5		142.9096	0.812469	3	2	2	0	